Chemical Characterization and Charge Carrier Dynamics of Crystalline Silicon(111) Surfaces Modified with Surface-Bound Organic Functional Groups

Thesis by

Lauren J. Webb

In Partial Fulfillment of the Requirements

for the Degree of

Doctor of Philosophy

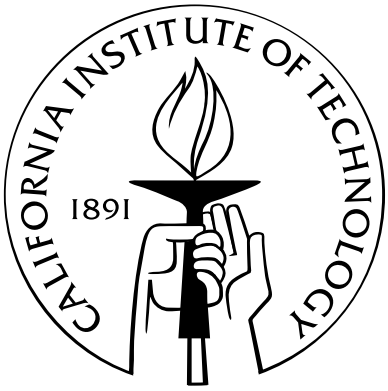

California Institute of Technology

Pasadena, California

2005

(Submitted May 26, 2005)

Acknowledgements

I have been exceptionally fortunate to have spent my time as a graduate student working with a number of colleagues who were not only great scientists, but wonderful and interesting people. Putting together this final statement of my work here at Caltech has made it clear to me how much I owe to so many people. Now that the time has come to express my thanks I find the task of doing this adequately a bit daunting, but here goes.

First and foremost I would like to thank my advisor, Prof. Nathan S. Lewis. Nate has been a constant source of ideas, encouragement, and unending critical analysis. Nate fosters an atmosphere in our group in which every detail of every idea is questioned relentlessly, and the rigor of his approach to all topics has been the best possible scientific training I could imagine. Beyond that, however, he has taught me to trust my instincts and to follow my own path, which is the greatest lesson any teacher can impart. I am very grateful for the opportunity to have worked with him. The members of my committee, Dr. Harry Gray, Dr. Rudy Marcus, and Dr. Jacqueline Barton, are all inspiring scientists and teachers, and it has been my great privilege to talk with them about my research and future plans. Finally I must thank the two directors of the Molecular Materials Resource Center during my time here, Dr. Michael Freund and Dr. Bruce Brunschwig, for their financial, technical, and moral support throughout my five-year love-hate relationship with the X-ray photoelectron spectrometer.

In the Lewis Group, David Michalak and Florian Gstrein have been my constant and invaluable sources of help and advice in lab, teaching me how to do just about everything necessary to complete this thesis. If I ever provide even a tenth of the support to someone else in lab as these two have given to me, I will consider myself a success. There have been a number of great people to work with on our semiconductor projects, including Julie

Biteen, David Knapp, E. Joseph Nemanick, and Matthew Traub. Working with them has made the day-to-day slog of graduate school more productive and certainly more enjoyable. Above that, these people, along with David Michalak, were enormously generous with their time, lab skills, and critical analysis during our synchrotron data collection runs at Brookhaven National Laboratory, for which I am truly grateful. I would also like to thank Agnes Juang for teaching me much of the previous chemical functionalization knowledge accumulated by former Lewis Group members.

I would like to thank everyone in the Lewis Group for keeping me on my toes for the last five years. Elizabeth Mayo has been a terrific friend from the very beginning of my time here at Caltech and has always been willing to discuss science or anything else at an impressive range of volumes. More generally, my fellow group members have challenged me on just about everything I did or said, science or otherwise. Short of shutting down entirely, it is impossible to be in this group without discussing and examining and reexamining, well, everything. This atmosphere may not be right for everyone, but I have benefited from it enormously. I am also deeply indebted to the two real heros of the Lewis Group, Nannette Pettis and Sherry Feick, without whom we would all wander in darkness and confusion.

Beyond the Lewis Group, I have spent much time collaborating with people who added tremendous depth to my education and experience, and whose help is in constant evidence in this thesis. Hongbin Yu from the Heath Group provided the STM data described herein and has been a great collaborator and a valuable source of ideas and discussion on all aspects of silicon surface structure. As a result of Hongbin's work, we turned to the computational expertise of Santiago Solares from the Goddard Group. The three of us have brought our completely different backgrounds to one very interesting problem in what has proven to be an ideal and extremely productive collaboration. At Rutgers University, Prof. Yves Chabal and his postdoc Sandrine Rivillon taught me everything I know about infrared spectroscopy and were generous with their time and equipment during my visits to their laboratory. Furthermore, through them an additional collaboration with Prof. Krishnan Raghavachari and his graduate student Matthew Halls at Indiana University helpfully provided computational techniques to understand our IR observations. At Brookhaven Na-

tional Lab, Ally Chan was tremendously helpful at getting me up and running on the synchrotron beamline and made the experience much more fun than I had any right to expect. A sabbatical spent by Dr. Wolfram Jaegermann in our laboratory led to an interesting trans-Atlantic collaboration with his postdoc, Ralf Hunger.

There are a number of people who have helped me on a more technical level, and I am deeply grateful for their efforts and assistance. Mike Roy of the machine shop kindly put up with my horrible technical drawing skills to generate some important experimental equipment. Harry Meyer at Oak Ridge National Lab collected helpful Auger electron spectroscopy data. Bengt Jaeckel of the Technische Universität Darmstadt provided low energy electron diffraction images described here. Dian Buchness has been a limitless source of information and assistance. My final original research proposals and this thesis benefited greatly from a number of people who provided me with comments and feedback: Julie Biteen, Matthew Traub, Christopher Thomas, David Michalak, Elizabeth Mayo, and Bruce Brunschwig. Thank you all.

Finally, I would like to thank the people without whom none of this would have been possible, my parents John Webb and Lynn Chmelir. I love you.

Abstract

Investigations of the chemical structure and charge carrier properties of alkylated crystalline silicon(111) surfaces are presented. Hydrogen-terminated Si(111) surfaces were alkylated with a series of saturated hydrocarbons through a chlorination/alkylation procedure and characterized using surface-sensitive techniques. High-resolution soft X-ray photoelectron spectroscopy (SXPS) identified 1 monolayer of H, Cl, and C on the H-, Cl- and CH_3-terminated surfaces, respectively. Surfaces functionalized with bulkier alkyls showed Si 2p binding energy shifts that suggest that unalkylated Si atoms are bonded to hydrogen. Alkylated Si(111) surfaces were further characterized using transmission infrared spectroscopy (TIRS). The Si–Cl stretching and bending motions were identified at 583 and 528 cm^{-1}, respectively. On the methyl-terminated Si(111) surface, a CH_3 symmetrical bending vibrational mode at 1257 cm^{-1} polarized perpendicular to the surface was observed. On the C_2H_5-terminated surface, a Si–H stretching and bending motion at 2080 and 627 cm^{-1}, respectively, were observed, confirming that unalkylated Si atoms are terminated with H atoms. Structural morphology of the CH_3-terminated Si(111) surface was investigated by low energy electron diffraction (LEED), which found that this surface retained a flat, unreconstructed (1 x 1) structure. Scanning tunneling microscopy (STM) images of CH_3-Si(111) were obtained at 4.7 and 77 K. The functionalized surface preserved the atomically flat morphology of freshly etched H-Si(111), and at 4.7 K individual methyl H atoms were clearly resolved for the first time.

Electronic passivation of the alkylated Si(111) surface was investigated through measurement of surface charge carrier recombination velocities (S), through time-resolved radio frequency (rf) photoconductivity decay methods. While unpassivated H- and Cl-terminated surfaces reacted rapidly in an air ambient to yield S>1400 cm s^{-1}, alkylated

surfaces preserved $S<$200 cm s^{-1} even when exposed to air for a period of weeks.

Finally, the two-step chlorination/alkylation route was compared to three other Si(111) surface functionalization techniques: (1) chlorination with Cl_2(g) followed by alkylation with an alkylmagnesium halide reagent, (2) Lewis acid-mediated reduction of a terminal alkene, and (3) anodization of the H-terminated Si(111) surface in diethyl ether containing 3.0 M CH_3MgI. The chemical properties and charge carrier recombination rates of each surface were measured as a function of time exposed to air.

Portions of the material presented here have appeared previously in the following references and are reproduced with permission:

Webb, L. J.; Lewis, N. S. “Comparison of the Electrical Properties and Chemical Stability of Crystalline Silicon(111) Surfaces Alkylated Using Grignard Reagents or Olefins with Lewis Acid Catalysts.” *J. Phys. Chem. B*, **2003**, *107*, 5404–5412.

Yu, H.; Webb, L. J.; Reis, R.; Solares, S. D.; Goddard, W. A.; Heath, J. R.; Lewis, N. S. “Low Temperature STM Images of Methyl-Terminated Si(111) Surfaces.” *J. Phys. Chem. B*, **2005**, *109*, 671–674.

Webb, L. J.; Nemanick, E. J.; Biteen, J. S.; Knapp, D. W.; Michalak, D. J.; Traub, M. C.; Chan, A. S. Y.; Brunschwig, B. S.; Lewis, N. S. “High-Resolution X-ray Photoelectron Spectroscopic Studies of Alkylated Silicon(111) Surfaces.” *J. Phys. Chem. B*, **2005**, *109*, 3930–3937.

Rivillon, S.; Chabal, Y. J.; Webb, L. J.; Michalak, D. J.; Lewis, N. S.; Halls, M. D.; Raghavachari, K. “Infrared Spectroscopy of Chlorine-Terminated Si(111) Surfaces.” *J. Vac. Sci. Technol. A*, in press.

Hunger, R.; Fritsche, R.; Jaechet, B.; Jaegermann, W.; Webb, L. J.; Lewis, N. S. “Chemical and Electronic Characterization of Methyl-Terminated Si(111) Surfaces by High-Resolution Synchrotron Photoelectron Spectroscopy.” *Phys. Rev. B*, in press.

Webb, L. J.; Biteen, J. S.; Brunschwig, B. S.; Chan, A. S. Y.; Knapp, D. W.; Meyer, H. M.; Nemanick, E. J.; Traub, M. C.; Lewis, N. S. “High-Resolution X-ray Photoelectron Spectroscopy of the Air Oxidation of Alkylated Crystalline Silicon(111) Surfaces.” to be submitted.

Contents

List of Figures

List of Tables

Chapter 1

Introduction to Silicon Surface Chemistry and Electrochemistry

1.1 Charge Carrier Dynamics at Semiconductor Surfaces and Interfaces

The semiconducting and light-absorbing properties of silicon have placed it at the center of modern electronic and photovoltaic devices. Because there has been extensive and prolonged interest in the semiconducting photophysics of Si, the behavior of the bulk crystal is well-understood.[1] At the crystal surface, however, Si atoms are no longer protected by the bulk material from chemical reactions with the environment, and molecular species can absorb onto or bond with surface atoms. These new molecular species can alter the electronic structure of the semiconductor at the surface, potentially influencing the electronic behavior of the entire material. To prevent this, electronic or photovoltaic devices made from Si are typically covered in thick layers of high-quality, annealed silicon dioxide to protect the surface from the ambient environment and prevent these deleterious chemical reactions. This strategy has been adequate for microelectronic devices that have been produced for the past several decades.

There is currently increasing interest in fabricating electronic devices of ever smaller size. In particular, nano-scale Si particles have been proposed for light-emitting[2] and memory[3] devices, and Si nanorods have potential for nano-scale photovoltaic devices,[4] thus thrusting Si into the world of "molecular electronics." As the Si crystal becomes smaller,

the ratio of surface area-to-volume increases dramatically, and the properties of the surface begin to dominate the properties of the device as a whole. In the limit of nanocrystals or nanotubes, where a very large percentage of the Si atoms present are at or very close to the surface, bulk Si crystal properties become meaningless. A primary obstacle for further research in this area will be definition of and subsequent control over surface electronic properties.

This situation becomes clear upon consideration of the behavior of electron and hole charge carrier pairs at the interface of a semiconducting crystal and another medium of differing electrochemical potential.[5] Figure 1.1(a) shows the effect of placing a n-type Si crystal into contact with a solution containing an electron acceptor/donor (A/A^-) pair with an electrochemical potential (E^0) more positive in energy than the Fermi level (E_F) of the semiconductor. As the potentials of the semiconductor and redox couple equilibrate, electrons from the dopant atoms in the n-type semiconductor will transfer across the semiconductor/liquid interface to acceptor molecules in solution, leaving a net positive charge in the crystal and a net negative charge in the solution (Figure 1.1(b)). Because the dopant atoms are fixed in the crystal lattice, the cationic centers cannot diffuse to the surface to match the negative charge in the solution, which is lined up at the crystal/liquid interface. The net positive charge in the semiconductor instead is spread over a much larger portion of the bulk crystal, called the depletion or space-charge region.

When the semiconductor is illuminated as shown in Figure 1.1(c), electrons are injected from the valence band (VB) into the conduction band (CB), leaving behind an electron vacancy, or hole. The electric field established by the space-charge region drives the majority charge carrier (electrons in the case of a n-type semiconductor) away from the crystal surface towards the back of the crystal, and drives the minority carrier (holes) across the semiconductor interface to the redox molecule in solution. The bulk charge carrier properties of any device created through this strategy are determined by the extent of the band bending, which is in turn described by the difference in E_F and $E^o(A/A^-)$, and the depth of the space-charge region (W). When a photovoltaic cell formed from such a method is illuminated, the total possible photopotential, called the built-in voltage (V_{bi}), is measured from the bottom of the CB to the band edge, indicated in Figure 1.1(b).[5]

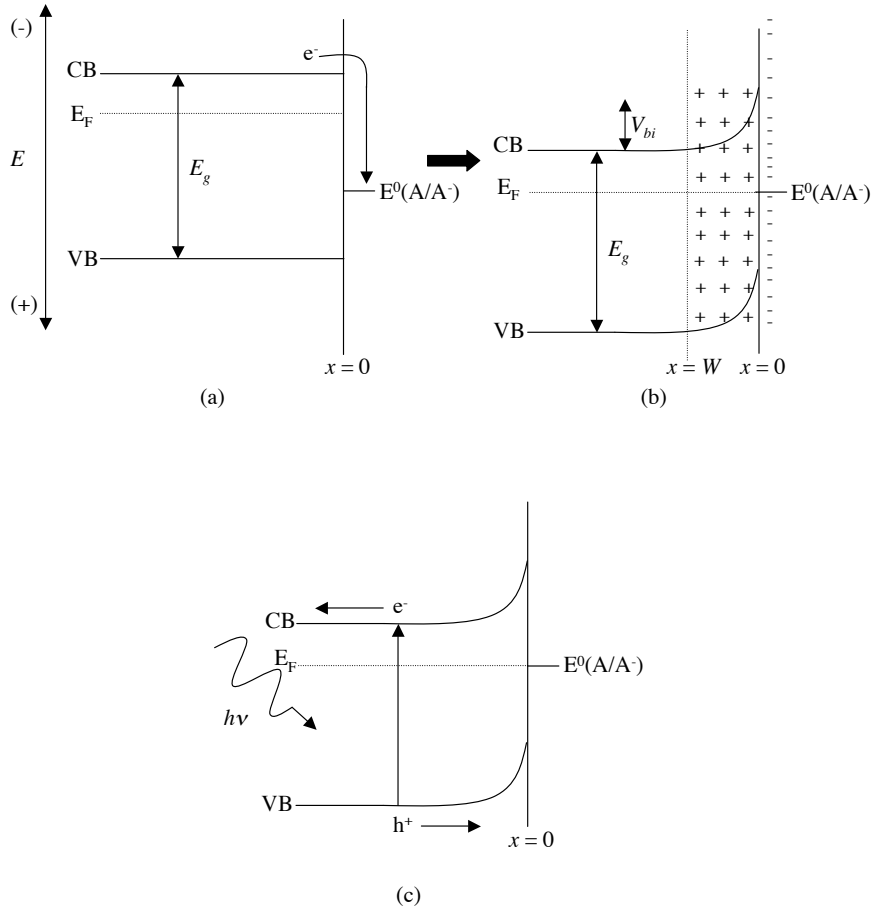

Figure 1.1: Energy band diagram of a n-type semiconductor immersed in a solution containing an electron donor-acceptor pair (E^0(A/A$^-$)). The x-axis is distance into the bulk crystal from the surface (x=0), and the y-axis is energy increasing positive in the downward direction. (a) Initial state with E_F of the semiconductor at a more negative potential than E^0(A/A$^-$), causing electrons to move from the semiconductor to acceptor species in solution; (b) After equilibration, a net negative charge is in solution, and a net negative charge in the semiconductor extends into the crystal for distance $x = W$ from the interface, resulting in bending of the semiconductor VB and CB by an amount called the built-in voltage, V_{bi}. (c) Upon illumination with $h\nu \geq E_g$, electrons are injected into the CB, leaving holes behind in the valence band. Figure adapted from Tan, *et al.*[5]

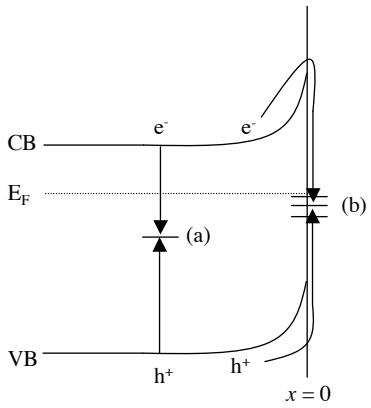

Figure 1.2: Charge carrier recombination processes at a semiconductor/liquid junction. Recombination of an electron-hole pair (a) in the bulk and (b) at the surface of the semiconductor crystal. Figure adapted from Lewis, *et al.*[6]

This picture is complete in the absence of other processes that allow electrons and holes to recombine and thus short the charge carrier gradient established by the semiconductor/liquid junction. For the work described herein, the two most important recombination pathways occur either in the bulk or at the surface, shown in Figure 1.2.[6] The flux (U) of charge carriers to a recombination site has been described by the Schokley-Reed-Hall equation:[6]

$$U = \frac{pn - n_i^2}{\tau_{p0}(n + n_1) + \tau_{no}(p + p_1)} \tag{1.1}$$

where n and p are the concentrations of electrons and holes, respectively, n_i is the total charge carrier concentration in the absence of external excitation, and n_1 and p_1 are carrier concentrations in electronic trap states:

$$n_1 = n_i e^{(E_T - E_i)/kT} \tag{1.2}$$

$$p_1 = p_i e^{(-E_T - E_i)/kT} \tag{1.3}$$

with E_i equal to the position of the Fermi level with no dopant atoms and E_T describing the energy of the electronic trap state. Finally, the lifetime of each charge carrier in Eq. 1.1 is given by:

$$\tau_{n0} = \frac{1}{\sigma \nu_{th} N_T} \tag{1.4}$$

$$\tau_{p0} = \frac{1}{\sigma \nu_{th} N_T} \tag{1.5}$$

where N_T is the number of electronically active trap states, σ is the cross-section for carrier capture on the surface, typically 10^{-15} cm^2, and ν_{th} is the thermal charge carrier velocity, which is 5.2 x 10^6 cm s^{-1} in n-type Si(111) at room temperature.[1,7,8] Eqs. 1.4 and 1.5 assume that σ remains the same for both electrons and holes. When recombination occurs at the surface, n and p are replaced in Eq. 1.1 by the surface concentration of electrons and holes, n_s and p_s, respectively, with

$$n_s = n_i e^{(-qV_{bi})/kT} \tag{1.6}$$

$$p_s = p_i e^{(-qV_{bi})/kT} \tag{1.7}$$

It is clear from Eqs. 1.1–1.3 that recombination achieves its maximum rate when charge carrier traps are located at the middle of the bandgap. These electronic states, in turn, are introduced into the crystal by lattice defects or chemical impurities. Bulk crystals of silicon can be manufactured to an unprecedented degree of purity (1 impurity in 10^{10} Si atoms in the crystals used in this work), ensuring that essentially no imperfection will be found in the Si crystal. Electron-hole recombination in the bulk will thus be exceptionally slow. If the Si surface has chemically reacted with its environment, however, new molecular orbitals in the bandgap can promote very high rates of surface charge carrier recombination and render a device useless.

The rate of surface electron-hole recombination (S) can be related directly to the number of electronic defects present at the surface through the surface lifetime of the charge carrier:[8]

$$S = N_T \sigma \nu_{th} = \frac{1}{\tau} \tag{1.8}$$

Given a surface atom density of 7.8 x 10^{14} cm^{-2} on Si(111),[1] determining S can lead to a direct determination of the number of defects of the Si surface. Assuming that the surface does not contain a significant number of structural defects, N_T offers an approximation of the number of surface defects caused by chemical bonding.

1.2 Chemical Modification of Silicon(111) Surfaces

In order to understand and control the introduction of electronic states on Si surfaces, a current topic of interest is the passivation of these surfaces with thin, molecular layers that can be manipulated through comparatively simple wet-chemical techniques. In order to study the resulting chemical and electronic structure of such surfaces it is necessary to begin with a well-defined template. The surface most commonly used in Si electronic and photovoltaic devices is cut along the $<100>$ crystal plane because this surface forms a high-quality interface with the crystalline SiO_2 insulating layer commonly added during device fabrication processes.[9] As can be seen from Figure 1.3(a), however, the (100) sur-

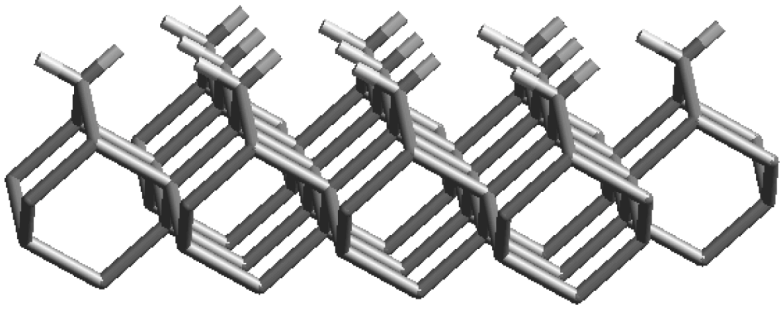

(a)

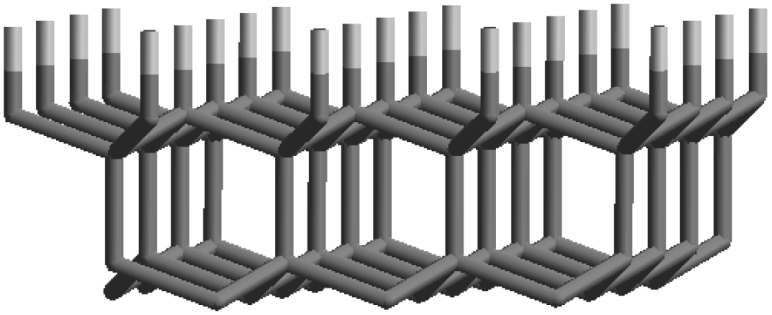

(b)

Figure 1.3: Structure of two common silicon crystal faces. (a) Si(100) surface; (b) Si(111) surface.

face is quite sterically hindered, with one surface Si dangling bond pointed directly at that of a neighboring Si atom. Only small atoms such as H or Cl will be able to bond to every surface Si atom, limiting the ability to perform interesting chemistry at this surface. The (111) surface, shown in Figure 1.3(b), has three of the Si tetrahedral bonds tied up in the bulk crystal and one Si dangling bond normal to the surface and available for chemical reactions. This is the least sterically hindered surface available on the Si crystal. Moreover, the H-terminated Si(111) surface can be made atomically flat over hundreds of Ångstroms through simple wet chemical etching of the native SiO_2 layer in aqueous fluoride solutions,[10] and thus provides an ideal starting material for surface alkylation.

The H-terminated Si(111) surface obtained through aqueous fluoride ion etching was the first surface prepared through simple wet-chemical techniques that demonstrated the concept of control over Si surface electronic properties through chemical bonding strategies. This surface became especially promising when attenuated total internal reflection infrared (IR) spectroscopy indicated that it was indeed atomically flat over very large areas, exhibited by a Si–H stretch that was perpendicular to the $<111>$ plane,[10] and photoconductivity decay measurements showed it had a low S of 0.25 cm s^{-1}.[11] This surface was found to oxidize rapidly in air, however, forming a silicon/native silicon oxide interface that was electrically defective and had essentially infinitely high S values.[8] There has been much interest in developing other chemical passivation strategies that prevent the extensive oxidation of the Si(111) surface while preserving the low surface charge carrier recombination velocity of the H-terminated surface.

One promising technique that has received much recent attention to solve the shortcomings of the H-terminated Si surface is the formation of surficial Si–C bonds.[12] To this end, the H-terminated Si surfaces of both single-crystal and porous Si substrates have been alkylated using alkylmagnesium reagents,[13,14] and halogenated surfaces have been further alkylated using alkylmagnesium or alkyllithium reagents.[15–21] Alkylation of the H-terminated surface has also been attempted using free-radical initiation methods such as irradiating with ultraviolet light,[19,22–25] chemical free-radical activation,[26,27] thermal activation,[26,28–34] or hydrosilation.[35–39] Other alkylation methods involve the formation of dangling Si surface bonds using scanning tunneling microscopy techniques[40] or the transition

metal-catalyzed reduction of a terminal alkene directly on the Si–H surface.[41] Additionally, several electrochemical functionalization methods have been described.[42–49] These alkylation techniques have also served as the starting point for bonding more interesting and complicated molecules to the surface[50] such as polymers,[51] saccharides,[52] and amines.[53,54]

A two-step surface alkylation procedure involving chlorination of H-terminated Si(111) followed by alkylation with an alkylmagnesium halide reagent is shown in Figure 1.4.[15,16] This reaction scheme was developed in our laboratory and has been analyzed extensively to characterize the chemical structure of the surface. X-ray photoelectron spectroscopy (XPS) demonstrated that this reaction proceeds without oxidizing the Si surface, shown by the absence of the silicon oxides in the Si 2p region of the XPS spectrum. XPS also showed that as longer alkyl chain lengths were introduced onto the surface, the ratio of the integrated areas of the C 1s : Si 2p peaks increased approximately monotonically. The ratio of integrated areas is proportional to the surface coverage of C atoms, and although it did not prove that the C is chemically bonded to the Si surface, it did show that the coverage of C increases in a manner predicted by the alkyl chain length. This is consistent with the hypothesis that this functionalization method forms a regular alkyl layer of controlled thickness on the Si(111) surface. On the Cl-terminated surface, high-resolution electron energy loss spectroscopy (HREELS) revealed a peak at 550 cm^{-1} corresponding to the surface Si–Cl stretch. When that surface was alkylated, the Si–Cl feature disappeared, and a new peak at 650 cm^{-1} was observed. This was assigned to the surface Si–C stretch, providing sufficient evidence for the first time that this surface was composed of surface-bound alkyl groups. The HREELS spectra were, however, unable to estimate the overall surface coverage of the Si–C feature.[16]

Although the chemical characterization and morphological properties of the alkylated Si(111) surface prepared through this two step chlorination/alkylation route had not yet been fully defined, there was considerable interest in how it would effect surface charge carrier behavior. Further work in this laboratory showed that this functionalization route generates alkyl-terminated surfaces that are sufficiently passivated to prevent electron-hole pair recombination on crystalline Si(111) surfaces during exposure to ambient air for periods of at least one month. Over this time, S values remained $<$25 cm s^{-1}, demonstrating

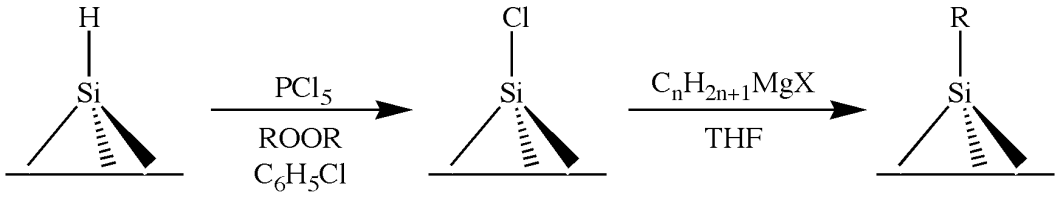

Figure 1.4: A two-step chlorination/alkylation functionalization route of Si(111).[16] A freshly etched H-terminated Si(111) is exposed to a saturated solution of PCl_5 in chlorobenzene with a small amount of peroxide added as a radical initiator. The Cl-terminated surface is then immersed in a solution of alkylmagnesium halide, $C_nH_{2n+1}MgX$, where n = 1 – 18 and X = Cl or Br, in tetrahydrofuran (THF).

that the surface is exceptionally stable.[8] This behavior was observed when the surface was terminated with both CH_3- and C_8H_{17}- groups, and further work in our laboratory has shown reasonable electronic passivation on surfaces alkylated with branched alkyls such as *i*-propyl- and *t*-butyl-, and even with bulky functional groups such as phenyl- and benzyl-.[55]

The initial success of this surface modification technique at chemical and electrical passivation is especially interesting in view of a simple steric model of the alkylated surface. The internuclear distance between adjacent atop sites on the Si(111) crystal face is 3.8 Å,[1] implying that a methyl group, with a van der Waals diameter of 2.5 Å,[46] is small enough to fit on every surface Si atom, and 100% surface coverage is possible. In contrast, the van der Waals diameter of a methylene group is approximately 4.5–5.0 Å,[56,57] so complete termination of Si atop sites on the unreconstructed Si(111) surface is not possible. Models of alkyl packing on the Si(111) surface have indicated that 50–55% surface coverage is the maximum obtainable for long straight-chain alkyl groups on the Si(111) surface.[57] These models were obtained by choosing initial conditions for packing arrangements and densities that seemed chemically reasonable, then optimizing the structure to find the minimum energy configuration. A number of surface packing arrangements were attempted and compared, but this technique is limited by the starting conditions and does not account for packing arrangements that are not regular enough for the small unit cell used in these calculations, but that still would provide high packing densities. Bulkier functional groups such as *t*-butyl- or benzyl- impose even more severe packing limitations on the alkylated Si(111) surface.

1.3 Summary

The work presented here addresses two intricately related questions on the chemical and electronic characteristics of alkylated Si(111) surfaces. First, Si(111) surfaces functionalized through the two-step chlorination/alkylation route were characterized with a number of surface-sensitive analytical techniques to determine the exact chemical and morphological structure of the Si-alkyl interface. Particular emphasis was placed on identifying a surface Si–C bond and determining the extent of alkyl group surface coverage. These

analyses were conducted on alkylated surfaces both after they were freshly prepared and as they oxidized in air over a time period of up to several weeks. The functionalization technique used throughout this research is described in detail in Chapter 2. In Chapter 3, XPS of these functionalized surfaces collected under high-resolution surface sensitive conditions is described and evidence for a monolayer of surface Si–C bonds is presented. Surface transmission infrared spectroscopy, which was used to characterize surface functional group vibrational modes, is described in Chapter 4. Detailed morphology of the CH_3-terminated Si(111) surfaces investigated by low energy electron diffraction scanning tunneling microscopy in ultra-high vacuum are described in Chapter 5. The stability of these alkylated surfaces as they were exposed to air for long time periods is detailed in Chapter 6.

The second major topic of this research is a description of the electronic properties of the alkylated surface, which were characterized both on the freshly prepared surface and and then monitored as the surfaces oxidized in air. This work is described in Chapters 7 and 8. Here experiments demonstrating electronic surface passivation are related to the structure of the alkyl layer, the electronic band structure of the silicon at the surface, and the functionalization reaction employed to prepare the modified surface. Finally, general conclusions of the current understanding of the alkylated Si(111) surface are summarized in Chapter 9.

Bibliography

[1] Sze, S. M. *The Physics of Semiconductor Devices;* Wiley: New York, 2nd ed.; 1981.

[2] Fauchet, P. M. *IEEE J. Sel. Top. Quant.* **1998,** *4*, 1020–1028.

[3] Ostraat, M. L.; De Blauwe, J. W.; Green, M. L.; Bell, L. D.; Brongersma, M. L.; Casperson, J.; Flagan, R. C.; Atwater, H. A. *Appl. Phys. Lett.* **2001,** *79*, 433–435.

[4] Kayes, B. M.; Atwater, H. A.; Lewis, N. S. *J. Appl. Phys.* **2004,** submitted.

[5] Tan, M. X.; Laibinis, P. E.; Nguyen, S. T.; Kesselman, J. M.; Stanton, C. E.; Lewis, N. S. *Prog. Inorg. Chem.* **1994,** *41*, 21–144.

[6] Lewis, N. S.; Rosenbluth, M. L. Theory of Semiconductor Materials. In *Photocatalysis: Fundamentals and Applications*; Serpone, N.; Pelizzetti, E., Eds.; Wiley INTERSCIENCE: New York, 1989.

[7] Sturzenegger, M.; Prokopuk, N.; Kenyon, C. N.; Royea, W. J.; Lewis, N. S. *J. Phys. Chem. B* **1999,** *103*, 10838–10849.

[8] Royea, W. J.; Juang, A.; Lewis, N. S. *Appl. Phys. Lett.* **2000,** *77*, 1988–1990.

[9] Hattori, T.; Takahashi, K.; Seman, M. B.; Nohira, H.; Hirose, M.; Kamakura, N.; Takata, Y.; Shin, S.; Kobayashi, K. *Appl. Surf. Sci.* **2003,** *212–213*, 547–555.

[10] Higashi, G. S.; Chabal, Y. J.; Trucks, G. W.; Raghavachari, K. *Appl. Phys. Lett.* **1990,** *56*, 656–658.

[11] Yablonovitch, E.; Allara, D. L.; Chang, C. C.; Gmitter, T.; Bright, T. B. *Phys. Rev. Lett.* **1986,** *57*, 249–252.

[12] Bent, S. F. *Surf. Sci.* **2002,** *500*, 879–903.

[13] Mitchell, S. A.; Boukherroub, R.; Anderson, S. *J. Phys. Chem. B* **2000,** *104*, 7668–7676.

[14] Yu, H. Z.; Boukherroub, R.; Morin, S.; Wayner, D. D. M. *Electrochem. Commun.* **2000,** *2*, 562–566.

[15] Bansal, A.; Li, X. L.; Lauermann, I.; Lewis, N. S.; Yi, S. I.; Weinberg, W. H. *J. Am. Chem. Soc.* **1996,** *118*, 7225–7226.

[16] Bansal, A.; Li, X.; Yi, S. I.; Weinberg, W. H.; Lewis, N. S. *J. Phys. Chem. B* **2001,** *105*, 10266–10277.

[17] He, J.; Patitsas, S. N.; Preston, K. F.; Wolkow, R. A.; Wayner, D. D. M. *Chem. Phys. Lett.* **1998,** *286*, 508–514.

[18] Okubo, T.; Tsuchiya, H.; Sadakata, M.; Yasuda, T.; Tanaka, K. *Appl. Surf. Sci.* **2001,** *171*, 252–256.

[19] Terry, J.; Linford, M. R.; Wigren, C.; Cao, R. Y.; Pianetta, P.; Chidsey, C. E. D. *Appl. Phys. Lett.* **1997,** *71*, 1056–1058.

[20] Terry, J.; Linford, M. R.; Wigren, C.; Cao, R. Y.; Pianetta, P.; Chidsey, C. E. D. *J. Appl. Phys.* **1999,** *85*, 213–221.

[21] Webb, L. J.; Lewis, N. S. *J. Phys. Chem. B* **2003,** *107*, 5404–5412.

[22] Boukherroub, R.; Wayner, D. D. M. *J. Am. Chem. Soc.* **1999,** *121*, 11513–11515.

[23] Cicero, R. L.; Linford, M. R.; Chidsey, C. E. D. *Langmuir* **2000,** *16*, 5688–5695.

[24] Effenberger, F.; Gotz, G.; Bidlingmaier, B.; Wezstein, M. *Angew. Chem.-Int. Edit.* **1998,** *37*, 2462–2464.

[25] Terry, J.; Mo, R.; Wigren, C.; Cao, R. Y.; Mount, G.; Pianetta, P.; Linford, M. R.; Chidsey, C. E. D. *Nucl. Instr. Methods Phys. Res. Sect. B* **1997,** *133*, 94–101.

[26] Linford, M. R.; Chidsey, C. E. D. *J. Am. Chem. Soc.* **1993,** *115*, 12631–12632.

[27] Linford, M. R.; Fenter, P.; Eisenberger, P. M.; Chidsey, C. E. D. *J. Am. Chem. Soc.* **1995,** *117*, 3145–3155.

[28] Sieval, A. B.; Demirel, A. L.; Nissink, J. W. M.; Linford, M. R.; van der Maas, J. H.; de Jeu, W. H.; Zuilhof, H.; Sudholter, E. J. R. *Langmuir* **1998,** *14*, 1759–1768.

[29] Sieval, A. B.; Linke, R.; Heij, G.; Meijer, G.; Zuilhof, H.; Sudholter, E. J. R. *Langmuir* **2001,** *17*, 7554–7559.

[30] Sung, M. M.; Kluth, G. J.; Yauw, O. W.; Maboudian, R. *Langmuir* **1997,** *13*, 6164–6168.

[31] Boukherroub, R.; Wojtyk, J. T. C.; Wayner, D. D. M.; Lockwood, D. J. *J. Electrochem. Soc.* **2002,** *149*, H59–H63.

[32] Boukherroub, R.; Wayner, D. D. M.; Sproule, G. I.; Lockwood, D. J.; Canham, L. T. *Nano Letters* **2001,** *1*, 713–717.

[33] Boukherroub, R.; Wayner, D. D. M.; Lockwood, D. J.; Canham, L. T. *J. Electrochem. Soc.* **2001,** *148*, H91–H97.

[34] Gelloz, B.; Sano, H.; Boukherroub, R.; Wayner, D. D. M.; Lockwood, D. J.; Koshida, N. *Appl. Phys. Lett.* **2003,** *83*, 2342–2344.

[35] Boukherroub, R.; Morin, S.; Bensebaa, F.; Wayner, D. D. M. *Langmuir* **1999,** *15*, 3831–3835.

[36] Buriak, J. M.; Allen, M. J. *J. Am. Chem. Soc.* **1998,** *120*, 1339–1340.

[37] Buriak, J. M.; Stewart, M. P.; Geders, T. W.; Allen, M. J.; Choi, H. C.; Smith, J.; Raftery, D.; Canham, L. T. *J. Am. Chem. Soc.* **1999,** *121*, 11491–11502.

[38] Zazzera, L. A.; Evans, J. F.; Deruelle, M.; Tirrell, M.; Kessel, C. R.; McKeown, P. *J. Electrochem. Soc.* **1997,** *144*, 2184–2189.

[39] Schmeltzer, J. M.; Porter, L. A.; Stewart, M. P.; Buriak, J. M. *Langmuir* **2002,** *18*, 2971–2974.

[40] Cicero, R. L.; Chidsey, C. E. D.; Lopinski, G. P.; Wayner, D. D. M.; Wolkow, R. A. *Langmuir* **2002,** *18*, 305–307.

[41] Saghatelian, A.; Buriak, J. M.; Lin, V. S. Y.; Ghadiri, M. R. *Tetrahedron* **2001,** *57,* 5131–5136.

[42] Allongue, P.; de Villeneuve, C. H.; Pinson, J.; Ozanam, F.; Chazalviel, J. N.; Wallart, X. *Electrochimica Acta* **1998,** *43,* 2791–2798.

[43] Allongue, P.; de Villeneuve, C. H.; Pinson, J. *Electrochimica Acta* **2000,** *45,* 3241–3248.

[44] Allongue, P.; de Villeneuve, C. H.; Cherouvrier, G.; Cortes, R.; Bernard, M. C. *J. Electroanal. Chem.* **2003,** *550,* 161–174.

[45] Dubois, T.; Ozanam, F.; Chazalviel, J.-N. *Electrochem. Soc. Proc.* **1997,** *97-7,* 296–310.

[46] Fidelis, A.; Ozanam, F.; Chazalviel, J. N. *Surf. Sci.* **2000,** *444,* L7–L10.

[47] Gros-Jean, M.; Herino, R.; Chazalviel, J. N.; Ozanam, F.; Lincot, D. *Mat. Sci. Eng. B* **2000,** *69,* 77–80.

[48] Henry de Villeneuve, C.; Pinson, J.; Bernard, M. C.; Allongue, P. *J. Phys. Chem. B* **1997,** *101,* 2415–2420.

[49] Lees, I. N.; Lin, H. H.; Canaria, C. A.; Gurtner, C.; Sailor, M. J.; Miskelly, G. M. *Langmuir* **2003,** *19,* 9812–9817.

[50] Linford, M. R.; Chidsey, C. E. D. *Langmuir* **2002,** *18,* 6217–6221.

[51] Juang, A.; Scherman, O. A.; Grubbs, R. H.; Lewis, N. S. *Langmuir* **2001,** *17,* 1321–1323.

[52] de Smet, L. C. P. M.; Stork, G. A.; Hurenkamp, G. H. F.; Sun, Q. Y.; Topal, H.; Vronen, P. J. E.; Sieval, A. B.; Wright, A.; Visser, G. M.; Zuilhof, H.; Sudholter, E. J. R. *J. Am. Chem. Soc.* **2003,** *125,* 13916–13917.

[53] Bocking, T.; James, M.; Coster, H. G. L.; Chilcott, T. C.; Barrow, K. D. *Langmuir* **2004,** *20,* 9227–9235.

[54] Wojtyk, J. T. C.; Morin, K. A.; Boukherroub, R.; Wayner, D. D. M. *Langmuir* **2002,** *18*, 6081–6087.

[55] Nemanick, E. J.; Hurley, P. T.; Lewis, N. S. **2004,** manuscript in preparation.

[56] Ewen, B.; Strobl, G. R.; Richter, D. *Faraday Discuss.* **1980,** *69*, 19–31.

[57] Sieval, A. B.; van den Hout, B.; Zuilhof, H.; Sudholter, E. J. R. *Langmuir* **2001,** *17*, 2172–2181.

Chapter 2

Experimental Details of Silicon Surface Alkylation through a Two-Step Chlorination/Alkylation Route

2.1 Introduction

The alkylated Si(111) surfaces described in this work were prepared almost exclusively through one experimental procedure, which will be described in detail here. Any differences in the alkylation procedure will be noted in subsequent chapters. A two-step chlorination/alkylation functionalization route shown in Figure 1.4 was adapted from Bansal, *et al.*[1] and further refined from Royea, *et al.*[2]

2.2 Experimental

2.2.1 Materials

Silicon(111) wafers that were n-type were obtained from a variety of sources depending on experimental conditions and will be described for each individual experiment. All solvents used in alkylation reactions were anhydrous, stored under N_2(g), and used as received from Aldrich Chemical Corp. Solvents were only exposed to the atmosphere of a N_2(g)-purged flush box. Water with a resistivity of $\geq$18.0 MΩ cm obtained from a Barnstead Nanopure system (Dubuque, IA) was used at all times. All chemicals were used as received except where noted.

2.2.2 Sample Preparation

2.2.2.1 Preparation of H-Terminated Si(111) Surfaces

Each Si wafer was cut into samples of approximately 1 cm^2. Throughout the functionalization procedure, care was taken to handle the wafer only by the extreme edge to avoid scratching the surface, which would cause severe structural defects that might influence chemical and electronic characterization efforts. Before chemical functionalization, each sample was cleaned by sequential rising in a flowing stream of H_2O, CH_3OH, acetone, CH_3OH, and H_2O, respectively. After cleaning, the sample was dried under a flowing stream of N_2(g). The Si wafer was then placed in 40% NH_4F(aq) (Transene, Inc.) for 20 min to etch away the native SiO_2 oxide layer and produce a H-terminated Si(111) surface. During the etching process, the wafers were agitated occasionally to remove bubbles that formed on the surface. After removal from the etching solution, the sample was rinsed thoroughly with H_2O and dried under a stream of N_2(g). The sample was then immediately inserted into the experimental apparatus or into the antechamber of a N_2-purged glove box, where all further chemical functionalization was conducted.

2.2.2.2 Preparation of Cl-Terminated Si(111) Surfaces

The H-terminated Si(111) surface was chlorinated by immersing the sample in a saturated solution of PCl_5 (99.998%, Alfa Aesar) in chlorobenzene to which a few grains of benzoyl peroxide had been added as a radical initiator. The reaction solution was heated to 90–100°C for 45 min. The sample was then removed from the reaction solution, rinsed with tetrahydrofuran (THF) and CH_3OH, and then blown dry under a flowing stream of N_2(g).

2.2.2.3 Preparation of C_nH_{2n+1}-Terminated Si(111) Surfaces

For alkylation, the Cl-terminated Si(111) sample was immersed in a 1.0–3.0 M solution of $C_nH_{2n+1}MgX$ in THF or diethyl ether with n = 1–14 and X = Cl or Br (Aldrich). Excess THF was added to each reaction solution to allow for solvent loss. The reaction solution was heated at 70–80°C for an amount of time dependent on the alkyl chain length, with longer chain lengths exposed for longer reaction times. The reaction times for each alkyl

Reagent	Reaction Time (hr)
CH_3MgX	2–3
C_2H_5MgX	3–5
C_4H_9MgX	2.5–5
$C_5H_{11}MgX$	5–16
$C_6H_{13}MgX$	16
$C_8H_{17}MgX$	16
$C_{10}H_{21}MgX$	24
$C_{14}H_{29}MgX$	40
$C_6H_5CH_2MgX$	16–18

Table 2.1: Alkylmagnesium halide reagents and reaction times for Si(111) surface alkylation with X = Cl or Br. All reactions were carried out in THF or diethyl ether + THF at 70–80°C.

chain length are given in Table 2.1. At the end of the reaction, the sample was removed from the alkylmagnesium solution and was rinsed with copious amounts of THF and CH_3OH, then immersed in CH_3OH and removed from the N_2-purged glove box. The sample was sonicated for 5 min in CH_3OH, sonicated in CH_3CN for a further 5 min, and then dried under a stream of N_2(g). Sonication was found to be important for completely removing residual Mg salts from the surface. After functionalization the sample was moved immediately into the experimental apparatus of interest. If the sample needed to be stored for some length of time it was moved back into the N_2(g)-purged glove box and sealed in a vial under N_2(g).

Bibliography

[1] Bansal, A.; Li, X.; Yi, S. I.; Weinberg, W. H.; Lewis, N. S. *J. Phys. Chem. B* **2001,** *105,* 10266–10277.

[2] Royea, W. J.; Juang, A.; Lewis, N. S. *Appl. Phys. Lett.* **2000,** *77,* 1988–1990.

Chapter 3

High-Resolution X-ray Photoelectron Spectroscopy of Functionalized Si(111) Surfaces

3.1 Introduction

Analytical techniques for surface chemistry are generally limited by the vanishingly small amount of material available for observation. The density of Si surface atoms along the <111> plane is 7.8 x 10^{14} cm^{-2},[1] substantially less than Avogadro's number, and traditional solution phase analytical techniques developed to determine chemical bonding and structure, such as nuclear magnetic resonance, infrared spectroscopy, or mass spectrometry, are generally not possible.

One of the most useful techniques to characterize thoroughly the chemical composition of the alkylated Si(111) surfaces prepared herein is X-ray photoelectron spectroscopy (XPS), in which the kinetic energies of atomic core electrons are measured as they are photoejected from atoms of a solid material upon absorption of an incident X-ray of known energy. The measured kinetic energy of the photoelectron, E_{KE}, is a function of the X-ray excitation energy, $h\nu$, the binding energy of the electron in a specific core orbital, E_{BE}, and the work function of the instrument, ϕ:

$$E_{KE} = h\nu - E_{BE} - \phi \tag{3.1}$$

Because Eq. 3.1 is a function of the excitation energy and the instrument work function,

which are both instrument specific, it is often more helpful to rearrange Eq. 3.1 to express binding energy,

$$E_{BE} = h\nu - E_{KE} - \phi \tag{3.2}$$

which is independent of the instrument on which it was collected. Photons in the X-ray region of the spectrum penetrate the entire sample to excite photoelectrons throughout the material, but the mean free path of a electron moving through a crystalline material such as silicon is fairly short before it is scattered by collision with a lattice phonon. The only photoelectrons that can escape the material to vacuum and can be measured by the electron detector originate from atoms that are relatively close to the surface. This allows the bulk material, which would otherwise dominate the signal, to be screened out, which produces an analytical technique that is highly sensitive to surface composition. Although X-rays photoeject core electrons that are not involved in chemical bonding, the core orbitals that contain these electrons are still influenced by the atoms' valence interactions. Changes in the electron density surrounding an atom caused by interactions with more or less electronegative elements will cause the core electrons to be held more or less tightly, respectively. This will result in small but measurable shifts in the core electron binding energy spectrum on the order of a few electron volts (eV). The shift in core electron energy can then be used to determine the extent of any bonding in which the atom participates.

Because of the importance of surfaces and interfaces of silicon in modern electronic devices, XPS of Si surfaces, usually prepared in ultra-high vacuum (UHV) conditions, has been explored and reported in the literature. In particular, the Si 2p core electron peak has been identified as a useful peak for chemical analysis of Si surfaces. This peak is spin-orbit split into a $2p_{3/2}$ and $2p_{1/2}$ doublet, with the $2p_{3/2}$ component centered at 99.4 binding electron volts (BeV).[1,2] One of the most well-studied surfaces to date is the Si/SiO_2 interface on both the (111) and (100) oriented surfaces. Silicon oxidation states from Si^{+} to Si^{4+} appear at approximately 1 eV intervals above the Si^{0} 2p core level peak.[1–5] Measuring the location of this silicon oxide peak allows the exact oxidation state of Si to be determined. Furthermore, XPS of surface Si atoms has shown that when bonded to more electronegative elements such as Cl, Br, C, and even H, the Si 2p core level peak is shifted

to higher binding energies by $<$1 eV.[6–15] This small shift can be measured under high-resolution conditions, and chemical bonds between Si and other elements can be analyzed.

When the two-step chlorination/alkylation Si surface functionalization route that is the subject of this report was first developed in our laboratory, XPS data on the functionalized surface was collected.[16,17] Several conclusions were drawn from this initial work. First, with proper exclusion of H_2O and O_2 from the reaction conditions, the full functionalization chemistry could be conducted without the formation of surface silicon oxides. This was important because surface functionalization was initially investigated as a way to slow Si surface oxidation processes, and it would have been deeply inconvenienced if the modification technique itself led to unwanted oxidation. Second, after the first chlorination step it was possible to see the appearance of a small peak 1.1 eV higher in binding energy than the Si 2p peak that quantitatively corresponded to $\approx$0.7 of a monolayer of Si atoms. This signal was attributed to surface Si atoms bonded to more electronegitve Cl atoms that were drawing away electron density, slightly shifting the signal for the surface Si 2p peak to higher binding energies than for the Si bulk peak. Finally, survey scan spectra of the alkyl-terminated surface demonstrated that the ratio of the integrated areas of C 1s:Si 2p increased monotonically with the number of C atoms in the alkyl chain. This was strong evidence for a surface-bound alkyl group introduced in a controlled manner by the chlorination/alkylation reaction, but did not prove the existence of a surface Si–C bond.

These measurements were carried out on an XPS instrument at the California Institute of Technology that was not able to resolve the shifts in the Si 2p binding energy of $<$0.6 eV, which would have been necessary to investigate the presence of a surface Si–C bond on the fully alkylated surface. This instrument also used a high-energy X-ray source that resulted in ejected photoelectrons having enough kinetic energy to escape from up to 15 Å of Si crystal, meaning that the topmost layer of Si atoms only made up $\sim$20% of the total experimental signal. Both of these factors prevented previous XPS investigations of the alkylated Si(111) surface from identifying possible Si atoms that might be bonded to the carbon atom of the alkyl group. Although this XPS instrument continues to be important for monitoring the functionalization reaction in our laboratory as seen below, it could not fully analyze the modified surface. For higher resolution surface sensitive measurements,

it was necessary to use a lower energy X-ray excitation source. To do this a synchrotron "soft" X-ray source was used to resolve and quantify surface Si atoms bonded to Cl, H, C, and O and to investigate the chemical species present on the nonalkylated portions of the functionalized Si surfaces. These results for freshly prepared CH_3-, C_2H_5-, and $C_6H_5CH_2$-terminated Si surfaces are reported here.

3.2 Experimental

3.2.1 Materials and Methods

Silicon(111) wafers polished on one side and having a thickness of 525 μm were obtained from Crysteco (Wilmington, OH). These n-type samples were doped with P to a resistivity of 2.0–8.5 Ω cm. A full description of the alkylation procedure can be found in Chapter 2.

3.2.2 Instrumentation

3.2.2.1 XPS Measurements

Preliminary spectroscopic data on functionalized Si(111) surfaces were collected using an M-Probe XPS system in our laboratory. For these experiments, 1486.6 eV X-rays generated from a Al Kα source illuminated the sample from an incident angle of 35° off the surface. Photoelectrons emitted along a trajectory of 35° off the surface were collected by a hemispherical analyzer. Samples were inserted via a quick-entry load lock into the UHV system and were kept at a base pressure of $\leq$1 x 10^{-9} Torr. All samples were sufficiently electrically conductive at room temperature so that no compensation for charging effects was required. On each sample, a "survey" scan of core photoelectron binding energies over a range of 1–1000 binding eV (BeV) was collected to identify all chemical species present on the surface.

A simple model that had been developed previously[18] was used to determine the sample surface composition based on the relative intensities of the O 1s, C 1s, Cl 2s and 2p, and Si 2p peaks observed in the survey scan XP spectra. The equivalent monolayer coverage of

an overlayer species, Φ_{ov}, can be expressed as

$$\Phi_{ov} = \left[\left(\frac{\lambda \sin\theta}{a_{ov}}\right)\left(\frac{\mathrm{SF}_{Si}}{\mathrm{SF}_{ov}}\right)\left(\frac{\rho_{Si}}{\rho_{ov}}\right)\left(\frac{I_{ov}}{I_{Si}}\right)\right] \tag{3.3}$$

where λ is the photoelectron penetration depth (1.6 nm on this instrument); θ is the photoelectron takeoff angle with respect to the surface (35°); a_{ov} is the atomic diameter of the overlayer species; and ρ_x and I_x are the volumetric density and integrated area of the signal of the overlayer and Si, as indicated. The sensitivity factors (SF_x) of the overlayer or substrate atoms used by the ESCA 2000 software package employed in this analysis were 0.90, 1.00, 2.49, 1.70, and 2.40 for the Si 2p, C 1s, O 1s, Cl 2s, and Cl 2p peaks, respectively. The solid-state volumetric densities (ρ_{ov}) of C, O, and Cl (3, 0.92, and 2.0 g cm^{-3}, respectively)[18,19] were used to calculate the atomic diameter of the overlayer species (0.19, 0.30, 0.30 nm for C, O, and Cl, respectively) through the equation

$$a_{ov} = \left(\frac{A_{ov}}{\rho_{ov} N_A}\right)^{1/3} \tag{3.4}$$

where A_{ov} is the atomic weight of the overlayer species and N_A is Avogadro's number. The volumetric density of Si is ρ_{Si} = 2.328 g cm^{-3}.[20] The integrated areas under the overlayer and substrate peaks, I_{ov} and I_{Si}, respectively, were determined by the ESCA 2000 software package.

3.2.2.2 SXPS Measurements

High-resolution SXPS experiments were performed on beamline U4A at the National Synchrotron Light Source (NSLS) at Brookhaven National Laboratory.[3] The sample was introduced through a quick-entry load lock into a two-state UHV system that was maintained at pressures of $\leq$1 x 10^{-9} Torr. The beamline had a spherical grating monochrometer that selected photon energies of 10–200 eV with a resolution of 0.1 eV. The selected excitation energy was not calibrated independently because this study was principally concerned with shifts in the Si 2p binding energy in reference to the bulk Si 2p peak, as opposed to the determination of absolute binding energies. Samples were illuminated at an incident en-

ergy of 140 eV, and the emitted photoelectrons were collected normal to the sample surface by a VSW 100-mm hemispherical analyzer that was fixed at 45° off the axis of the photon source. The beam intensity from the synchrotron ring was measured independently, and the data in each scan were normalized to account for changes in photon flux during the scan. No charging or beam-induced damage was observed on the samples during data collection. The limited range of excitation energies available at this beamline, although well-suited for high surface-resolution Si 2p core-level spectroscopy, prevented measurement of SXPS survey scans of the surface.

The escape depth of Si 2p photoelectrons was calculated using an empirical relation described by Seah.[21] The size of the Si atom, a_{Si}, was determined using Eq. 3.4 (A_{Si} = 28.086 g mol^{-1} and ρ_{Si} = 2.328 g cm^{-3})[20] yielding a_{Si} = 0.272 nm. The electron mean free path, λ_{Si}, was then calculated from the empirical relation[21]

$$\lambda_{Si} = (0.41\text{nm}^{-1/2}\text{eV}^{-1/2}) a_{Si}^{1.5} E_{Si}^{0.5} \tag{3.5}$$

where E_{Si} is the photoelectron kinetic energy (37 eV for Si 2p photoelectrons under our measurement conditions). Using this method, λ_{Si} of photoelectrons in the Si 2p peak was calculated to be 3.5 Å. Electron escape depths in Si measured under similar conditions have been reported to be 3.2–3.6 Å.[2,22] The penetration depth of the measurement can be calculated from $l_{Si} = \lambda_{Si} \sin\theta$, where θ is the collection angle off the surface. Data presented here were collected at θ = 90°, so l_{si} = 3.5 Å.

To identify features in the Si 2p region in addition to the Si 2p bulk peak, the background signal was determined using a Shirley fitting procedure[23–25] and subtracted from the original spectra. The background-subtracted spectra were then processed to deconvolute, or "strip," the Si $2p_{1/2}$ peak from the spin-orbit doublet.[1,2] To perform the spin-orbit stripping procedure, the energy difference between the Si $2p_{1/2}$ and Si $2p_{3/2}$ peaks was fixed at 0.6 eV and the Si $2p_{1/2}$ to Si $2p_{3/2}$ peak area ratio was fixed at 0.51.[1,2,17,18] The residual spectrum composed of Si $2p_{3/2}$ peaks was then fit to a series of Voigt line shapes[26] that were 5% Lorentzian and 95% Gaussian functions.[18,27] If more than one peak was needed to fit the spectrum, the full widths at half-maximum (fwhm) of all peaks were allowed to vary

by $\pm$25% from each other.[28] Occasionally, results from the peak fitting procedure for a given spectrum would differ greatly with small changes in the initial conditions of the peak fit. To avoid bias in selecting a representative fit, multiple fits of the same data set with different initial conditions were averaged, and the average peak center and area, along with the standard deviation, are reported. This standard deviation represents a confidence level of the curve fitting procedure, as opposed to an estimate of random errors over multiple experimental measurements on nominally identical surfaces. Standard deviations obtained through this process were neglected if they were below the sensitivity of the instrument (0.01 eV, 0.02 monolayers).

A simple overlayer-substrate model was employed to calculate monolayer surface coverage. This model was independent of instrumental sensitivity factors, although it assumed negligible differences in the photoionization cross sections of surface and bulk Si species.[1,18,27] In this method, the number density of modified surface Si atoms, $\Gamma_{Si,surf}$, was deduced from the ratio of the integrated area under the Si peak assigned to the surface atoms, $I_{Si,surf}$, to the integrated area of the Si peak assigned to bulk Si atoms, $I_{Si,bulk}$, with

$$\frac{I_{Si,surf}}{I_{Si,bulk}} = \frac{\Gamma_{Si,surf}}{n_{Si,bulk} l_{Si} - \Gamma_{Si,surf}} \tag{3.6}$$

In this expression, $n_{Si,bulk}$ is the number density of bulk crystalline Si atoms (5.0 x 10^{22} cm^{-3}),[20] and l_{Si} is 3.5 Å. Substituting $I = I_{Si,surf}/I_{Si,bulk}$ and $\Gamma_{Si,bulk} = n_{Si,bulk} l_{Si}$ into Eq. 3.6 and rearranging yields

$$\Gamma_{Si,surf} = \frac{I}{1+I} \Gamma_{Si,bulk} \tag{3.7}$$

Dividing the calculated value of $\Gamma_{Si,surf}$ by the number density of atop sites on the Si(111) surface, 7.8 x 10^{14} cm^{-2},[1] gives the monolayer coverage of modified Si atoms. The distance between the first and second Si layers along a vector perpendicular to the Si(111) crystal face is 1.6 Å,[9] implying that an electron escape depth of 3.5 Å will sample 2.2 monolayers of the Si crystal.

3.3 Results

3.3.1 H-Terminated Si(111) Surfaces

3.3.1.1 XPS Results

Survey scan XPS data from a freshly etched H-terminated Si(111) surface exhibited peaks only for the Si 2p (99.9 BeV) and Si 2s (151.1 BeV) orbitals (Figure 3.1(a)). Peaks observed at successive intervals of 17.5 BeV higher than the two principal peaks are characteristic of crystalline silicon samples and have been identified previously as plasmon loss features that arise for the Si 2s and 2p photoelectrons.[29,30] The lack of C and O signals indicated that these elements were not present above the detection limit of the instrument, which was $\sim$0.3 monolayer for C and 0.2 monolayer for O.

3.3.1.2 SXPS Results

Figure 3.2(a) shows the high-resolution SXPS data of the Si 2p region of a freshly prepared H-terminated Si(111) sample. As expected, a spin-orbit doublet was observed for bulk Si. As seen in the inset of Figure 3.2(a), no silicon oxide signals were detected in the binding energy region up to 5 eV above the bulk peak, even under these surface-sensitive conditions.

Figure 3.2(b) shows the SXPS data remaining after background subtraction and stripping of the Si $2p_{1/2}$ component of the Si spin-orbit doublet signal. The stripped data were fit to a series of three Voigt functions: the bulk Si $2p_{3/2}$ peak, a peak shifted higher in core binding energy by 0.15 eV, and a small foot shifted 0.55 eV higher in binding energy. The 0.15 eV shift is consistent with expectations for surface Si atoms bonded to H, which display photoelectrons 0.114–0.250 eV higher in binding energy than those of bulk Si.[6–8] The magnitude and direction of this shift is consistent with expectations because H (of Pauling electronegativity χ_P = 2.20) is somewhat more electronegative than Si (χ_P = 1.90).[31] The small peak shifted 0.55 eV higher than the bulk Si $2p_{3/2}$ is possibly due to surface bound -OH groups that might have formed during the short time the sample was exposed to water vapor in air ($<$5 min) when it was placed into the vacuum system; however, no further

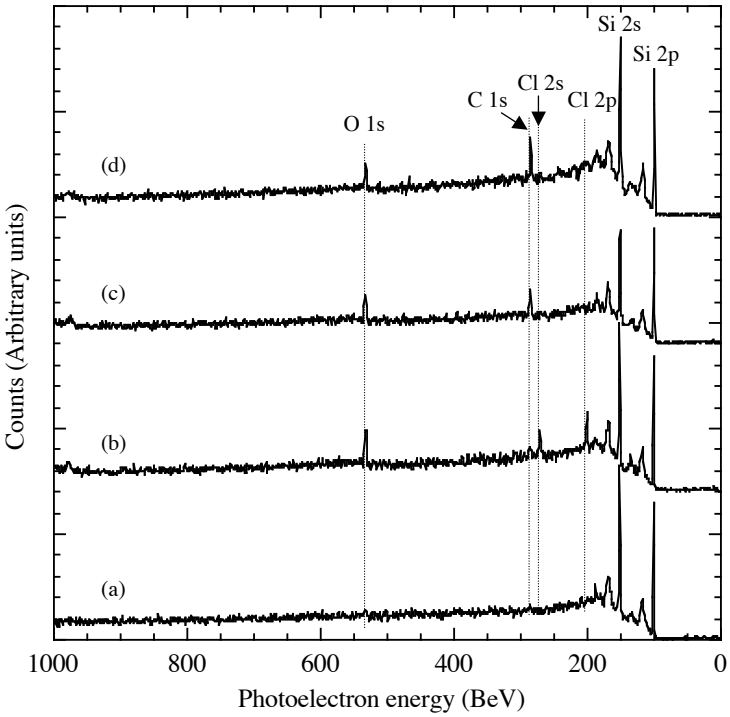

Figure 3.1: Survey XPS of functionalized Si(111) surfaces prepared through a two-step chlorination/alkylation method: (a) H-Si(111), (b) Cl-Si(111), (c) CH_3-Si(111), (d) C_2H_5-Si(111). Peak positions are given in the text.

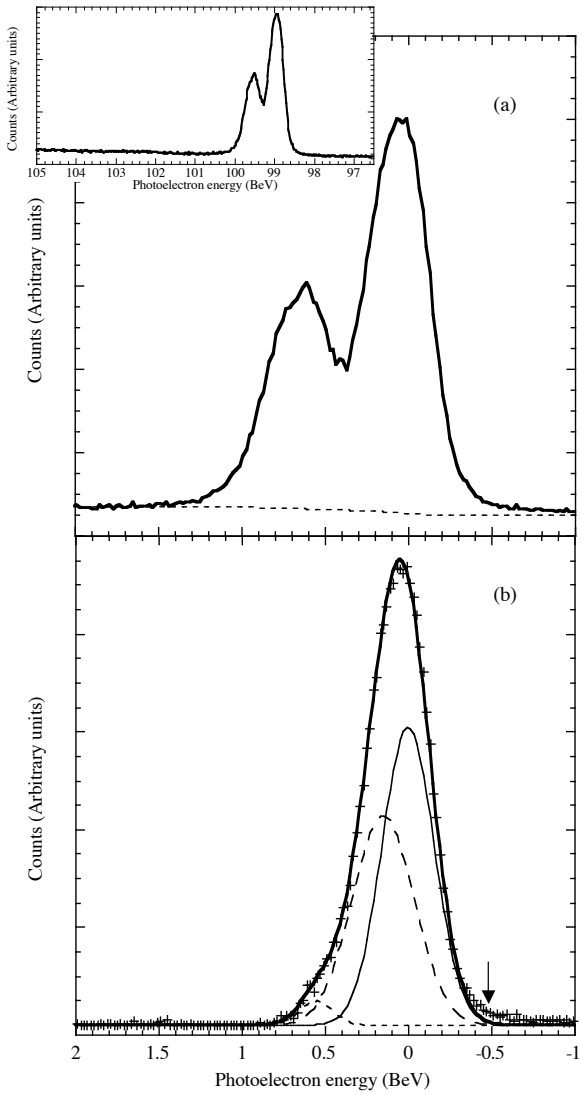

Figure 3.2: (a) SXPS results for the Si 2p region of a freshly prepared H-Si(111) surface and calculated background displayed relative to the binding energy (BeV) of the bulk Si $2p_{3/2}$ signal. The inset shows the entire energy region that was examined, displayed as a function of the absolute binding energy measured before any data processing. (b) Background-subtracted Si $2p_{3/2}$ region curve-fit as described in the text. Crosses, raw data; thin solid line, center at 98.89 BeV; long dashes, center at 99.04 BeV; short dashes, center at 99.44 BeV; thick solid line, calculated curve fit. The arrow identifies a feature discussed in the text.

experiments were conducted to determine the identity of this peak.

The low-binding-energy tail of the Si $2p_{3/2}$ region shown in Figure 3.2(b) displayed a small signal that was not explained by the peak-fitting procedure. This feature, identified by an arrow in Figure 3.2(b), appeared consistently in the Si $2p_{3/2}$ spectra of all of the functionalized surfaces reported here and has been observed occasionally in the literature on chemically modified Si surfaces.[4,8,15,32] Limited efforts have been undertaken to investigate the source of this signal on an unreconstructed Si surface, and there have been suggestions that this peak results from Si defects.[8] The small size of this feature did not interfere with the surface chemical analysis that was the focus of our investigations and will not be discussed further.

Table 3.1 summarizes the peak positions and surface coverages deduced from the fitting of the high-resolution SXP spectra. The absolute energies of the bulk Si $2p_{3/2}$ peaks observed for these surfaces are reported in Table 3.1, but because neither the excitation energy nor the work function of the instrument was measured during the experiment, the absolute energy observed has little meaning and will not be discussed further. On the H-Si(111) surface the +0.15 BeV peak was found to represent 1.02 monolayer (ML) of coverage (Eq. 3.7). The peak shifted by a binding energy of +0.55 eV had a coverage of 0.11 ML, again calculated using Eq. 3.7.

3.3.2 Cl-Terminated Si(111) Surfaces

3.3.2.1 XPS Results

As shown in Figure 3.1(b), a survey XPS scan of the Cl-terminated surface exhibited the expected bulk Si 2s and 2p peaks; a O 1s peak at 531.2 BeV; and Cl 2p and 2s peaks at 199.5 and 270.3 BeV, respectively. Use of Eq. 3.3 produced a value of 0.73 $\pm$ 0.13 or 0.59 $\pm$ 0.08 ML for the Cl surface coverage depending on whether the Cl 2s or Cl 2p peak was used. The same method produced a value of 1.4 $\pm$ 0.6 ML for the coverage of O. If this oxygen were present as silicon oxide, the Si 2p oxide peaks at 101–105 BeV in the high-resolution photoelectron spectrum should contain approximately 50% of the total Si 2p intensity, because the instrumental configuration used in this work probed only 2.2

Surface	Bulk peak[a] binding energy (eV)	peak 2 shift (eV)	peak 3 shift (eV)	Equivalent Monlayer Coverage–Eq. 3.7 peak 2 (ML)	peak 3 (ML)	Total ML
H-Si(111)	98.89	0.15	0.55	1.02	0.11	1.13
Cl-Si(111)[b]	98.67±0.04	0.83[c]	1.37[c]	0.99±0.04	0.16[c]	1.14±0.04
CH_3-Si(111)[d]	98.17±0.02	0.34±0.01	–	0.85±0.03	–	0.85±0.03
C_2H_5-Si(111)[d]	98.20±0.01	0.19[c]	0.61±0.01	1.02±0.12	0.19±0.01	1.21±0.13
$C_6H_5CH_2$-Si(111)[d]	98.23±0.02	0.15±0.02	0.57±0.02	1.10±0.25	0.39±0.08	1.49±0.33

Table 3.1: SXPS energies and monolayer coverages of Si $2p_{3/2}$ peaks on functionalized Si surfaces. [a]Absolute energies for the bulk Si $2p_{3/2}$ peak are reported for completeness, but are of limited use because the excitation energy was not calibrated. [b]Error reported is one standard deviation from multiple, identically prepared, surfaces. [c]Variability in peak fitting results was below the detection limit of the instrument and was not considered meaningful. [d]The reported standard deviation is from multiple fits of the spin-orbit-stripped spectra from the same surface and represents a confidence level in the curve fitting procedure.

monolayers of the sample. SXPS data of the Si 2p region of the Cl-terminated surface (shown below), however, clearly indicated a lack of observable SiO_2, consistent with the hypothesis that the O 1s signal observed on these surfaces was due to absorbed adventitious oxygen as opposed to silicon oxide.

3.3.2.2 SXPS Results

The SXPS peaks in the Si 2p region of the Cl-Si(111) surface, shown in Figure 3.3(a) were very different from those of the H-terminated Si surface. After the background had been removed and the spectrum stripped of the Si $2p_{1/2}$ peak, a second Si $2p_{3/2}$ signal was observed at a binding energy +0.83 eV relative to the bulk Si $2p_{3/2}$ peak (Figure 3.3(b)). This second peak was assigned to Si bound to Cl (χ_P = 3.16).[31] Chlorine-terminated Si(111) surfaces prepared using UHV techniques have been reported previously to display Si 2p binding energy XPS shifts of 0.7–0.9 eV,[9–14] in good agreement with our observations. The signal at +0.83 BeV from the bulk Si $2p_{3/2}$ peak represented an equivalent coverage of 0.99 ML. A third peak, located at a binding energy 1.37 eV higher than the Si $2p_{3/2}$ peak, was much smaller in amplitude, comprising 0.16 of a monolayer. This binding energy shift is consistent with expectations for a Si atom bonded to two Cl atoms, which should exhibit a chemical shift approximately twice that of a Si monochloride species.

3.3.3 Alkyl-Terminated Si(111) Surfaces

3.3.3.1 XPS Results

Figure 3.1(c) displays a survey XP spectrum of the CH_3-terminated Si(111) surface. The absence of Cl 2p and 2s peaks clearly indicated that Cl was eliminated after exposure to the methylmagnesium halide reagent, while a C 1s signal appeared at 284.7 BeV. A O 1s signal, ascribed to adventitious oxygen, was also visible on the functionalized surface at 531 BeV, representing 1.27 $\pm$ 0.01 ML of surface monolayer coverage. As discussed above for the Cl-terminated surface, inspection of the core-level spectrum in the CH_3-terminated surface (shown below) demonstrates that this O signal could not be ascribed to oxidized silicon species.

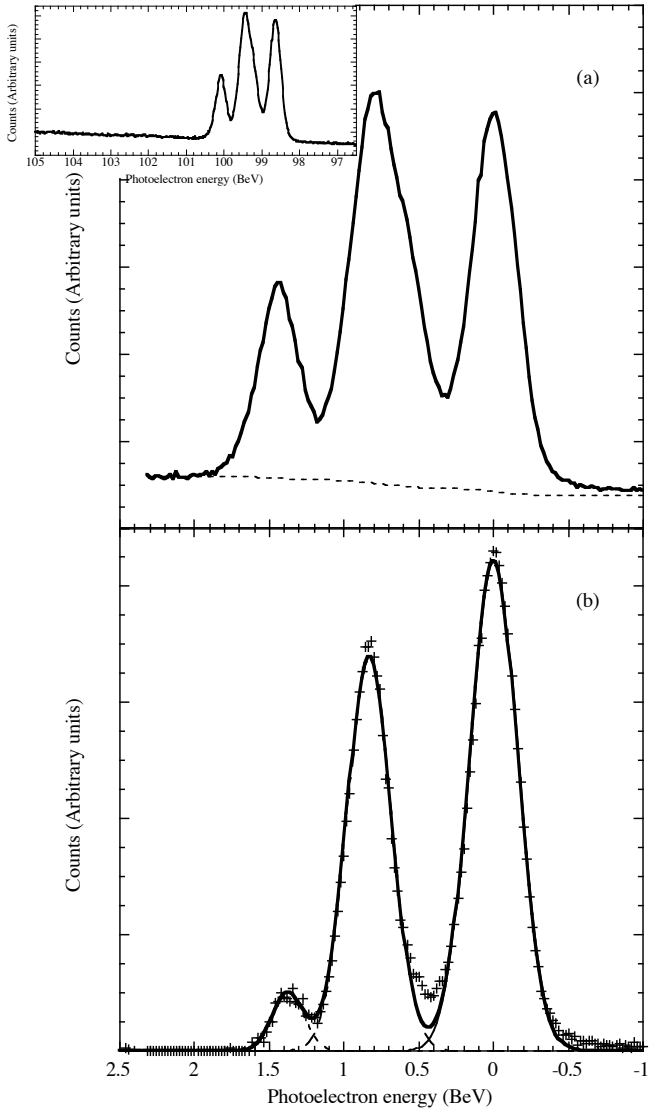

Figure 3.3: (a) SXPS results for the Si 2p region of a freshly prepared Cl-Si(111) surface and calculated background displayed relative to the binding energy (BeV) of the bulk Si $2p_{3/2}$ signal. The inset shows the entire energy region that was examined, displayed as a function of the absolute binding energy measured before any data processing. (b) Background-subtracted Si $2p_{3/2}$ region curve-fit as described in the text. Crosses, raw data; thin solid line, center at 98.64 BeV; long dashes, center at 99.47 BeV; short dashes, center at 100.01 BeV; thick solid line, calculated curve fit.

To determine the effect of alkylating the surface with groups that were sterically prevented from bonding to every Si atop site, the Si(111) surface was functionalized with a variety of straight-chain alkyls. The XPS survey scan of the C_2H_5-Si(111) surface (Figure 3.1(d)) resembled that of the CH_3-terminated Si(111) surface. This behavior was expected because the presence of adventitious hydrocarbon on the surface is known to complicate XPS analysis of terminating groups of similar C chain lengths.[17] The O 1s signal at 531 BeV (0.7 ± 0.2 ML) was ascribed to adventitious sources and not silicon oxides.

3.3.3.2 SXPS Results

Figure 3.4 shows the high-resolution SXPS data of the Si 2p region for a CH_3-terminated Si(111) sample. A Si $2p_{3/2}$ peak was observed 0.34 eV higher in binding energy than the bulk Si peak, consistent with expectations for a surface Si atom bonded to the more electronegative C (χ_P = 2.55)[31] in the terminating methyl group. This second peak represented a coverage of 0.85 ML (Table 3.1). As seen in the inset of Figure 3.4, no signals were detected at binding energies greater than 1.0 eV relative to the bulk Si $2p_{3/2}$ peak, indicating the absence of detectable oxidized silicon.

To investigate the effects of functionalization using longer alkylating agents containing methylene groups, C_2H_5-Si(111) surfaces were prepared and analyzed by SXPS. High-resolution SXPS data from the Si $2p_{3/2}$ peak on the freshly prepared C_2H_5-Si(111) surface, shown in Figure 3.5(a), exhibited a Si $2p_{3/2}$ peak 0.19 eV higher in binding energy than the bulk Si $2p_{3/2}$ peak. This shifted Si peak represented 1.02 ML of surface coverage. Similar to what was observed on the H-terminated surface, a third peak was present at 0.61 eV higher in energy than the bulk Si $2p_{3/2}$ peak, in this case with a relative area corresponding to 0.19 of a monolayer. This peak possibly indicates a small oxygen-containing layer that could not be eliminated as the sample was introduced from air into the SXPS vacuum chamber. The total surface coverage of the two shifted peaks was 1.21 ML.

The peak +0.19 higher in energy than the bulk Si $2p_{3/2}$ signal was approximately halfway between the peak energies for Si–H and Si–C signals observed on the H- and CH_3-terminated surfaces, respectively. To determine whether this peak resulted from two independent surface Si moieties, it was fitted by two peaks having the same energy shifts,

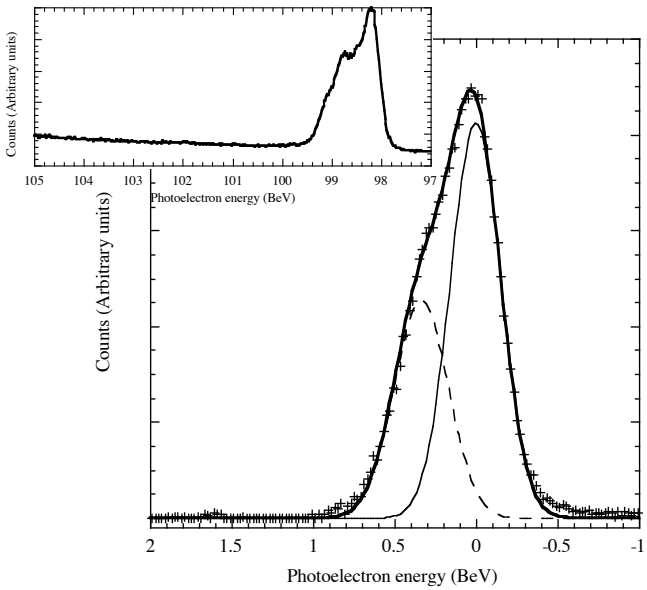

Figure 3.4: SXPS results for the Si $2p_{3/2}$ region of a freshly prepared CH_3-Si(111) surface after background subtraction and spin-orbit striping and displayed relative to the binding energy of the bulk Si $2p_{3/2}$ signal. Crosses, raw data; thin sold line, center at 98.17 BeV; long dashes, center at 98.51 BeV; thick solid line, calculated curve fit. The inset shows the entire energy region that was examined, displayed as a function of the absolute binding energy measured before any data processing.

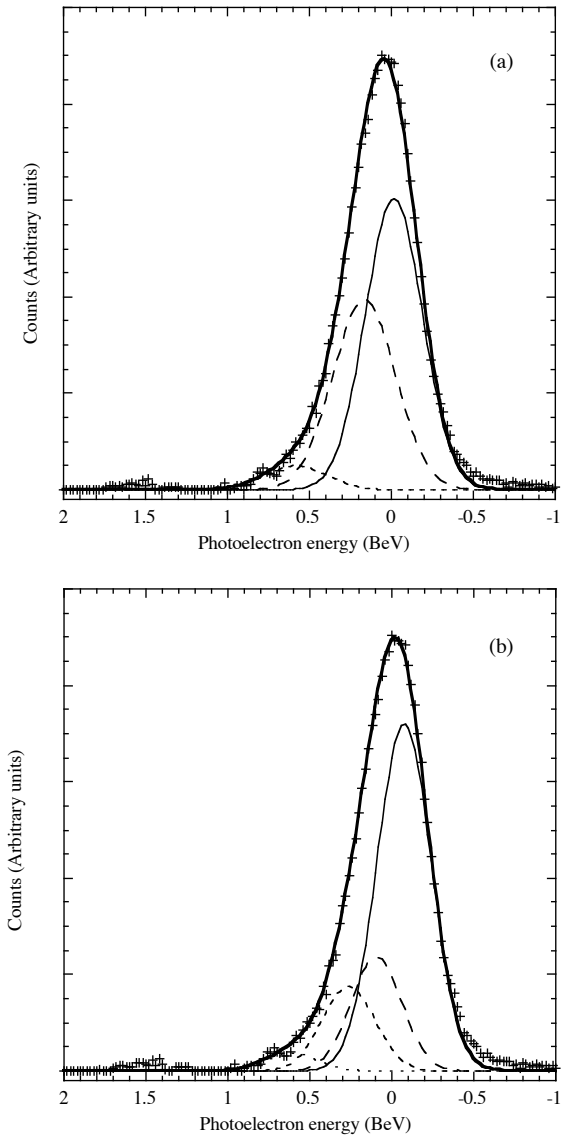

Figure 3.5: (a) SXPS results for the Si $2p_{3/2}$ region of a freshly prepared C_2H_5-Si(111) surface after background subtraction and spin-orbit stripping and displayed relative to the binding energy of the bulk Si $2p_{3/2}$ signal. Crosses, raw data; thin solid line, center at 98.20 eV; long dashes, center at 98.39 eV; short dashes, center at 98.80 eV; thick solid line, calculated curve fit. (b) Same sample with the surface feature deconvoluted into two peaks representing Si–H (+0.18 eV) and Si–C (+0.34 eV).

shapes, and widths as those found on the H- and CH_3-Si surfaces. Although the fitting parameters were very constrained, there is a possibility that this procedure will result in overfitting of these spectral data. As shown in Figure 3.5(b). this procedure produced a best fit with the two peaks at +0.18 and +0.34 eV representing coverages of 0.53 and 0.43 ML, respectively. A third peak, at +0.69 eV representing a coverage of 0.11 ML, was also present in the fit.

To investigate the effects of functionalization using bulkier alkylating agents, $C_6H_5CH_2$-terminated Si(111) was prepared and studied by SXPS (Figure 3.6). As shown in Table 3.1, a Si $2p_{3/2}$ peak was observed at +0.15 eV from the bulk peak with a coverage of 1.10 ML. A smaller peak 0.57 eV higher in binding energy than the bulk Si peak was also detected and was found to represent a coverage of approximately 0.39 ML. The coverage calculations are dependent on the calculated value of the electron escape depth, so a 0.2 Å increase in the calculated escape depth (to 3.7 Å) would produce a decrease in the calculated coverage of the two combined peaks to 1.2 ML.

3.3.4 High-Resolution SXPS of CH_3-Terminated Si(111) Surfaces Collected at Varying Excitation Energies

Methyl-terminated Si(111) surfaces were prepared at the California Institute of Technology and shipped to Berlin for further high-resolution synchrotron-based SXPS analysis. This data was collected by Dr. Ralf Hunger of the Institute of Materials Science at the Technische Universität Darmstadt in Darmstadt, Germany, and is described extensively in Hunger, *et al.*[33] Because this work provided important evidence for both the chemical and electronic structure of the CH_3-terminated surface, important observations are summarized here.

Once the methyl-terminated Si(111) surfaces were placed under UHV, they were annealed by heating to 500°C for 15 min, which did not alter substantially Si or C spectroscopic features. Samples were illuminated with excitation energies between 115–650 eV on beamline U49/2-PGM2 at the BESSY II synchrotron facility in Berlin, and analyzed with a Phoibos model 150 electron analyzer (SPECS).[34] Because this beamline had a

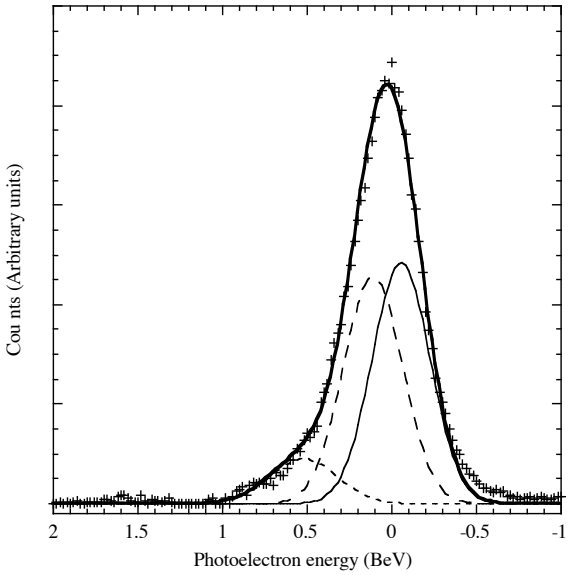

Figure 3.6: SXPS results for the Si $2p_{3/2}$ region of a freshly prepared $C_6H_5CH_2$-Si(111) surface after background subtraction and spin-orbit stripping and displayed relative to the binding energy of the Si $2p_{3/2}$ signal. Crosses, raw data; thin solid line, center at 98.22 BeV; long dashes, center at 98.39 BeV; short dashes, center at 98.80 BeV; thick solid line, calculated curve fit.

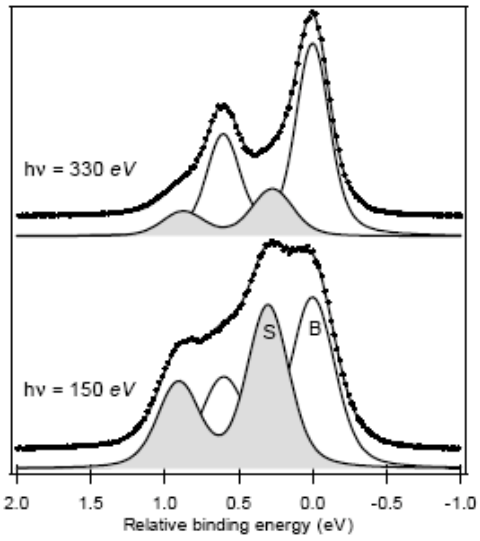

Figure 3.7: SXPS of the Si 2p region of the CH_3-teriminated Si(111) surface collected at different excitation energies. Spectra are displayed after background subtraction and before spin-orbit striping as a function of relative binding energy (eV) above the center of the Si $2p_{3/2}$ signal. Top: $h\nu$ = 330 eV; bottom: $h\nu$ = 150 eV. Closed circles are raw data and the solid lines are the calculated curve fits. The surface (S) and bulk (B) peaks were fit as described in the text. From Hunger, *et al*.[33]

greater range of accessible excitation energies than the beamline at NSLS, photoelectrons from the CH_3-terminated surface were collected at a variety of different excitation energies, and therefore electron escape depths from the Si crystal lattice (λ_{Si} in Eq. 3.5). The results of this analysis are shown in Figure 3.7. At the lowest excitation energy, 150 eV, the spectrum was essentially identical to that shown in Figure 3.4. When the excitation energy was raised to 330 eV, and photoelectrons from deeper in the Si crystal lattice were collected, the Si peak previously assigned to surface Si atoms bound to the carbon atom of the methyl group diminished in relative intensity of the overall signal. This verifies that the Si 2p signal shifted to slightly higher binding energies is indeed due to the top most layer of Si atoms and can only be observed when experimental conditions are optimized for highly surface sensitive parameters. A Shirley background was fit and subtracted from the original spectrum, then the Si 2p spin-orbit doublet was fit to a Voigt function with a Lorentzian width of 0.055 eV. The energy difference between the Si $2p_{1/2}$ and Si $2p_{3/2}$ peak as fixed at 0.605 eV and the Si $2p_{1/2}$ to Si $2p_{3/2}$ peak area ratio was fixed at 0.52. This surface Si 2p peak, labeled S in Figure 3.7, was shifted 0.30 eV higher in binding energy from the bulk component (B) and represented a total relative signal intensity of 0.96 compared with the bulk component.

The high-resolution photoelectron spectrum of the C 1s peak at 285 BeV was also collected in these experiments through excitation of the surface with $h\nu$ = 300 eV. After subtraction of a Shirley-type background from the spectrum, the C 1s signal was fit to a series of Voigt functions where the Lorentzian width was held at 0.15 eV. The C 1s signal was composed of four peaks, labeled C^0–C^3 in Figure 3.8. They were assigned to C bound to the more electropositive Si atom, located at 284.27 eV (C^0), C contamination from adventitious sources, at 285.47 eV (C^3), and two smaller peaks at 284.65 and 285.03 eV (C^1 and C^2) identified as originating from C 1s atoms of the surface-bound methyl group in the first and second C–H stretching vibrationally excited states. The observation of these vibrational signals for the first time on Si(111)[33] demonstrates the exceptionally clean nature of the CH_3-Si(111) surface prepared by this alkylation method.

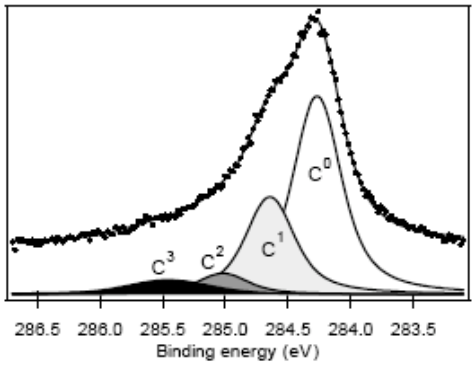

Figure 3.8: SXPS of the C 1s region on the CH_3-terminated Si(111) surface collected at $h\nu$ = 330 eV. Spectra are displayed after background subtraction as a function of absolute measured binding energy. Closed circles are raw data and solid lines are the calculated curve fits, obtained as described in the text. C^0: carbon from the methyl group bonded to Si; C^1 and C^2: C–H vibrational stretching features from the carbon from the methyl group bonded to Si; C^3: non-methyl adventitious carbon. From Hunger, *et al*.[33]

3.4 Discussion

Replacement of the H-terminated Si surface by a Si–Cl layer has been shown to yield a metastable intermediate surface that can be subsequently treated with an alkylmagnesium halide reagent, in an energetically favorable reaction, to drive the alkylation of Si to completion. The observed evolution of the high-resolution X-ray photoelectron spectra from the H- to Cl- to alkyl-terminated Si(111) surfaces clearly supported this formulation of the chemical transformations in the two-step chlorination/alkylation functionalization process. The H-terminated Si surface exhibited a distinct peak at +0.15 eV relative to the bulk Si $2p_{3/2}$ peak, in accord with expectations for surficial Si–H bonds exhibiting a positive chemical shift due to the slightly increased electronegativity of H compared to Si. The determination that this surface has 1 monolayer coverage of such Si–H bonds is in agreement with other spectroscopically derived assignments of the structure of the NH_4F-etched Si(111) surface.[35]

Treatment with PCl_5 eliminated the +0.15 eV Si $2p_{3/2}$ peak observed on H-terminated Si(111) and produced peaks characteristic of a monochlorinated Si surface. The measured quantity of surface Si–Cl groups was close to 1 ML, with peaks representing possible dichloro Si species accounting for $<$0.20 monolayer, and with essentially no peaks that could be attributed to trichloro Si species. Similar peak intensities and positions have been observed previously for H-terminated Si surfaces exposed to Cl_2(g) under rigorously oxygen-free conditions.[15] Although XPS survey scans of the Cl-terminated sample showed some amount of O 1s signal, no SiO_2 was detected between 101 and 105 BeV even under the highly surface sensitive conditions used in this investigation. The adventitious species could result from a number of sources, including absorbed solvent from the wet-chemical preparation techniques, adsorbed pump oil vapor introduced in the quick-entry load lock, or contaminating dust particles covered with oxygen-containing organic molecules that were not possible to avoid when working in standard laboratory conditions. The Si 2p region, which has specific and extensively studied spectroscopic shifts introduced by Si^{+}–Si^{4+} oxides[1,2] was examined instead to address this issue. The lack of peaks from oxidized silicon demonstrates that the functionalization reaction proceeded without measurable Si oxidation

under ambient pressure conditions in a N_2(g) atmosphere.

The SXPS data also indicated that alkylation of the chlorinated Si surface proceeded without detectable silicon oxide formation. The lack of Cl signals on the methylated Si surface is consistent with the formation of a nearly full monolayer of Si–CH_3 bonds. The peak +0.30 – 0.34 eV in binding energy relative to the bulk Si $2p_{3/2}$ peak is close to what has been observed previously for surficial Si atoms bonded to alkyl groups.[15,36,37] Previous SXPS studies of hydrocarbons introduced in UHV onto the Si(111)-(7 x 7) surface have reported a Si $2p_{3/2}$ peak shifted by $\sim$0.5 eV from the bulk Si $2p_{3/2}$ peak, in accord with an expected shift of 0.4–0.5 eV based on simple electronegativity considerations.[36,37] Methylated Si surfaces prepared by treatment of a chlorinated Si(111) surface with CH_3-Li have also been reported to display Si $2p_{3/2}$ SXPS peaks that are shifted by 0.27 eV from the bulk Si signal.[15] For the surfaces described here, the calculated coverage of the overlayer species was consistent with formation of nearly a full monolayer of Si–CH_3 groups, with only a very small amount of adventitious carbon sources seen in high-resolution scans of the C 1s region of the CH_3-Si(111) surface. Furthermore, although some amount of adventitious O was again observed, the absence of peaks shifted by $>$1 eV relative to bulk Si $2p_{3/2}$ indicated that no silicon oxide with higher oxidation states was formed on the methylated surface.

Silicon(111) surfaces were further functionalized with longer, bulkier hydrocarbons such as C_2H_5- and $C_6H_5CH_2$-. Interestingly, no Si–Cl signals were detected on such surfaces, even when the alkyl group was sterically precluded from bonding to every Si atop site on an unreconstructed Si(111)-(1 x 1) surface. Additionally, no oxide was detected on any alkylated surface. Contamination of the surface by Mg salts from the alkylmagnesium halide reagent was eliminated because no evidence for the Mg $K_1L_{23}L_{23}$ Auger peak at 307 eV was observed in the XPS survey spectra of any alkylated surface (Figure 3.1(c)–(d)).

Because no elements other than Si, C, and O were detected in wide XPS scans of surfaces alkylated by the chlorination/alkylation procedure and because a negligible amount of oxidized Si was present on such alkylated surfaces, the unalkylated surface Si atoms are either reconstructed or have been terminated with Si–H bonds, presumably resulting from the quenching of the alkylmagnesium halide reagent and work-up of the sample with CH_3OH.

The Si–C binding energy shift is no more than 0.2 eV greater than that of Si–H, making reliable decomposition of the two peaks difficult, even under these high-resolution conditions. However, fitting the single integrated peak at +0.19 eV above the Si $2p_{3/2}$ bulk peak to two peaks at known Si–C and Si–H binding energy shifts resulted in a deconvolution of the spectrum that was consistent with expectations for termination of a monolayer of Si atop atoms on such surfaces with either Si–C or Si–H bonds. Scanning probe microscopy studies or other independent spectroscopic signatures of such surfaces are required to assign the packing and fractional coverage of such systems by either Si–C or Si–H groups, and will be described in later chapters.

3.5 Conclusion

High-resolution SXPS studies of crystalline Si(111) surfaces functionalized through a two-step wet-chemical route, involving chlorination of H-Si(111) followed by alkylation with a variety of alkylmagnesium halide reagents, have shown that on the H- or Cl-terminated Si(111) surface, a component of the Si 2p signal is shifted to higher binding energies than the bulk Si 2p peak, indicating a bonding interaction between a surface Si atom and an overlayer species that is more electronegative than the Si in the crystal lattice beneath the surface. Functionalization with CH_3-, an alkyl group that can, in principle, bond to every atop site on the unreconstructed Si(111) surface, produced an SXPS signal in the Si $2p_{3/2}$ region that was shifted to slightly higher energies than the bulk Si $2p_{3/2}$ peak. The magnitude of this shift (+0.34 eV) is consistent with expectations for surface Si atoms bonded to the C atom of the methyl group. The intensity of this positively shifted signal corresponded to approximately 0.85 monolayer on the Si(111) surface. A similar, but lower-energy, peak was also observed on silicon surfaces that were functionalized with longer and bulkier functional groups that are sterically prohibited from forming bonds to every Si atop site on the Si(111) surface. The SXPS data indicate that such surfaces are partially alkyl-terminated and are either reconstructed or terminated with Si–H bonds at unalkylated sites. No evidence was found for Si–OR moieties or other oxidized Si species that could, in principle, contribute to the bonding of such surfaces. The detailed spectroscopic characterization of

such functionalized surfaces is a required step in understanding the interesting chemical and electronic characteristics of these alkylated Si systems.

Acknowledgment

This research was carried out in part at the National Synchrotron Light Source, Brookhaven National Laboratory, which is supported by the U.S. Department of Energy, Division of Materials Sciences and Division of Chemical Sciences, under Contract DE-AC02-98CH 10886.

Bibliography

[1] Himpsel, F. J.; McFeeley, F. R.; Taleb-Ibrahimi, A.; Yarmoff, J. A.; Hollinger, G. *Phys. Rev. B.* **1988,** *38*, 6084–6096.

[2] Himpsel, F. J.; Meyerson, B. S.; McFeeley, F. R.; Morar, J. F.; Taleb-Ibrahimi, A.; Yarmoff, J. A. Core Level Spectroscopy at Silicon Surfaces and Interfaces. In *Proceedings of the 1988 Enrico Fermi School on Photoemission and Absorption Spectroscopy of Solids and Interfaces with Synchrotron Radiation*; Varenna: North Holland, 1988.

[3] Keister, J. W.; Rowe, J. E.; Kolodziej, J. J.; Niimi, H.; Tao, H. S.; Madey, T. E.; Lucovsky, G. *J. Vac. Sci. Technol. A* **1999,** *17*, 1250–1257.

[4] Ohishi, K.; Hattori, T. *Jpn. J. Appl. Phys.* **1994,** *33*, L675–L678.

[5] Grunthaner, P. J.; Hecht, M. H.; Grunthaner, F. J.; Johnson, N. M. *J. Appl. Phys.* **1987,** *61*, 629– 638.

[6] Bjorkman, C. H.; Alay, J. L.; Nishimura, H.; Fukuda, M.; Yamazaki, T.; Hirose, M. *Appl. Phys. Lett.* **1995,** *67*, 2049–2051.

[7] Blase, X.; Dasilva, A. J. R.; Zhu, X. J.; Louie, S. G. *Phys. Rev. B* **1994,** *50*, 8102–8105.

[8] Karlsson, C. J.; Owman, F.; Landemark, E.; Chao, Y. C.; Martensson, P.; Uhrberg, R. I. G. *Phys. Rev. Lett.* **1994,** *72*, 4145–4148.

[9] Durbin, T. D.; Simpson, W. C.; Chakarian, V.; Shuh, D. K.; Varekamp, P. R.; Lo, C. W.; Yarmoff, J. A. *Surf. Sci.* **1994,** *316*, 257–266.

[10] Bogart, K. H. A.; Donnelly, V. M. *J. Appl. Phys.* **1999,** *86*, 1822–1833.

[11] Layadi, N.; Donnelly, V. M.; Lee, J. T. C. *J. Appl. Phys.* **1997,** *81*, 6738–6748.

[12] Cheng, C. C.; Guinn, K. V.; Donnelly, V. M.; Herman, I. P. *J. Vac. Sci. Technol. A-Vac. Surf. Films* **1994,** *12*, 2630–2640.

[13] Yarmoff, J. A.; Shuh, D. K.; Durbin, T. D.; Lo, C. W.; Lapianosmith, D. A.; McFeely, F. R.; Himpsel, F. J. *J. Vac. Sci. Technol. A-Vac. Surf. Films* **1992,** *10*, 2303–2307.

[14] Schnell, R. D.; Rieger, D.; Bogen, A.; Himpsel, F. J.; Wandelt, K.; Steinmann, W. *Phys. Rev. B* **1985,** *32*, 8057–8065.

[15] Terry, J.; Linford, M. R.; Wigren, C.; Cao, R. Y.; Pianetta, P.; Chidsey, C. E. D. *J. Appl. Phys.* **1999,** *85*, 213–221.

[16] Bansal, A.; Li, X. L.; Lauermann, I.; Lewis, N. S.; Yi, S. I.; Weinberg, W. H. *J. Am. Chem. Soc.* **1996,** *118*, 7225–7226.

[17] Bansal, A.; Li, X.; Yi, S. I.; Weinberg, W. H.; Lewis, N. S. *J. Phys. Chem. B* **2001,** *105*, 10266–10277.

[18] Haber, J. A.; Lewis, N. S. *J. Phys. Chem. B* **2002,** *106*, 3639–3656.

[19] Greenwood, N. N.; Earnshaw, A. *Chemistry of the Elements;* Reed Educational and Professional Publishing Ltd: Oxford, 2nd ed.; 1997.

[20] Sze, S. M. *The Physics of Semiconductor Devices;* Wiley: New York, 2nd ed.; 1981.

[21] Seah, M. P. Quantification of AES and XPS. In *Practical Surface Analysis,* Vol. 1, 2nd ed.; Briggs, D.; Seah, M. P., Eds.; John Wiley & Sons: Chichester, 1990.

[22] Pi, T. W.; Hong, I. H.; Cheng, C. P.; Wertheim, G. K. *J. Electron Spectrosc. Relat. Phenom.* **2000,** *107*, 163–176.

[23] Shirley, D. A. *Phys. Rev. B* **1972,** *5*, 4709–4714.

[24] Contini, G.; Turchini, S. *Comput. Phys. Commun.* **1996,** *94*, 49–52.

[25] Proctor, A.; Sherwood, P. M. A. *Anal. Chem.* **1982,** *54*, 13–19.

[26] Sherwood, P. M. A. Data Analysis in XPS and AES. In *Practical Surface Analysis*, Vol. 1; Briggs, D.; Seah, M. P., Eds.; John Wiley & Sons Ltd: New York, 1990.

[27] Webb, L. J.; Lewis, N. S. *J. Phys. Chem. B* **2003,** *107*, 5404–5412.

[28] Chakarian, V.; Shuh, D. K.; Yarmoff, J. A.; Hakansson, M. C.; Karlsson, U. O. *Surf. Sci.* **1993,** *296*, 383–392.

[29] Cheng, K. L.; Cheng, H. C.; Liu, C. C.; Lee, C.; Yew, T. R. *Japan. J. Appl. Phys.* **1995,** *34*, 5527–5532.

[30] Stinespring, C. D.; Wormhoudt, J. C. *J. Appl. Phys.* **1989,** *65*, 1733–1742.

[31] Allen, L. C. *J. Am. Chem. Soc.* **1989,** *111*, 9003–9014.

[32] Hricovini, K.; Gunther, R.; Thiry, P.; Talebibrahimi, A.; Indlekofer, G.; Bonnet, J. E.; Dumas, P.; Petroff, Y.; Blase, X.; Zhu, X. J.; Louie, S. G.; Chabal, Y. J.; Thiry, P. A. *Phys. Rev. Lett.* **1993,** *70*, 1992–1995.

[33] Hunger, R.; Fritsche, R.; Jaeckel, B.; Jaegermann, W.; Webb, L. J.; Lewis, N. S. *Phys. Rev. B.* **2004,** in press.

[34] Mayer, T.; Lebedev, M. V.; Hunger, R.; Jaegermann, W. *Appl. Surf. Sci.* **2005,** in press.

[35] Dumas, P.; Chabal, Y. J.; Higashi, G. S. *J. Electron Spectrosc. Relat. Phenom.* **1990,** *54*, 103–108.

[36] Simons, J. K.; Frigo, S. P.; Taylor, J. W.; Rosenberg, R. A. *Surf. Sci.* **1996,** *346*, 21–30.

[37] Rochet, F.; Jolly, F.; Bournel, F.; Dufour, G.; Sirotti, F.; Cantin, J. L. *Phys. Rev. B* **1998,** *58*, 11029–11042.

Chapter 4

Transmission Infrared Spectroscopy of Methyl- and Ethyl-Terminated Silicon(111) Surfaces

4.1 Introduction

Fourier transform infrared spectroscopy (FTIR) is a popular analytical technique for investigating the chemistry and structure of modified semiconductor surfaces.[1,2] On Si(111) surfaces, FTIR was important in characterizing the freshly etched H-terminated surface.[3,4] In these pioneering studies, polarized IR radiation was used to determine that the H-terminated Si(111) surface prepared through etching in NH_4F(aq) is ideally flat when a sharp Si–H stretch at 2083 cm^{-1} was observed by illumination with p-polarized light, thus indicating the Si–H bond is perpendicular to the surface. When s-polarized light was used, only a small Si–H stretch was observed and was attributed to the small number of Si surface atoms present along a terrace step edge or defect site on the otherwise flat surface.[4] Another application of FTIR to semiconductor surface chemistry has been monitoring the oxidiation of the H-terminated Si(111) surface through the growth of Si–O–Si bonds from the characteristic longitudinal optical (LO) and transverse optical (TO) Si–O–Si stretching motions found at 1252 and 1065 cm^{-1}, respectively.[5]

These IR studies have been possible by using attenuated total internal reflection (ATR) IR techniques, which maximize signal from the substrate surface atoms and therefore highlight vibrational modes from surface chemical bonds. In this experimental configuration,

the IR beam is focused on the beveled edge of a semiconductor crystal and then internally reflects off the surface/absorbate (or vacuum) interface a number of times before exiting through the other end of the crystal.[2,6] For a semiconductor crystal of only several centimeters in length on which both the front and back surfaces are polished and etched, the IR beam could internally reflect off the surface/absorbate interface dozens of times, resulting in a large boost in the signal of absorbed IR light. This amplification allows IR absorptions from surface features to be measured accurately with standard FTIR laboratory equipment.

Although ATR IR allows the measurement of vibrational features associated with surface chemical bonds with great success, there are several problems that limit its utility. The overall path length through the substrate crystal can be quite long. By the time the IR beam has emerged from the substrate, crystal lattice phonons absorb virtually all infrared light near their vibrational energy, and possible surface vibrational modes in that region are undetectable. In silicon, this prevents standard ATR IR measurements of surface vibrations below 1500 cm^{-1}.[5] By limiting the number of times the IR beam internally reflects off the surface/absorbate interface, the total path length through the Si crystal can be shortened, and this window can be extended to 900 cm^{-1}, although with a corresponding loss of signal from surface vibrational modes.[5,7,8]

To further the investigation of the alkylated Si(111) surfaces that are the subject of this report, FTIR techniques would be ideal for identifying and characterizing surface Si–C bonds unambiguously for the first time. This would be an important validation of the model of the surface/overlayer structure formed through the two-step chlorination/alkylation functionalization route that is proposed in Figure 1.4. Previous observations of the surface Si–C stretching vibration on modified (111) and (100) surfaces through high-resolution electron energy loss spectroscopy (HREELS) have tentatively placed the energy of the Si–C stretching motion at 650–700 cm^{-1},[9–15] well within the region accessible by standard IR detectors but hidden and not previously detected on a Si surface investigated through ATR IR because of the large signal of the crystal phonon vibrations.

In the past several years, Dr. Yves Chabal and his laboratory at Rutgers University have been developing the technique of transmission infrared spectroscopy (TIRS) for sur-

face analysis in which the IR beam is transmitted through a crystal substrate polished on both the front and back surfaces. The IR beam passes through the surface/absorbate interface only twice, as it enters and exits the crystal. The substantially lower signal of surface vibrational features relative to ATR IR must be made up for by the sensitivity of the detector used. Modern DTGS detectors are capable of fulfilling these high-sensitivity requirements.[16] Because the beam passes through the bulk of the substrate only once, the crystal lattice phonon vibrations do not completely absorb the beam in the region below 900 cm^{-1}. If these phonon vibrations are subtracted from the spectra accurately, surface features in that energy region can be observed. This was demonstrated by the Chabal laboratory on a Cl-terminated Si(111) surface prepared by heating the H-terminated Si(111) surface at 95°C in a 0.3% mixture of Cl_2(g)/N_2(g) for 30 min. The TIR spectra of this surface revealed two features at 584 and 527 cm^{-1}, which were later identified as the Si–Cl stretching and bending modes, respectively.[17,18] With this demonstrated sensitivity for low energy vibrational absorptions, it is now feasible to measure the surface Si–C bond of an alkylated surface directly.

In the present report, TIRS was collected on H-, Cl-, CH_3, and C_2H_5-terminated Si(111) surfaces. Emphasis was placed on observing features in the low wavenumber region of the IR spectrum, 400–1300 cm^{-1}, that has previously been inaccessible to ATR IR spectroscopic investigations of Si surface chemistry. The strength of vibrational modes corresponding to Si–H and Si–Cl stretching and bending motions was used to quantify the extent of the surface functionalization after each step of a chlorination/alkylation reaction. Evidence for a Si–C vibrational stretch between 600–800 cm^{-1} was sought on both methyl- and ethyl-terminated surfaces, as well as evidence for other surface-termination groups on sites on the ethyl-terminated surface that are not alkyl-terminated.

4.2 Experimental

4.2.1 Materials and Methods

Float-zone grown n-Si(111) from Silicon Valley Microelectronics (San Jose, CA) was used. This material was doped with P to a resistivity $>$30 Ω cm and polished on both sides to a thickness of $>$450 μm. Samples were cut to a size of approximately 2 cm by 4 cm. Functionalization of the surface with CH_3- and C_2H_5- was accomplished according to the procedures given in Chapter 2 with several modifications. First, the NH_4(aq) etching solution was degassed by bubbling with N_2(g) in a partly sealed container for at least 1 hr before the Si sample was immersed in the solution. This was done to ensure a flat surface free of etch pits. Second, no N_2(g) line was available in the N_2(g)-purged glove box in which functionalization was performed. At the end of the chlorination step the sample was thoroughly rinsed with tetrahydrofuran (THF) and CH_3OH, then THF again, which was allowed to evaporate off of the sample surface. After each functionalization step the sample was moved through ambient air into the sample compartment of the FTIR instrument. Care was taken to move the sample from the preparation chamber to the instrument as quickly as possible to prevent the growth of silicon oxides. After TIRS data were collected, the sample was again moved quickly through air back to the antechamber of the N_2(g)-purged glove box.

4.2.2 Instrumentation

All TIRS spectra were collected using a Nicolet Nexus 670 FTIR that contained a N_2(g)-purged sample chamber. Spectra were recorded using the Omnic software package between 400–4000 cm^{-1} at a resolution of 4 cm^{-1} in transmission mode with a room temperature DTGS detector. The instrument configuration is shown in Figure 4.1. For maximum signal, the incident IR beam illuminated the surface from an incident angle, θ, of 74° off surface normal, which is the Brewster angle for silicon. At the Brewster angle p-polarized light is transmitted through the wafer while s-polarized light is reflected, preventing the use of traditional polarization experiments to determine the orientation of surface motions.

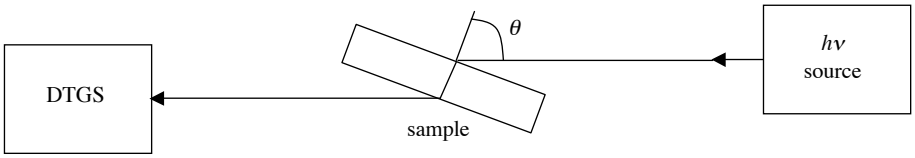

Figure 4.1: Configuration of TIRS experiments. For maximum signal to the detector, θ = 74°, while for polarization-type experiments, θ = 30°.

To circumvent this limitation, spectra were also recorded by illuminating with an incident beam angle of 30° off surface normal. As the incident beam moves closer to surface normal, the interaction with vibrational motions perpendicular to the surface becomes weaker, and the interaction with motions parallel to the surface begins to dominate the signal. By comparing spectra collected at 74° and 30° it was possible to determine which observed vibrational modes were perpendicular to the surface and which were parallel, thus providing the same information as a polarization-dependent measurement. This strategy is referred to as a "polarization-type" experiment.

After the sample was placed on the angle-controlled stage, the chamber was closed and purged with N_2(g) continuously. A spectrum was collected as the sum of 1000 consecutive scans. Five consecutive spectra were recorded in this manner, and in general the fifth spectrum was free of CO_2(g) and contained only small amounts of H_2O. This is the spectrum that is presented here. All data processing to determine peak centers and integrated areas were done without manipulation of the sample spectrum. For presentation purposes, the spectra shown here were occasionally processed to remove any residual H_2O signal and smooth the spectrum background with a linear function. The extent of any spectrum processing for cosmetic purposes is noted on each figure.

The single beam spectrum of each surface was dominated in the low wavenumber region by Si lattice phonon vibrations, and so each sample was referenced to the surface of its precursor to subtract out common components of the signal. The H-terminated Si(111) surface was referenced to the native oxide-covered surface, the Cl-terminated surface was referenced to the H-terminated surface, and the alkyl-terminated surface was referenced to the Cl-terminated surface. When these difference spectra are displayed in absorbance mode, peaks that are positive represent features that grew in during a surface reaction, while negative peaks are chemical features that disappeared during the reaction. Features common to both raw spectra such as Si–Si phonon peaks cancel and appear as flat regions. Extensive experience determined that if the sample was not placed into the sample holder carefully after sequential surface modification steps, the difference spectrum contained large contributions from Si–Si phonon bands in the low wavenumber region of the spectrum. No attempt was made to account for additional contributions to inconsistent

phonon absorption such as sample temperature.

4.3 Results

4.3.1 H-Terminated Si(111) Surfaces

TIR spectra of the H-terminated Si(111) surface were collected with an incident IR beam angle, θ, of 74° and 30° off surface normal. These spectra are shown in Figure 4.2. At an illumination angle of 74°, both the Si–H stretching (ν, 2083 cm^{-1}) and bending (δ, 627 cm^{-1}) motions were clearly visible.[4,19–21] Because the H-terminated surface was referenced against the SiO_2 surface from which it was made, the Si–O–Si motions LO and TO (1224 and 1058 cm^{-1}, respectively) were seen as negative peaks because they disappeared during sample etching in NH_4F(aq). Apart from a small absorption feature at 2400 cm^{-1} from atmospheric CO_2(g) contamination in the FTIR sample chamber, no other significant peaks were observed.

The Si–H stretching mode (2083 cm^{-1}) and the LO Si–O–Si mode (1224 cm^{-1}) decreased in intensity when the incident IR beam was moved from the Brewster angle to 30° off surface normal. The Si–H bending (627 cm^{-1}) and the TO Si–O–Si modes (1058 cm^{-1}) remained approximately as intense at both spectra collection angles. This effect is expected to distinguish between vibrational motions that are perpendicular to the surface, and thus do not interact strongly with an IR beam that is close to surface normal. This demonstrates that the Si–H stretching mode is indeed perpendicular to the surface, as predicted by the model of an atomically flat Si(111) surface terminated with hydrogen that has been observed in previous ATR IR experiments.[4]

4.3.2 Cl-Terminated Si(111) Surfaces

4.3.2.1 Experimental Results

The difference TIR spectra of Cl-terminated Si(111) at two different data collection angles are shown in Figure 4.3, with the low wavenumber region shown in greater detail in Figure 4.4. The Cl-terminated single beam spectrum was referenced to the H-terminated sample

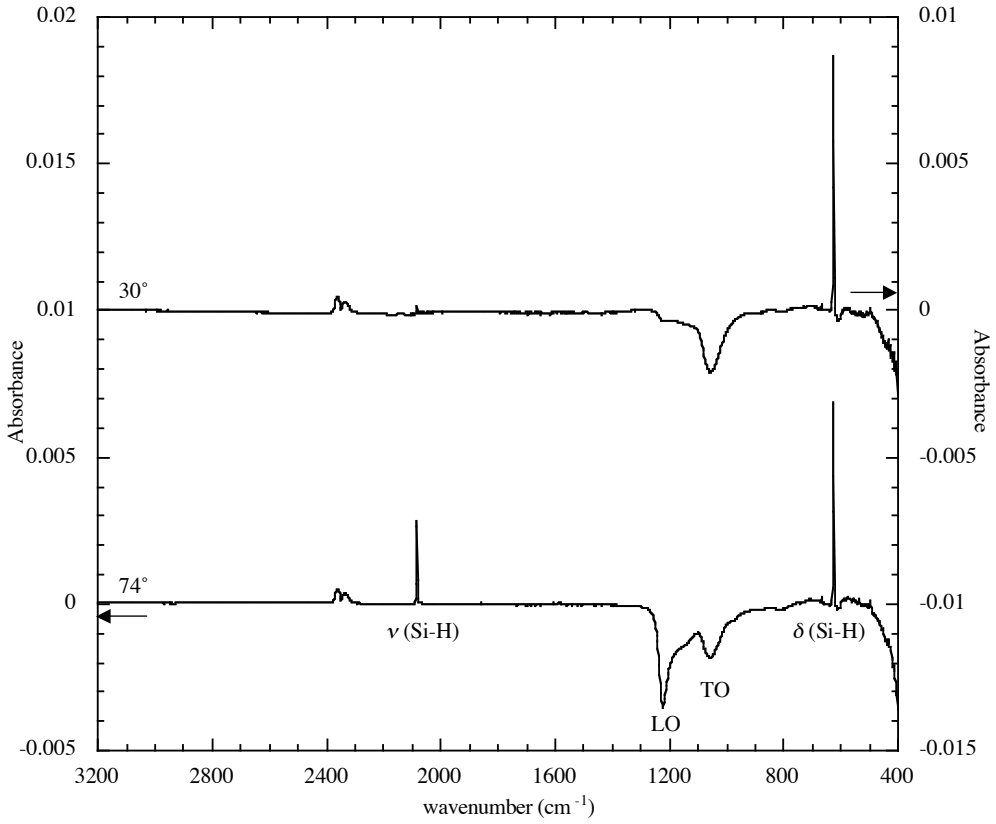

Figure 4.2: TIRS and proposed peak assignments of the H-terminated Si(111) surface collected at an incident beam angle of 74° (bottom) and 30° (top) off surface normal. The spectra are on the same scale of absorbance (absorbance units), although they are offset for easier viewing. Data are shown after subtraction of H_2O and flattening of the baseline.

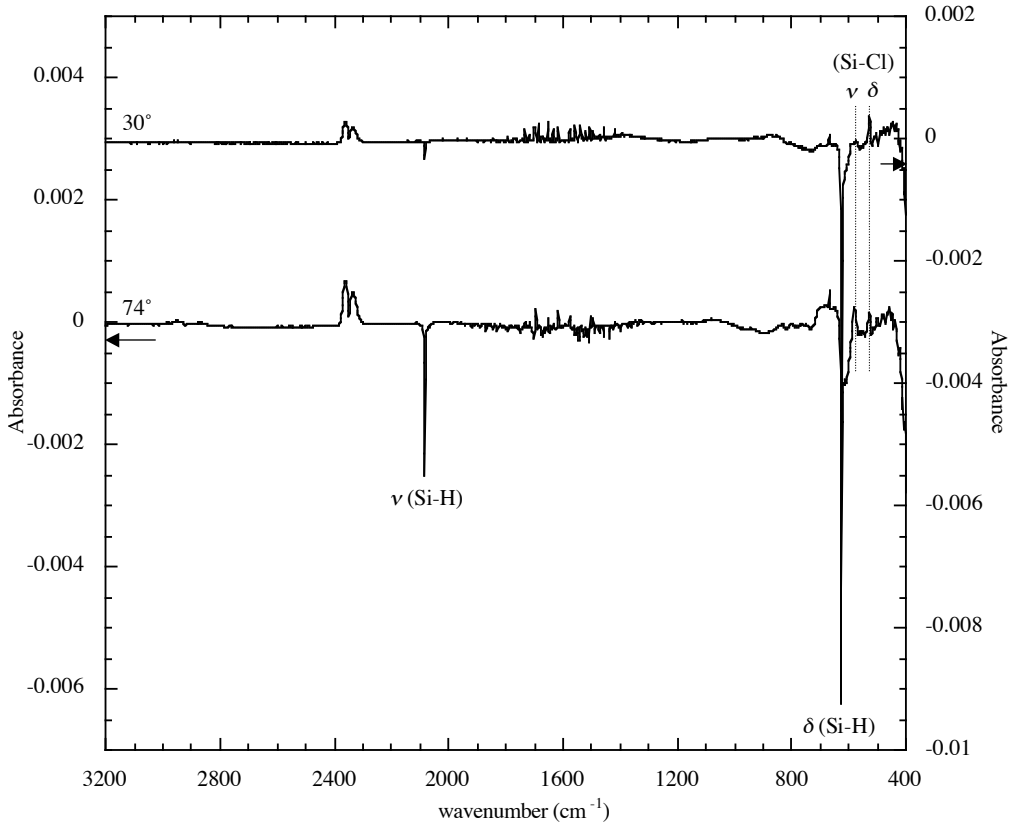

Figure 4.3: TIRS and proposed peak assignments of the Cl-terminated Si(111) surface collected at an incident beam angle of 74° (bottom) and 30° (top) off surface normal. The spectra are on the same scale of absorbance (absorbance units), although they are offset for easier viewing. Data are shown after subtraction of H_2O and flattening of the baseline.

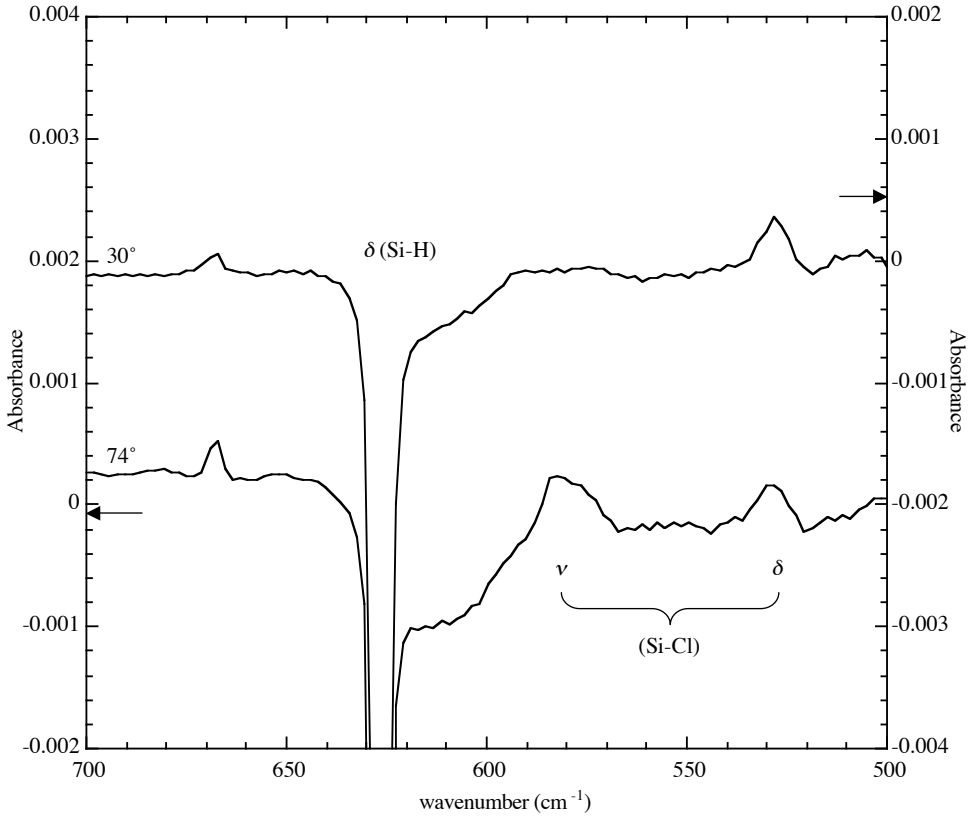

Figure 4.4: TIRS and proposed peak assignments of the Cl-terminated Si(111) surface collected at an incident beam angle of 74° and 30° off surface normal shown in the low wavenumber region. The spectra are on the same scale of absorbance (absorbance units), although they are offset for easier viewing. Data are shown after subtraction of H_2O and flattening of the baseline.

of that wafer, so that modes associated with the Cl-terminated surface appear as positive features, while modes present on the H-terminated surface appear as negative features in the spectra. As expected from previous spectra of the freshly etched surface, the Si–H stretching vibrational mode appeared greatly reduced when observed with an IR incident angle of 30° off surface normal compared to spectra collected at the Brewster angle, while the Si–H bending mode appeared equally strongly negative in both configurations. Two peaks appeared on the Cl-terminated surface, at 583 and 528 cm^{-1}, that were not observed on the H-terminated surface. Polarization-type studies revealed that the strength of the mode at 583 cm^{-1} was greatly reduced when probed at an incident IR angle of 30° rather than at the Brewster angle, indicating that it is a mode that is perpendicular to the surface. The mode at 528 cm^{-1} demonstrated similar absorptivity at either collection angle, indicating that it is a bending motion that is parallel to the surface. Previous HREELS[9,22] and FTIR[17,23–25] studies have identified the Si–Cl stretching motion between 500–625 cm^{-1}. Given the absence of any other chemical features of this surface, as seen by both survey scan and high-resolution X-ray photoelectron spectroscopy (Chapter 3), these two peaks are assigned to surface Si–Cl vibrational modes, although which particular motions they represent is not immediately clear, and will be discussed further in Section 4.3.2.2. As seen previously on the H-terminated surface, CO_2(g) in the sample compartment was observed in a peaks at 2400 cm^{-1} and 667 cm^{-1}, which can be seen in Figure 4.4.

The relative integrated area under each curve was used as a qualitative measurement of the extent of surface coverage. Without separate consideration of the relative oscillator strengths and cross-sections of each IR absorption feature this technique cannot be used to identify quantitatively the absolute monolayer coverage of each chemical species involved in a surface vibrational motion, but it is a useful tool for comparison between surfaces. Peak areas were estimated with the Omnic software package used to collect and analyze all TIRS data, and are given in Table 4.1. The ratio of the area under the observed stretching mode to bending mode is also given as a useful aid for quickly comparing vibrational features on different surfaces. On the freshly etched H-terminated surface examined at an incident IR beam angle of 74°, the area of the Si–H stretching mode at 2083 cm^{-1} was 1.48 x 10^{-2} $\pm$ 0.03 x 10^{-2}, while the area of the bending mode at 627 cm^{-1} was 3.31 x 10^{-2} $\pm$ 0.08

		TIRS peak area		
-R	θ	ν(Si–H)	δ(Si–H)	ν:δ(Si–H)[a]
-H	74°	(1.48±0.03)x10^{-2}	(3.31±0.08)x10^{-2}	0.45±0.02
	30°	(1.36±0.1)x10^{-3}	(4.2±0.2)x10^{-2}	0.033±0.002
-Cl	74°[b]	(-1.45±0.07)x10^{-2}	(-3.7±0.3)x10^{-2}	0.39±0.05
	30°[b]	(-1.35±0.03)x10^{-3}	(-4.4±0.6)x10^{-2}	0.031±0.005

Table 4.1: Integrated areas of TIRS peaks on H- and Cl-terminated Si(111) surfaces assigned to Si–H and Si–Cl modes. [a] Ratio of the integrated area of the stretching mode ν to the bending mode δ. [b] Negative areas identify features on the H-terminated surface that appear as negative peaks in the difference spectrum of the Cl-terminated surface.

x 10^{-2}. The ratio of the area under the observed stretching mode to the observed bending mode was 0.45 $\pm$ 0.02. When this surface was chlorinated, the area of the negative Si–H stretching peak in the difference spectrum attributed to hydrogen that had been removed from the surface was -1.45 x 10^{-2} $\pm$ 0.07 x 10^{-2}. The corresponding values for the Si–H bending motion at 627 cm^{-1} on this surface was -3.7 x 10^{-2} $\pm$ 0.3 x 10^{-2}. The overall ratio of the Si–H stretching to Si–H bending mode on the Cl-terminated Si(111) surface was 0.39 $\pm$ 0.05. Within the error of the experiment and the area determination technique, the relative amount of Si–H present on the freshly etched surface that then disappeared on the Cl-terminated surface was the same, supporting the hypothesis that hydrogen atoms on the freshly etched surface are quantitatively replaced by chlorine atoms when the surface is exposed to the PCl_5 solution. The integrated areas of both Si–H vibrational modes when scanned at an incident IR beam angle of 30°, given in Table 4.1, confirm this conclusion.

In a separate study, Dr. Sandrine Rivillon of the Chabal laboratory at Rutgers University compared three methods of Si(111) surface chlorination: exposing the H-Si(111) surface to PCl_5, to Cl_2(g) illuminated by UV light to form a Cl· radical, and to Cl_2(g) heated to 95°C to generate the Cl· radical. Comparing the two Si–Cl modes on these three surfaces led to the conclusion that there were no substantive chemical differences in these Cl-terminated surfaces prepared through different functionalization methods.[18]

4.3.2.2 Calculations of the Cl-Si(111) Surface

The quantitative disappearance of the Si–H stretching and bending modes on the chlorinated surface, as well as previous photoelectron spectroscopy evidence that indicates the Cl-terminated surface is free of other chemical groups (Chapter 3), strongly suggests that the vibrations at 583 and 528 cm^{-1} are associated with a single chlorine species having two normal modes. Variation of the incident angle of the infrared beam relative to the surface plane showed that the 583 cm^{-1} mode was polarized perpendicular to the surface while the 528 cm^{-1} mode was polarized parallel to the surface. This set of observations cannot, however, differentiate between monochloride or trichloride terminations of the silicon surface. Qualitatively, the monochlorinated surface would have a higher stretching frequency and a lower bending frequency, while the trichlorinated surface would have symmetric and

asymmetric frequencies with the appropriate polarizations. For the monochloride, the low frequency mode at 528 cm^{-1} would be associated with the Si–Cl bending vibration, while for the trichloride, this same feature could be associated with the asymmetric stretch of the $Si–Cl_3$ mode. A theoretical investigation of the structures formed from the interaction of chlorine with the Si(111) surface was performed by Prof. Krishnan Raghavachari and his student Matthew Halls at Indiana University. These calculations are described in Rivillon, *et al*.,[18] but will be repeated here for clarity.

Calculations on Cl-terminated silicon surfaces were done with an approach that mixed components of a periodic surface unit cell and a Si cluster model. This method was employed because the presence of a low frequency (528 cm^{-1}) mode suggested that examining the substrate silicon motion would be important for fully modeling the surface stretching motions. While a calculation based on periodic boundary conditions can be used to represent the uniform coverage properly, techniques for the computation of force constants and vibrational frequencies are better developed in cluster models. The approach used here combined these two methods to derive the geometry of the surface from a periodic unit cell calculation, and then used these geometric parameters in a medium-sized cluster model to derive the vibrational modes. Previously two-layer cluster models have been used to investigate the bond energy for Cl desorption as well as the Si–Cl stretching frequency for the Cl-passivated Si(111) surface.[26]

The geometric parameters for a monochlorinated surface were obtained from complete optimization of a periodic unit cell that contained four layers of silicon atoms. The surface silicon atoms were terminated with the bound chlorine atoms while the bottom layer silicon atoms were terminated with hydrogen. A B-LYP gradient corrected density functional[27,28] with the polarized 6-31G* basis set[29] was used in these calculations. The optimized Si–Cl distance was found to be 2.11 Å, slightly shorter than the corresponding distance of 2.14 Å found for a hydrogen-terminated Si_{10} cluster (adamantane-cage model for Si(111)) containing a single surface chlorine atom.

The geometric parameters obtained with the periodic unit cell were then used to generate truncated cluster models to analyze the vibrational modes of this system. A cluster model containing seven chlorine atoms was generated to represent the local environment

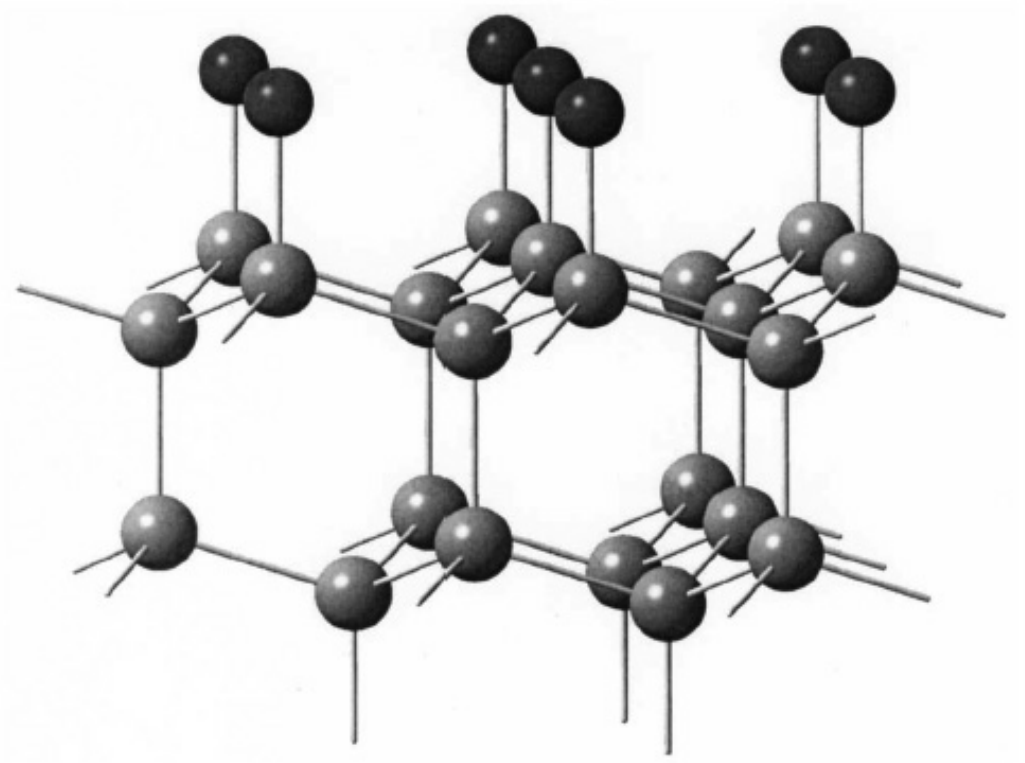

Figure 4.5: Silicon cluster model used in calculations of Si–Cl vibrational modes at the B-LYP/6-31G* theoretical level. Gray atoms are Si and black atoms are Cl. Figure from Rivillon, *et al.*[18]

and interactions of surface chlorine atoms. The central surface chlorine was surrounded by six other chlorines in a lattice-like structure, shown in Figure 4.5. This cluster, $Si_{22}H_{21}Cl_7$, was the smallest cluster that produced a qualitatively correct description of the collective vibrations (*vide infra*) in the system. It contained seven first-layer silicon atoms each attached to a chlorine atom, six second-layer Si atoms, six third-layer Si atoms, and three fourth-layer Si atoms. All of the remaining broken Si–Si backbonds were terminated with hydrogen atoms to remove any artifacts that might arise from the presence of nonphysical unpaired spins. The overall point group symmetry of the cluster model was C_{3v}.

The harmonic vibrational frequencies of the cluster model were calculated at the B-LYP/6-31G* theoretical model. The hydrogen atoms in the cluster were replaced with their isotropic analogs (D or T) in the vibrational analysis to prevent any nonphysical mixing of their vibrations with those of the Cl atoms. The lack of full periodicity in the cluster model, coupled with the presence of seven chlorine atoms, yielded many more vibrational modes than were seen experimentally. However, a careful investigation of the vibrational modes and their associated intensities indicated a clear emergence of collective vibrational modes even in such a small cluster model. For example, among the seven different Si–Cl stretching vibrations in our cluster model, a collective vibration, polarized perpendicular to the surface, occurred at 552 cm^{-1}. This vibration occurred at the highest frequency and had an intensity more than twice that of all the other six modes combined, clearly indicating that this vibration was emerging as the allowed surface stretching mode. In a similar manner, a mode parallel to the surface was calculated at 494 cm^{-1} belonging to the degenerate "*e*" representation of the C_{3v} point group. This mode emerged as a bending vibration with a strong intensity, but was dominated by the motion of the surface silicon atoms parallel to the surface and had only a small component associated with the surface-bound chlorine atoms. The calculations suggest that this behavior is caused by the lighter mass of silicon as compared to chlorine. The parallel motion of surface silicon atoms in their relatively stiff potential shifts the absorption frequency of this "bending" mode to a value fairly close to that of the corresponding stretching mode. Although this bending mode is submerged in the lattice phonons, it has a strong computed intensity and is clearly associated with the surface. A low-intensity bending mode associated mostly with chlorine atom motion was

also evident. This mode occurred at a much lower frequency ($\sim$100 cm^{-1}), which was beyond the range for which experimental data could be collected.

The emergence of two strong surface modes, a perpendicular mode at 552 cm^{-1} and a parallel mode at 494 cm^{-1}, is in excellent agreement with the experimental observations in the present work. This supports the assignment of the mode at 583 cm^{-1} to a Si–Cl stretching motion and the mode at 528 cm^{-1} to a bending motion. The calculated value of 552 cm^{-1} for the Si–Cl stretching mode is in good agreement with previous results (538 cm^{-1})[26] at the B3-LYP/6-31G* level using a two-layer cluster model. The slightly low values of the computed frequencies compared to the experimental values could have been due to the use of the B-LYP density functional or to the relatively small size of the clusters used to describe such collective vibrations.

Similar models were attempted in the periodic unit cell calculations for surface $SiCl_3$ groups, but this surface configuration produced very large steric repulsions. The van der Waals radius of chlorine is 1.8 Å,[30] indicating that optimal distance between the chlorine atoms should be $\geq$3.6 Å. Since the Si–Si distance on the Si(111) surface is only 3.8 Å,[31] even with best possible dihedral rotations, no reasonable configurations containing $SiCl_3$ groups on all surface silicon atoms could be generated. In an additional attempt to perform calculations on this surface, $SiCl_3$ groups were attached to the seven surface silicon atoms in the cluster shown in Figure 4.5. The resulting optimized structure (not shown) was highly distorted and was not a realistic surface configuration. The presence of a uniform trichlorinated Si(111) surface can therefore be ruled out based solely on steric considerations.

4.3.3 CH_3-Terminated Si(111) Surfaces

The Cl-terminated surface was functionalized with CH_3- groups using a methylmagnesium halide solution. After quenching the alkylating reagent, the resulting surface was again analyzed by TIRS. The spectra acquired from two different incident angles of the IR beam, 74° and 30° off normal, are shown in Figure 4.6. These spectra were referenced against the spectra of the Cl-terminated samples from which they were made, and so negative peaks

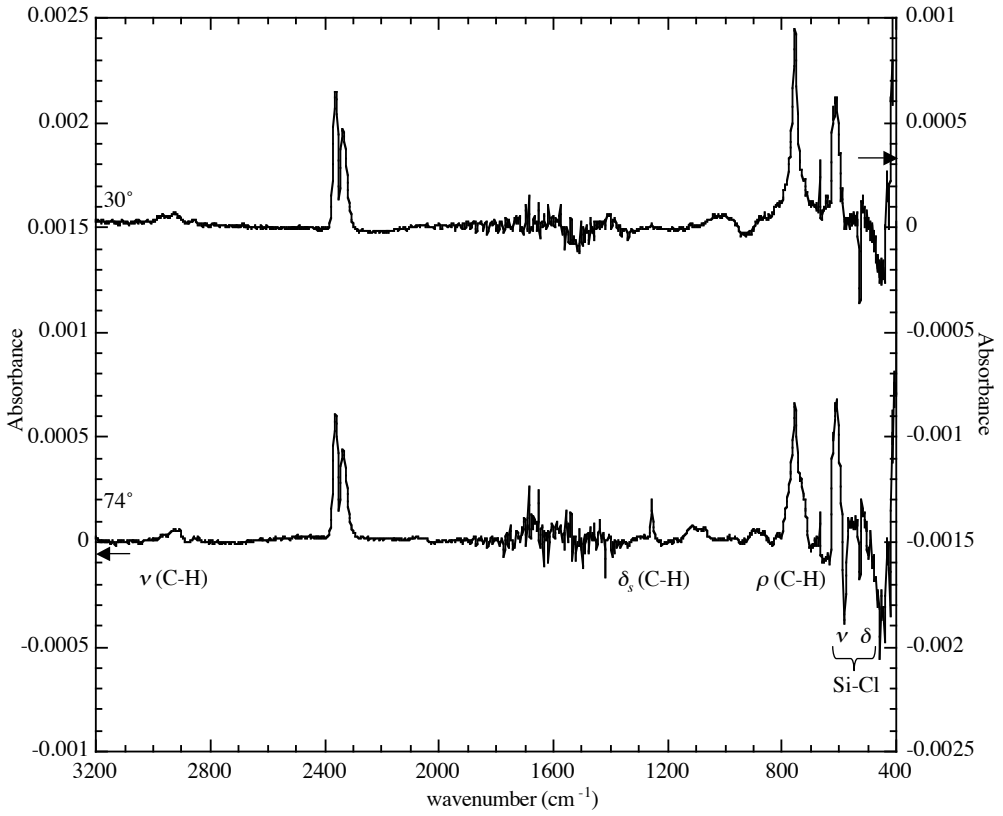

Figure 4.6: TIRS and proposed peak assignments of the CH_3-terminated Si(111) surface collected at an incident beam angle of 74° (bottom) and 30° (top) off surface normal. The spectra are on the same scale of absorbance (absorbance units), although they are offset for easier viewing. Data are shown after subtraction of H_2O and flattening of the baseline.

		TIRS peak area				
-R	θ	ν(Si–Cl)	δ(Si–Cl)	ν:δ(Si–Cl)[a]	δ_s(C–H)	ρ(C–H)
-Cl	74°	(1.0±0.2)x10^{-2}	(3.7±0.9)x10^{-3}	3±1	–	–
	30°	–	(3.8±0.6)x10^{-3}	–	–	–
-CH_3	74°	(-7±2)x10^{-3},[b]	(-2.3±0.01)x10^{-3}	3±1	(2.2±0.2)x10^{-3}	(1.8±0.2)x10^{-2}
	30°	–	(-2.8±1.6)x10^{-3}	–	–	(1.7±0.3)x10^{-2}
-C_2H_5	74°	(-5±1)x10^{-3}	(-3±1)x10^{-3}	1.9±0.6	–	–
	30°	–	(-3.6±0.5)x10^{-3}	–	–	–

Table 4.2: Integrated areas of TIRS peaks on Cl- and CH_2-terminated Si(111) surfaces assigned to Si–Cl and C–H modes. [a] Ratio of the integrated area of the stretching mode ν to the bending mode δ. [b] Negative areas identify features on the H-terminated surface that appear as negative peaks in the difference spectrum of the Cl-terminated surface.

in the absorption spectrum represent features of the Cl-terminated surface that disappeared during the alkylation reaction. On the Cl-terminated Si surfaces shown in Figures 4.3 and 4.4, the integrated areas of the Si–Cl stretching and bending modes at 583 and 528 cm^{-1}, respectively, when examined at an IR incident angle of 74°, were found to be 1.0 x 10^{-2} $\pm$ 0.2 x 10^{-2} and 3.7 x 10^{-3} $\pm$ 0.9 x 10^{-3}, respectively (Table 4.2). Similar areas were found for the corresponding negative Si–Cl features when the CH_3-terminated surface was examined under identical scan conditions, shown in Table 4.2. Measurement of the areas of the Si–Cl bending mode when observed at an IR incident angle of 30° gave similar results. This indicates that all Cl initially present on the surface is removed during the alkylation reaction, in agreement with previous XPS observations described in Chapter 3. On the CH_3-terminated Si surface, a small, broad peak centered at $\sim$2068 cm^{-1} was observed, possibly indicating that a small amount of surface Si–H contamination was present. Unfortunately, the region near the Si–H bending mode at 626 cm^{-1} was obscured by a large Si–Si phonon mode, so it was not possible to determine if the peak at 2068 cm^{-1} did indeed represent surface Si–H groups.

New distinct peaks of the C–H stretching modes appeared around 2900 cm^{-1} on the CH_3-terminated surface, shown in Figure 4.7. Vibrational absorption features at 2856, 2909, 2928, and 2965 cm^{-1} were measured on the surface when the spectra were collected at an incident IR beam angle of both 74° and 30°, although all observed features were reduced in intensity when the incident IR beam angle was moved to 30°. From a simple group theory argument, a CH_3- group should have two IR-active vibrational modes, an a_1 symmetric stretching mode and an e asymmetric stretching mode at slightly higher wavenumber.[32] Previous investigations of CH_3-terminated porous Si surfaces, with an amorphous surface structure but high surface IR signal, have observed broad C–H symmetric and asymmetric stretches centered at $\sim$2900 and 2970 cm^{-1}, respectively.[33] FTIR studies of silicon oxide surfaces terminated with trimethylsilane have also reported methyl C–H stretches at 2904 and 2963 cm^{-1}.[34] Other investigations of alkylated porous Si have observed C–H stretching at 2860 and 2936 cm^{-1} from a terminating 6-trifluoroacetamindohexyl group, in which all C–H bonds are on methylene (CH_2) groups.[35] With this information,[36] the peaks at 2909 and 2965 cm^{-1} likely represent the methyl C–H symmetric and asymmetric

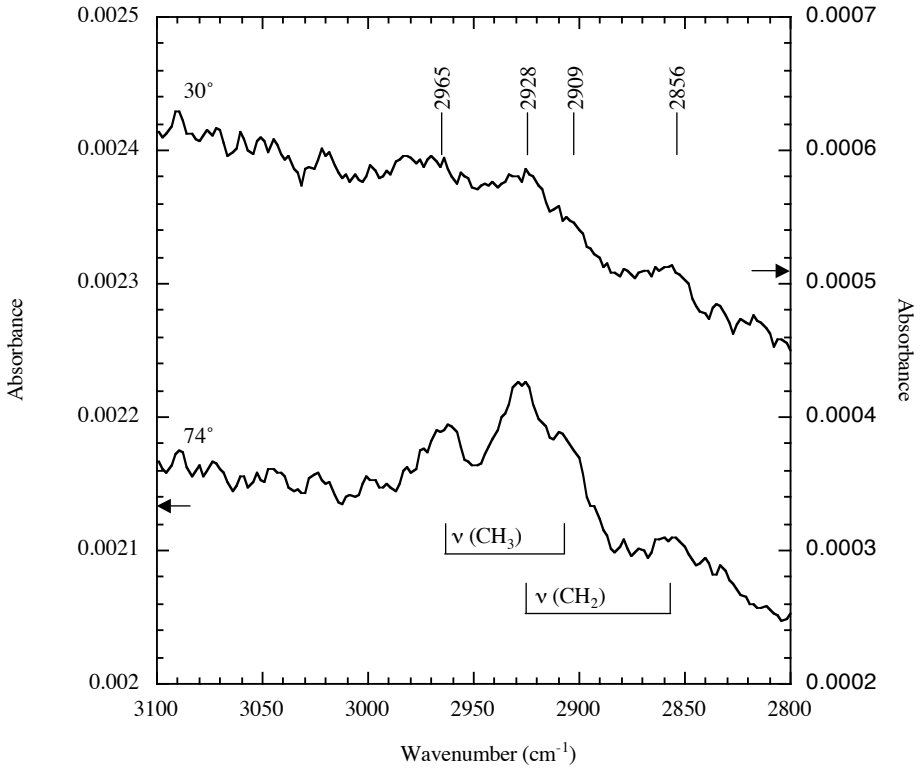

Figure 4.7: TIRS and proposed peak assignments of the C–H stretching region of the CH_3-terminated Si(111) surface collected at an incident beam angle of 74° (bottom) and 30° (top) off surface normal. Positions of relevant peaks are noted above the spectra. Spectra are shown without alteration such as background smoothing on the same scale, but are offset for clarity.

stretching vibrations, respectively, while the peaks at 2856 and 2928 cm^{-1} are possibly from methylene C–H stretching motions. These methylene signals could originate from hydrocarbon contamination that is known to be present on the CH_3-terminated Si(111) surface prepared through the two-step chlorination/alkylation route.

The low wavenumber region of vibrational absorptions on the CH_3-Si(111) surface collected from two different incident IR beam angles, along with proposed peak assignments, are shown in Figure 4.8. When the surface was examined with the IR beam incident on the surface at the Brewster angle, a sharp feature at 1257 cm^{-1} was clearly visible, but was not seen when the IR beam was moved towards surface normal. This peak was assigned as the C–H symmetric bending, or "umbrella," mode of the methyl group.[33,37] The polarization-type experiments revealed that it is a motion that is perpendicular to the Si(111) surface. This demonstrates that the methyl group introduced to the surface through the two-step chlorination/alkylation route is oriented perpendicular to the surface, consistent with the model of surface alkyl bonding proposed in Figure 1.4. A second sharp peak at 757 cm^{-1} appeared at both data collection angles. This absorption energy is expected for a methyl C–H rocking mode,[37] which would be parallel to the surface if it originates on a methyl group normal to the Si(111) surface, and therefore is expected to be observed even when the incident IR beam is itself near to surface normal. The integrated areas for both of these peaks at both data collection angles are given in Table 4.2.

Another feature present in the spectrum collected at an IR incident angle of 74° off normal was a small, broad absorption near 1100 cm^{-1}, corresponding possibly to the TO mode of Si–O–Si. Interestingly, this feature was not observed when the TIR spectrum of the CH_3-terminated surface was collected at an incident angle of 30° off surface normal. It was already demonstrated (Figure 4.2) that because the TO mode is parallel to the Si(111) surface, it should appear with equal intensity no matter what angle the surface is illuminated with the IR beam. Because the spectra in Figure 4.8 were taken from two different samples, inclusion of the TO peak on one sample could possibly have been caused by small variations in the amount of O incorporated in the near-surface Si lattice that cannot be prevented by the alkylation technique used here. The amount of oxide on the surface was estimated by assuming that the native silicon oxide was 15 Å thick, and by determining the

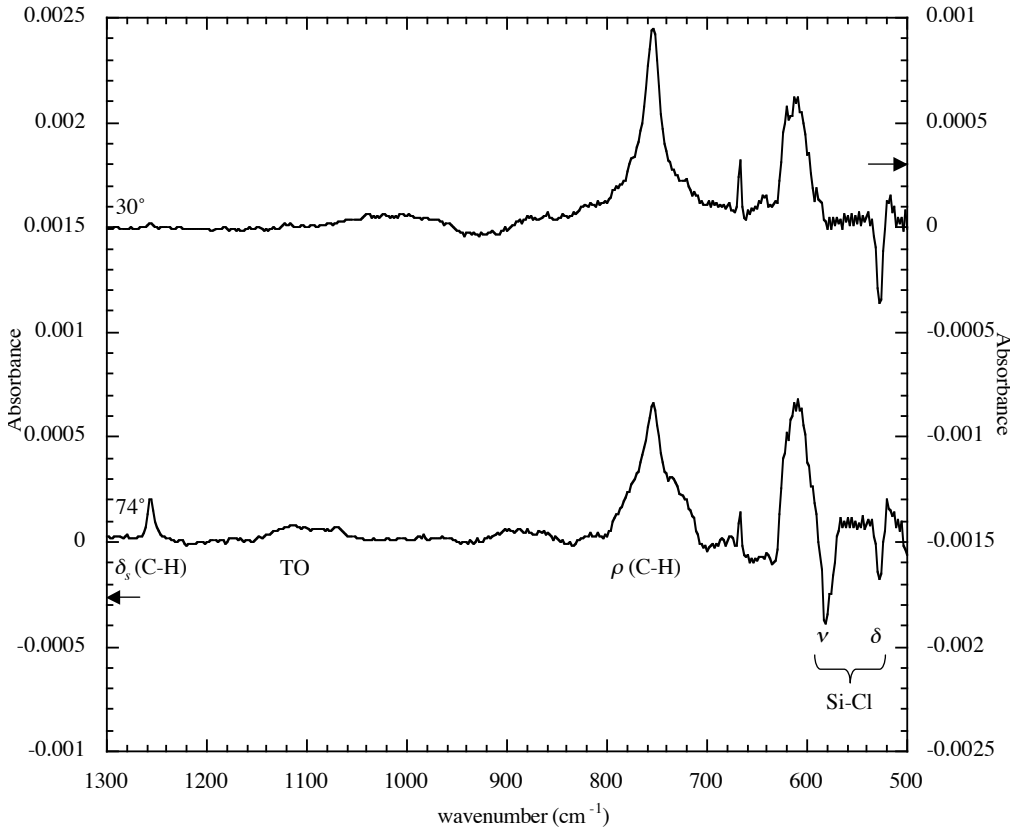

Figure 4.8: TIRS and proposed peak assignments of the CH_3-terminated Si(111) surface collected at an incident beam angle of 74° (bottom) and 30° (top) off surface normal shown in the low wavenumber region. The spectra are on the same scale of absorbance (absorbance units), although they are offset for easier viewing. Data are shown after subtraction of H_2O and flattening of the baseline.

ratio of the integrated areas of the TO peak on the CH_3-terminated surface to that on the native oxide surface (negative peak in Figure 4.2). The TO peak on the CH_3-terminated surface corresponded to a possible Si–O–Si coverage of 0.03 ML, or approximately 0.5 Å.

In the low energy region of the TIR spectrum, shown in Figure 4.8, a feature at ≈730 cm^{-1} was observed as a large shoulder on the methyl C–H rocking motion peak when data was collected at the Brewster angle that disappeared when the IR beam was moved towards surface normal. This polarization-type behavior indicated it could be a surface motion positioned perpendicular to the Si(111) surface plane, although this was higher in energy than most proposed Si–C stretches previously identified by HREELS investigations.[10–15] Finally, Figure 4.8 shows a broad feature at ∼620 cm^{-1} at both data collection angles. This corresponded to a Si–Si lattice phonon mode that was not perfectly subtracted from the CH_3-terminated surface by referencing with the Cl-terminated surface, possibly due to a slight difference in placement of the two surfaces in the IR sample holder or a small temperature variation during data collection.[38] A sharp absorption at 667 cm^{-1} was also observed from atmospheric CO_2(g) contamination in the IR sample compartment.

4.3.4 C_2H_5-Terminated Si(111) Surfaces

To collect infrared spectra of a surface on which complete alkyl termination is not possible, TIRS was also conducted on a Cl-terminated surface that had been exposed to a solution of ethylmagnesium halide. TIR spectra of the C_2H_5-terminated surface after subtraction of H_2O and baseline smoothing is shown in Figure 4.9. The peaks corresponding to Si–Cl stretching and bending modes at 583 and 528 cm^{-1} were observed as negative features in the spectrum, demonstrating that they decreased as the Si–Cl surface was exposed to the alkylating solution. As on the CH_3-terminated Si surface, the integrated areas of peaks attributed to Si–Cl bending and stretching motions were used as a reference to determine the extent of replacement of the chlorine by alkyl groups on the surface through the functionalization procedure. As shown in Table 4.2, when the Si–Cl bending mode at 528 cm^{-1} was examined, the integrated area of the positive feature on the Cl-terminated surface was identical to that of the negative feature on the C_2H_5-terminated surface, within the error

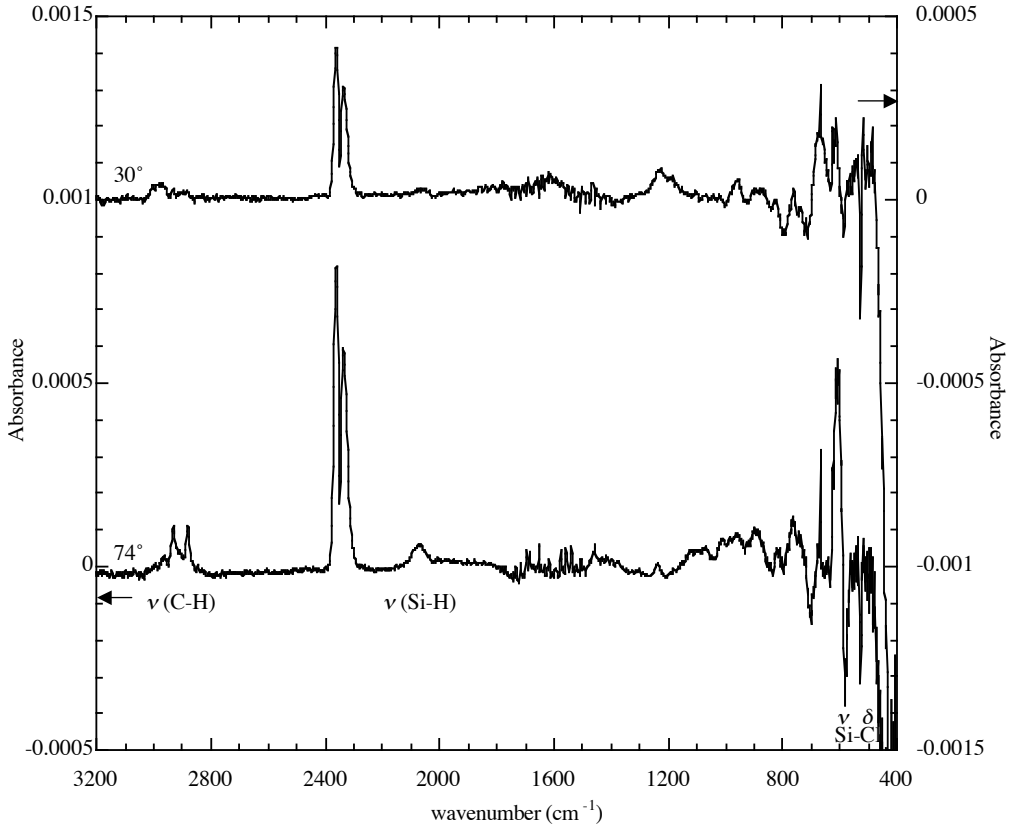

Figure 4.9: TIRS and proposed peak assignments of the C_2H_5-terminated Si(111) surface collected at an incident beam angle of 74° (bottom) and 30° (top) off surface normal. The spectra are on the same scale of absorbance (absorbance units), although they are offset for easier viewing. Data are shown after subtraction of H_2O and flattening of the baseline.

of the experiment. This supports previous XPS observations that all Cl is removed from the Si surface during exposure to the alkylmagnesium halide solution, even on a surface where not all atop Si(111) atoms can be bonded to the alkyl group. The data from the Si–Cl stretching mode (583 cm^{-1}) was not as conclusive, although measurement of the area under this peak could have been hampered by interference from the Si–Si phonon region directly above 600 cm^{-1}.

A broad peak on the C_2H_5-terminated Si(111) surface centered at approximately 2080 cm^{-1} was observed when TIRS was collected with an incident IR beam 74° off surface normal and was not seen when the data collection angle was reduced to 30°. This was near the energy of the peak representing the Si–H stretching motion (2083 cm^{-1}) observed in the spectrum of the freshly etched Si(111) surface seen previously in Figure 4.2. This peak could correspond to surface Si–H atoms that were present on the surface after the alkylation, consistent with the hypothesis that if no more Cl is left on a C_2H_5-terminated surface, the remaining Si atop sites might be bonded with H atoms. The Si–H signal from this surface would no longer be the sharp peak characteristic of a highly ordered surface with a single termination layer, but instead be broad and amorphous, representing Si–H bonds in a variety of chemical environments.

Upon close inspection of the low wavenumber region of this surface, a feature at 627 cm^{-1} was apparent no matter at what IR beam incident angle the spectra were collected, possibly corresponding to the Si–H bending vibrational mode. This can be seen in Figure 4.10. Like the probable Si–H stretching feature at ≈2080 cm^{-1}, the shape and size of this peak were difficult to determine because the peak was partly buried by a strong Si–Si phonon mode at ≈610 cm^{-1}. This Si–H feature would be expected for a mixed surface monolayer comprised partly of Si–H and partly Si–C bonds, again consistent with the hypothesis that the C_2H_5-terminated Si(111) surface is partly covered with Si–H bonds after the two-step chlorination/alkylation functionalization procedure. The only other peak seen in this region was a sharp absorption feature at 667 cm^{-1} from CO_2 contamination in the sample chamber. It is interesting to note that neither the CH_3- symmetrical bending (1250 cm^{-1}) or C–C stretching vibrational modes (1000 – 1050 cm^{-1}) were observed.

The C–H stretching region near 2900 cm^{-1} is shown in Figure 4.11. Examination of

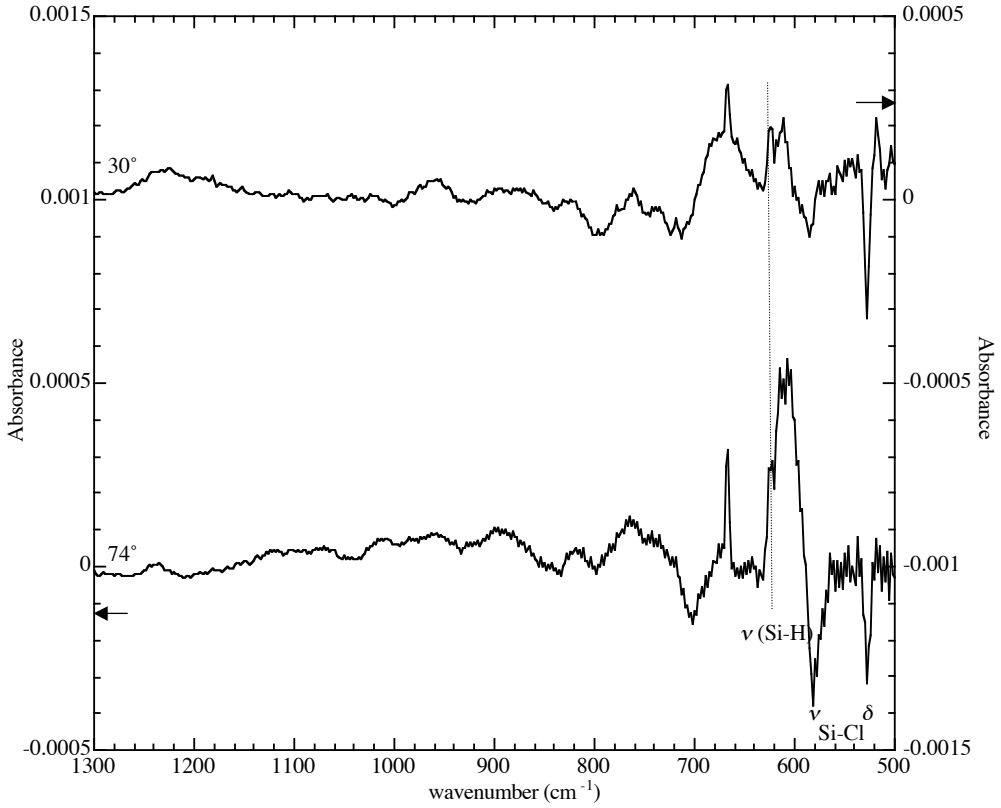

Figure 4.10: TIRS and proposed peak assignments of the C_2H_5-terminated Si(111) surface collected at an incident beam angle of 74° (bottom) and 30° (top) off surface normal shown in the low wavenumber region. The spectra are on the same scale of absorbance (absorbance units), although they are offset for easier viewing. Data are shown after subtraction of H_2O and flattening of the baseline.

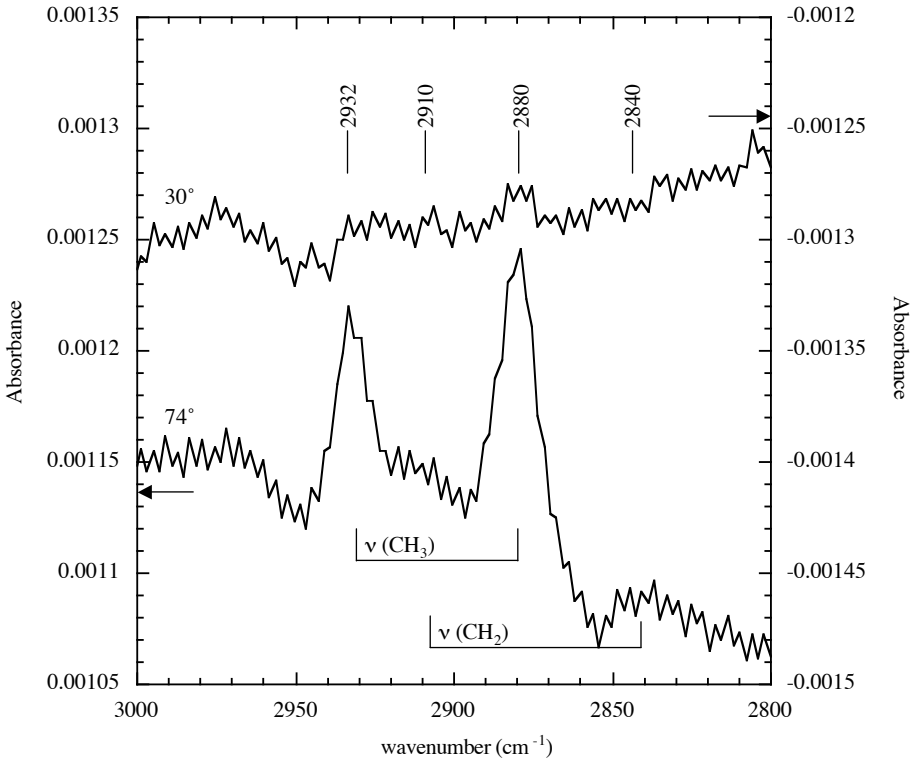

Figure 4.11: TIRS and proposed peak assignments of C–H stretching region of C_2H_5-terminated Si(111) examined at an incident beam angle of 74° (bottom) and 30° (top) off surface normal. The spectra are shown before any data manipulation was conducted. The spectra are on the same scale, but are offset for easier comparison.

	TIRS peak location			
-R	$\overline{\nu}$ (cm^{-1})	intensity[a]	assignment	$\perp$ to surface?
-H	2083	s	ν (Si–H)	yes
	627	s	δ (Si–H)	no
-Cl	583	m	ν (Si–Cl)	yes
	528	m	δ (Si–Cl)	no
$-CH_3$	2965	m	ν_a $(C–H)_{CH_3}$	
	2928	s	ν_a $(C–H)_{CH_2}$	
	2909	m	ν_s $(C–H)_{CH_3}$	
	2856	w	ν_s $(C–H)_{CH_2}$	
	1257	m	δ_s $(C–H)_{CH_3}$	yes
	1100	w	TO (Si–O–Si)	
	757	s	ρ $(C–H)_{CH_3}$	no
$-C_2H_5$	2932	s	ν_a $(C–H)_{CH_3}$	
	2910	m	ν_a $(C–H)_{CH_2}$	
	2880	s	ν_s $(C–H)_{CH_3}$	
	2840	w	ν_s $(C–H)_{CH_2}$	
	2080	m	ν (Si–H)	yes
	627	m	δ (Si–H)	no

Table 4.3: Assignment of TIRS peaks observed on functionalized Si(111) surfaces. [a] Qualitative assessment of peak intensity: s = strong, m = medium, w = weak.

this region revealed four vibrational absorptions at 2840, 2880, 2910, and 2932 cm^{-1} on the surface examined by the IR beam 74° off surface normal. Previous observations of an ethyl group on the Si(111) surface have been limited in scope,[39,40] but ZnO and ZrO_2 surfaces have been ethylated, and vibrational absorption features with four distinct peaks have been observed.[41,42] Based on these previous observations, as well as IR from self-assembled alkyl monolayers on gold,[36] the C–H stretching vibrational modes observed on the C_2H_5-terminated Si(111) surface at 2840 and 2910 cm^{-1} are assigned to the CH_2 methylene unit, while the peaks at 2880 and 2932 cm^{-1} are assigned to the CH_3 methyl group. A summary of surface vibrational features observed on samples here is given in Table 4.3.

4.4 Discussion

By comparing the TIR spectrum of a freshly prepared Cl-terminated Si(111) surface referenced against a H-Si(111) sample to the TIR spectrum of that H-terminated surface, the area under the Si–H stretching and bending vibrational modes on both surfaces revealed that all surface H atoms were removed, consistent with the hypothesis that chlorination by PCl_5 replaces surface H atoms with Cl atoms quantitatively. Furthermore, the small full width at half maximum (fwhm) of the Si–Cl stretching and bending modes on the Cl-terminated Si(111) surface indicated that the surface was highly homogeneous. Because the Cl-terminated surfaces were made from atomically flat, H-terminated Si surface, this high homogeneity indicates that PCl_5 chlorination of the H-Si(111) sample does not lead to extensive roughening or pitting of the surface.[18]

It is unexpected to measure the stretching and bending motions of the Si–Cl bond so close in energy, separated by only 60 cm^{-1}, given that they correspond to very different motions. One possible explanation is that the surface is terminated with $SiCl_3$ groups and that the two modes associated with the Si–Cl surface are the symmetric and asymmetric Si–Cl stretching vibrational modes. Another possible explanation is that the surface is indeed terminated by single Si–Cl bonds, but that the Si atom is in motion in both the stretching and bending vibrational modes while the heavier surface Cl atom remains motionless. In this case, both the stretching and the bending of the surface Si–Cl bond would involve the

distortion of three Si–Si backbonds, which would have similar displacement energies. Calculations on a mixed periodic unit cell/Si cluster model were used to distinguish these two scenarios. These calculations confirmed that the trichlorinated $SiCl_3$ surface is sterically prohibited. Given that high-resolution XPS data described in Chapter 3 detected no $SiCl_3$ species, these calculations confirm that surface Si atoms cannot be triply bonded to Cl, but instead strongly suggest that the surface consists of monochlorinated Si species. Furthermore, calculations identified the mode at 528 cm^{-1} as originating from a Si–Cl bending motion in which the Si is displaced, accounting for the unusually close energy of the Si–Cl stretching and bending modes.

When this monochlorinated surface was exposed to an alkylmagnesium halide solution, the Si–Cl stretching and bending peaks were used to determine the extent of chlorine removal by the alkylating reagent. Within the detection limit of the instrument and the accuracy of the measurement technique, the Cl was completely removed during exposure to the alkylmagnesium halide reagent. Although the surface modification procedure is conducted under rigorously O_2- and H_2O-free conditions to avoid oxidizing the Si surface, occasionally TIRS evidence for Si–O–Si vibrational modes was observed near 1100 cm^{-1}. This was present in amounts of <1 Å, however, indicating that this indeed is not an important part of the fully functionalized alkyl-terminated surface. This is consistent with extensive high-resolution XPS evidence on the freshly prepared alkyl-terminated Si(111) surface.

The observation of the Si–Cl stretching and bending vibrational modes at 583 and 528 cm^{-1} is a clear demonstration of the utility of TIRS for investigating extremely low wavenumber vibrational absorptions on the Si surface, which was the original goal of this research. With this capability, it should be possible to measure the infrared absorption of the surface Si–C stretching motion, which has been predicted from previous HREELS experiments to be between 600–700 cm^{-1}. There was, however, no conclusive evidence of a Si–C vibrational mode found in the experiments presented here. On the CH_3-terminated surface, two regions were examined carefully for evidence of the Si–C stretch. The first was $\sim$730 cm^{-1}, where a broad shoulder on the C–H rocking mode appeared at an incident IR beam angle of 74°, but disappeared when the IR beam was moved to an incident an-

gle of 30°. This is representative of a surface-associated vibrational mode that is oriented perpendicular to the Si surface, as seen for example in the Si–Cl and Si–H stretching motions at 583 and 2083 cm^{-1}, respectively. HREELS investigations of this bond have placed the Si–C stretching vibration below 700 cm^{-1},[10–15] much lower in energy than the peak observed here at 730 cm^{-1}. While this does not mean that the actual infrared absorption could be at a higher energy, it is not possible to conclude that this feature actually results from the Si–C vibrational absorption.

The second absorption region that was investigated closely was the area between 600–620 cm^{-1}, which was often obscured by a large Si–Si phonon vibration that was particularly difficult to reduce in the difference spectrum. In order to subtract this feature out of the difference spectrum fairly, TIR spectra of a SiO_2-covered Si wafer were recorded at an incident beam angle of 74° and 73°. Because the surface was deliberately offset in the sample holder, when the difference spectrum of these two samples was calculated, it consisted of a large Si–Si phonon vibration covering the area 600–620 cm^{-1}. This was then used as a background spectrum that was subtracted from the difference spectrum of the CH_3-terminated Si(111) surface. If the Si–Si phonon background is subtracted correctly, any feature remaining under that region should be uncovered after the subtraction is completed. This procedure, however, revealed nothing on the CH_3-terminated surface, even after the Si–Si lattice phonon appeared to be completely accounted for (data not shown). Given the demonstrated sensitivity to vibrational absorptions in this region, particularly for ν and δ(Si–Cl), the lack of any clear signal that can be definitely attributed to the surface Si–C stretching mode in this region is disappointing, but it must be left to further research in this area to investigate further.

4.5 Conclusion

Comparison of TIRS observations of H- and Cl-terminated Si(111) surfaces has shown that all terminating hydrogen atoms on the freshly etched Si surface are replaced with Cl atoms when this surface is exposed to PCl_5 and a radical generating reagent. Polarization-type studies of the Si–Cl stretching and bending modes at 583 and 526 cm^{-1}, respectively, con-

firm the conclusion from SXPS studies that the Cl-terminated surface is monochlorinated. Observation of these modes, furthermore, is strong confirmation that TIRS is a technique that should continue to be used to observe low energy surface vibrational modes that have been heretofore obscured by Si–Si phonon vibrations from the lattice crystal. Polarization-type behavior of the CH_3- symmetric bending or "umbrella" mode at 1257 cm^{-1} identified this as a feature that is perpendicular to the surface, consistent with the expectations for a surface-bound methyl group defined by the tetrahedral geometry of Si and C. Although no direct observation of the Si–C stretching vibrational mode near 650 cm^{-1} was made in these studies, observations of C–H stretching and bending vibrations on both the CH_3- and C_2H_5-terminated Si(111) surfaces demonstrate cleanly alkylated surfaces that warrant extensive further investigation with transmission IR spectroscopy.

Bibliography

[1] Chabal, Y. J. *Surf. Sci.* **1986,** *168*, 594–608.

[2] Chabal, Y. J. *Surf. Sci. Rep.* **1998,** *8*, 211–357.

[3] Yablonovitch, E.; Allara, D. L.; Chang, C. C.; Gmitter, T.; Bright, T. B. *Phys. Rev. Lett.* **1986,** *57*, 249–252.

[4] Higashi, G. S.; Chabal, Y. J.; Trucks, G. W.; Raghavachari, K. *Appl. Phys. Lett.* **1990,** *56*, 656–658.

[5] Chabal, Y. J.; Weldon, M. K.; Queeney, K. T.; Esteve, A. Vibrational Studies of Ultra-Thin Oxides and Initial Silicon Oxidation. In *Fundamental Aspects of Silicon Oxidation*; Chabal, Y. J., Ed.; Springer: New York, 2001.

[6] Harrick, N. J. *Internal Reflection Spectroscopy;* John Wiley & Sons: New York, 1967.

[7] Sperline, R. P.; Jeon, J. S.; Raghavan, S. *Appl. Spectrosc.* **1995,** *49*, 1178–1182.

[8] Queeney, K. T.; Fukidome, H.; Chaban, E. E.; Chabal, Y. J. *J. Phys. Chem. B* **2001,** *105*, 3903–3907.

[9] Bansal, A.; Li, X.; Yi, S. I.; Weinberg, W. H.; Lewis, N. S. *J. Phys. Chem. B* **2001,** *105*, 10266–10277.

[10] Yamada, T.; Kawai, M.; Wawro, A.; Suto, S.; Kasuya, A. *J. Chem. Phys.* **2004,** *121*, 10660–10667.

[11] Yoshinobu, J. *Solid State Commun.* **1986,** *60*, 801–805.

[12] Huang, C.; Widdra, W.; Wang, X. S.; Weinberg, W. H. *J. Vac. Sci. Technol. A* **1993,** *11*, 2250–2254.

[13] Widdra, W.; Huang, C.; Yi, S. I.; Weinberg, W. H. *J. Chem. Phys.* **1996,** *105*, 5605–5617.

[14] Hamaguchi, K.; Machida, S.; Nagao, M.; Yasui, F.; Makai, K.; Yamashita, Y.; Yoshinobu, J. *J. Phys. Chem. B* **2001,** *105,* 3718–3723.

[15] Widdra, W.; Huang, C.; Briggs, G. A. D.; Weinberg, W. H. *J. Electron Spectrosc.* **1993,** *64/65,* 129–136.

[16] Chabal, Y. J. **2005,** Personal communication.

[17] Rivillon, S.; Amy, F.; Chabal, Y. J.; Frank, M. M. *Appl. Phys. Lett.* **2004,** *85,* 2583–2585.

[18] Rivillon, S.; Chabal, Y. J.; Webb, L. J.; Michalak, D. J.; Lewis, N. S.; Halls, M. D.; Raghavachari, K. *J. Vac. Sci. Technol. B* **2004,** in press.

[19] Weldon, M. K.; Queeney, K. T.; Gurevich, A. B.; Stefanov, B. B.; Chabal, Y. J.; Raghavachari, K. *J. Chem. Phys.* **2000,** *113,* 2440–2446.

[20] Lebib, S.; Roca i Cabarrocas, P. *Eur. Phys. J. Appl. Phys.* **2004,** *26,* 17–27.

[21] Caudano, Y.; Thiry, P. A.; Chabal, Y. J. *Surf. Sci.* **2002,** *502-503,* 91–95.

[22] Gao, Q.; Cheng, C. C.; Chen, P. J.; Choyke, W. J.; Yates, J. T. *J. Chem. Phys.* **1993,** *98,* 8308–8323.

[23] Robinson, M. B.; Dillon, A. C.; George, S. M. *J. Vac. Sci. Technol. A* **1995,** *13,* 35–41.

[24] Dillon, A. C.; Wise, M. L.; Robinson, M. B.; George, S. M. *J. Vac. Sci. Technol. A* **1995,** *13,* 1–10.

[25] Sneh, O.; Wise, M. L.; Ott, A. W.; Okada, L. A.; George, S. M. *Surf. Sci.* **1995,** *334,* 135–152.

[26] Ricca, A.; Musgrave, C. B. *Surf. Sci.* **1999,** *430,* 116–125.

[27] Becke, A. D. *Phys. Rev. A* **1988,** *38,* 3098–3100.

[28] Lee, C. T.; Yang, W. T.; Parr, R. G. *Phys. Rev. B* **1988,** *37,* 785–789.

[29] Hehre, W. J.; Radom, L.; Schleyer, P. v. R.; Pople, J. A. *Ab Initio Molecular Orbital Theory;* John Wiley & Sons: New York, 1986.

[30] Pauling, L. *The Nature of the Chemical Bond;* Cornell University Press: Ithica, NY, 1960.

[31] Sze, S. M. *The Physics of Semiconductor Devices;* Wiley: New York, 2nd ed.; 1981.

[32] Oxton, I. A. *J. Mol. Struct.* **1979,** *56,* 57–68.

[33] Fidelis, A.; Ozanam, F.; Chazalviel, J. N. *Surf. Sci.* **2000,** *444,* L7–L10.

[34] Schmohl, A.; Khan, A.; Hess, P. *Superlattice. Microst.* **2004,** *36,* 113–121.

[35] Lees, I. N.; Lin, H. H.; Canaria, C. A.; Gurtner, C.; Sailor, M. J.; Miskelly, G. M. *Langmuir* **2003,** *19,* 9812–9817.

[36] Arnold, R.; Terfort, A.; Woll, C. *Langmuir* **2001,** *17,* 4980–4989.

[37] Kaltchev, M.; Tysoe, W. T. *Surf. Sci.* **1999,** *430,* 29–36.

[38] Rivillon, S. **2005,** Personal communication.

[39] Fellah, S.; Teyssot, A.; Ozanam, F.; Chazalviel, J. N.; Vigneron, J.; Etcheberry, A. *Langmuir* **2002,** *18,* 5851–5860.

[40] Yang, C. S.; Bley, R. A.; Kauzlarich, S. M.; Lee, H. W. H.; Delgado, G. R. *J. Am. Chem. Soc.* **1999,** *121,* 5191–5195.

[41] Oleinik, A. A.; Dodonov, V. A.; Lysenko, G. N.; Druzhkov, O. N. *Russ. Chem. B+* **1994,** *43,* 1577–1579.

[42] Ferguson, J. D.; Weimer, A. W.; George, S. M. *J. Vac. Sci. Technol. A* **2005,** *23,* 118–125.

Chapter 5

Structural Characterization of Methyl-Terminated Silicon(111) Surfaces by Low Energy Electron Diffraction and Scanning Tunneling Microscopy

5.1 Introduction

Taken together, X-ray photoelectron and infrared spectroscopy studies described in Chapters 3 and 4 strongly support the hypothesis that the two-step chlorination/alkylation functionalization route results in a surface-bound alkyl group oriented perpendicular to the Si(111) surface as predicted by the tetrahedral geometry of Si and C. Moreover, the evidence suggests that virtually all of the atop Si atoms on the CH_3- and C_2H_5-terminated surface are bonded either to an alkyl group or a hydrogen atom at the completion of functionalization. This is consistent with the conclusions of prior workers, who have suggested that functionalization with longer alkyl chains yields incomplete coverage of the Si(111) surface,[1] with the remainder of the sites being terminated by either -OH, -H, or other unidentified surface species.[2,3] Because the Si crystal substrate is highly ordered, these observations imply that the alkyl overlayer is itself well-ordered to accommodate a high density of surface-bound alkyl groups. Previous molecular modeling studies have indicated that methyl groups are the only saturated hydrocarbon moiety that can terminate

every Si atop site on the unreconstructed Si(111) surface.[2,4,5] Such complete chemical termination is expected to offer the most robust passivation of surface defects and to provide the best resistance to oxidation of the resulting Si surface over functionalization by hydrogen or chlorine atoms.

Although the chemical composition of alkyl-terminated surfaces has been thoroughly investigated in Chapters 3 and 4, there is still little information on the morphological structure or long-range order of the fully functionalized surface. Recent scanning tunneling microscopy (STM) images of the CH_3-terminated Si surface have revealed bright spots in a pattern consistent with a unreconstructed (1 x 1) adlattice structure on the Si surface.[6,7] For CH_3-terminated Si surfaces prepared through a two-step chlorination/alkylation route similar to that described here, photoelectron diffraction has been used to estimate the length of the Si–C bond as 0.18 nm.[2] Both of these results are again consistent with the hypothesis that the CH_3-terminated Si surface has an unreconstructed morphology defined by the tetrahedral geometry of both the sp^3 hybridized surface Si and atop methyl groups.

To explore this question further, it is necessary to determine the structure of the CH_3-terminated Si(111) surface in atomic detail. In the work described in this chapter, the structure of the CH_3-terminated Si(111) surface was investigated by low energy electron diffraction (LEED) to determine if the long-range order of the fully functionalized surface involves reconstruction of surface Si atoms. STM studies were then performed at low temperatures in ultra-high vacuum (UHV) conditions to investigate for the first time the local atomic structure of the fully methyl-terminated Si(111) surface prepared by the two-step chlorination/alkylation functionalization procedure.

5.2 Experimental

5.2.1 Materials and Methods

Silicon samples used in this work were (111)-oriented, Sb-doped, 0.005–0.02 Ω cm resistivity, n-type Si wafers having a miscut error of $\pm 0.5^\circ$. Samples were obtained from ITME (Poland). Low resistivity wafers were required to achieve adequate tunneling from

the substrate in UHV at the low temperatures used in this study. A flat along one side of the wafer was reported by the manufacturer to be cut along the $<1\bar{1}0>$ plane. This was confirmed with X-ray crystallography and through analysis of etch pits seen by STM. After the wafer was cut the orientation of the sample relative to the flat was marked and monitored throughout STM data collection.

For LEED experiments, CH_3-terminated Si(111) surfaces were prepared identically to the procedures described in Chapter 2, and then sealed under N_2(g) and mailed to the BESSY synchrotron facility in Berlin. For UHV STM studies, a slightly different cleaning and etching procedure was followed. The samples were cleaned and oxidized for 5 min at 80°C in a solution of 1:1:5 (vol) 30% H_2O_2:30% NH_3:H_2O and were then terminated with Si–H bonds by etching for 15 min in 40% NH_4F(aq) that had been purged with N_2(g) for approximately 45 min. The sample was then transported directly to the N_2(g)-purged glove box, although it was exposed to ambient air for approximately 5 min. Chlorination and methylation were then carried out as described in Chapter 2. After functionalization, the sample was mounted onto the STM stage and quickly introduced into the UHV chamber of the STM.

5.2.2 Instrumentation

LEED patterns were collected at electron energies of 40, 45, and 50 eV using a three-grid reverse-view LEED system (VG). Data were collected at the BESSY synchrotron facility in Berlin by Bengt Jaeckel of the Institute of Materials Science at the Technische Universität Darmstadt, Darmstadt, Germany.[8]

STM data were obtained on an Omicron low-temperature UHV STM using etched or mechanically cut Pt/Ir STM tips. Data were collected at 77 and 4.7 K by Dr. Hongbin Yu at the California Institute of Technology.[9]

5.3 Results

Figure 5.1 displays the LEED patterns of a CH_3-terminated Si(111) surface collected with primary electron energies of 40, 45, and 50 eV. These energies were used because they pro-

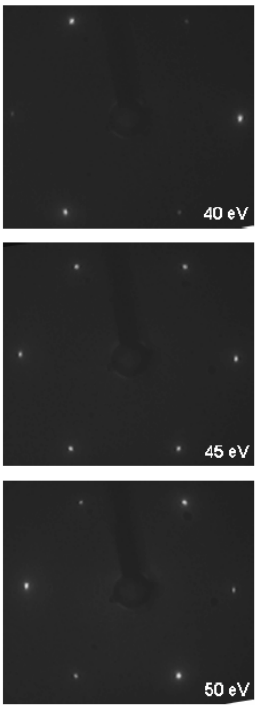

Figure 5.1: LEED pattern of CH_3-Si(111) taken with electron energies of 40, 45, and 50 eV. Electron energies are noted on the figure. Figure from Hunger, *et al*.[8]

duced a low electron penetration depth into the Si crystal, ensuring that the LEED pattern is representative of the alkyl overlayer and does not probe the structure of the underlying Si crystal lattice. The observed diffraction patterns exhibited a threefold symmetry corresponding to a (111)-(1 x 1) surface structure. This pattern is consistent with expectations for ideal, close-packed methyl termination of an unreconstructed Si(111) surface. The low intensity of the background and the sharpness of the diffraction spots indicate that the surface was well-ordered and consisted of extended, atomically flat terraces with relatively few defect sites. The low level of diffuse background, even at low electron kinetic energies, indicates that the diffraction pattern was the result of a commensurate CH_3- layer on top of a well-ordered Si(111) surface layer. The LEED pattern suggests that the quality of the methyl-terminated surface is comparable to that of the well-known wet-chemically prepared H-terminated Si(111) surface.[8]

Dr. Hongbin Yu has previously examined the structure of the freshly etched H-Si(111) surface prepared through the etching procedure described above by STM under UHV conditions at both 4.7 and 77 K. He found that H atoms on this surface were separated by 3.8 Å, identical to the atop Si–Si distance on the (111) surface.[10] Several attempts were made to collect STM images of the intermediate Cl-terminated Si(111) surface prepared through PCl_5 chlorination, but were unsuccessful. The reasons for this are unknown, but are perhaps due to the less rigorous cleaning procedure conducted on the freshly prepared Cl-terminated surface that might leave contaminating organic solvents present in high enough quantity to prevent tunneling between the sample and the STM under UHV conditions.

Figure 5.2 compares STM images of the morphology of the H-terminated Si(111) surface with that of the CH_3-terminated surface over a large surface area. A slight increase in the etch pit density was observed as a result of the chlorination/alkylation procedure, but large flat terraces, separated in height by single atomic steps, were observed on both surfaces. The lack of substantial defect sites or etch pits on the CH_3-terminated surface confirms the presence of a nearly atomically flat surface described by the LEED patterns.

Figure 5.3 shows STM images of the CH_3-terminated surface at 77 and 4.7 K, respectively. The image at 77 K, Figure 5.3(a), consisted of a series of triangularly shaped bright regions on a (1 x 1) structure, with spots separated by a distance of 0.38 ± 0.01 nm, labeled

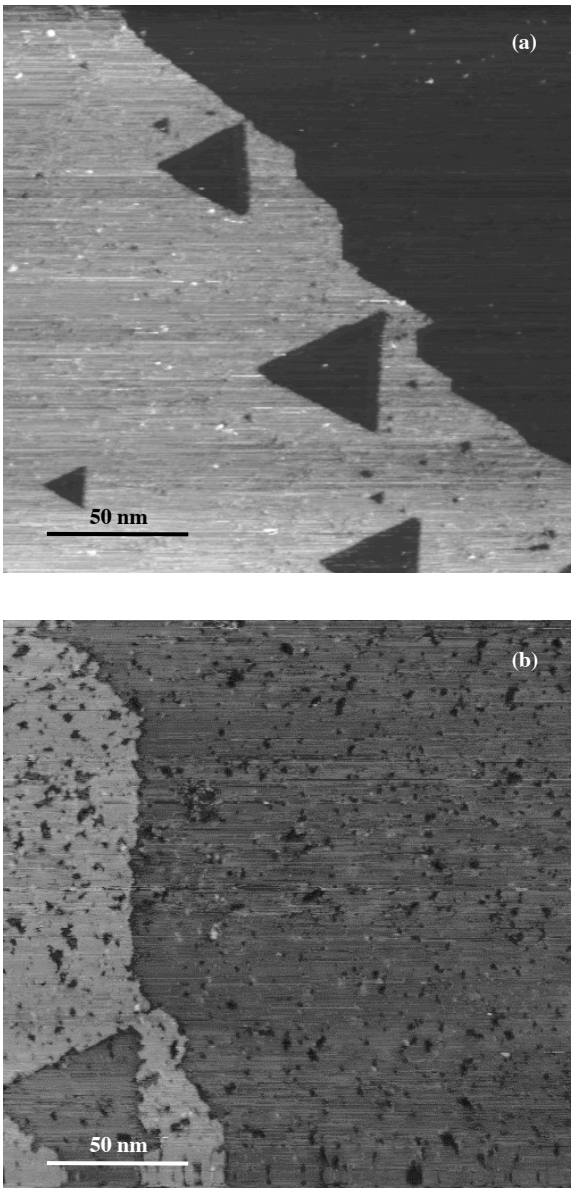

Figure 5.2: STM images of H- and CH_3-terminated Si(111) surfaces collected at 77 K shown in a 200 nm x 200 nm scan window. (a) H-Si(111); (b) CH_3-Si(111). In each image the scale bar is 50 nm. The black-to-light gray color change represents a single atomic step in both cases, although the contrast shading is not on the same scale. For color versions of these images see Yu, *et al*.[9]

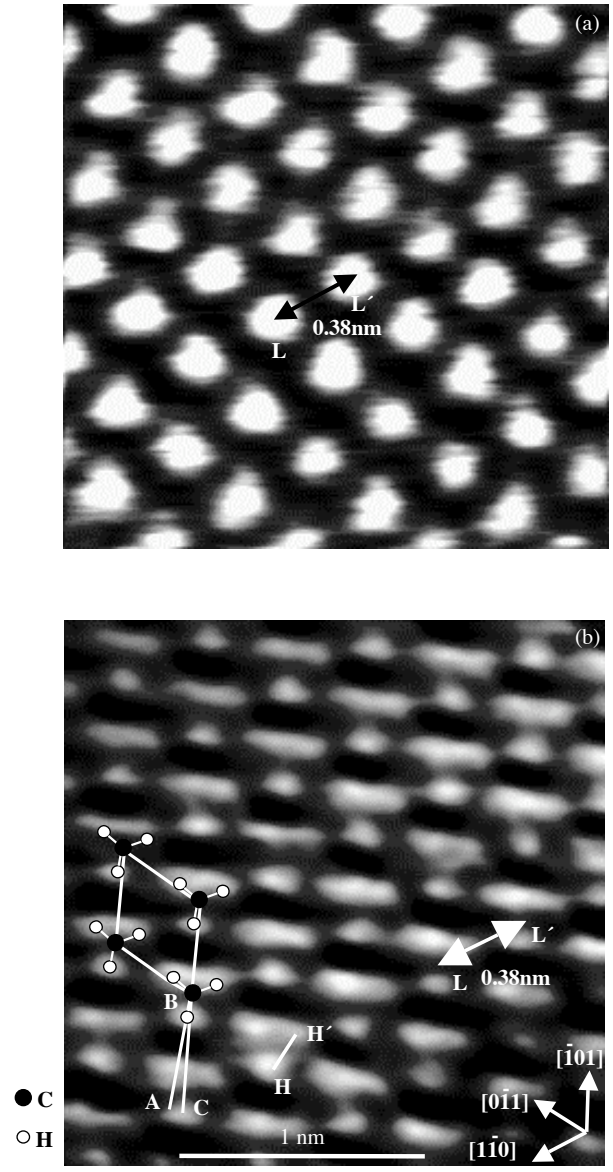

Figure 5.3: STM images of CH_3-terminated Si(111) surfaces at 77 and 4.7 K. (a) CH_3-Si(111) at 77 K; (b) CH_3-Si(111) at 4.7 K collected at a sample bias of V_s = -2.5 V and at a constant current of 0.05 nA. Length scale bar is 1 nm and the color range (dark = low; bright = high) is 0.05 nm. Features discussed in the text are noted. For color versions of these images see Yu, *et al.*[9]

as L and L'. This distance is equal to the spacing between atop sites on an unreconstructed Si(111) surface, and is consistent with previous STM observations of the placement of terminal H atoms on the freshly etched Si(111) surface. The ordering was quite robust, with relatively few defects observed over large regions of the surface.

STM images collected at 4.7 K (Figure 5.3(b)) revealed further structure in the CH_3-terminated surface, with the triangularly shaped regions each resolved into three spots separated from each other by an average distance of 0.18 ± 0.01 nm, indicated by H and H' on Figure 5.3(b). Four methyl group drawings are superimposed onto the image, assuming that the C atoms of the methyl groups are in registry with atop Si atoms, to illustrate the position and relative orientation of methyl groups on the Si(111) surface. The 0.18-nm distance between H atoms on the same methyl group is consistent with the distance between hydrogen atoms in a sp^3-hybridized geometry. The repulsions between H atoms on adjacent -CH_3 groups would be minimized if the C–H bonds on a methyl group were oriented directly toward the carbon atoms on adjacent CH_3- groups (i.e., if $\angle$ A–B–C = 0 in Figure 5.3). However, the STM data of Figure 5.3 indicated that the C–H bonds were rotated by $7 \pm 3^\circ$ away from the center of neighboring -CH_3 group ($\angle$ A–B–C = 7° in Figure 5.3(b)).

The orientation of this rotation relative to the location of the underlying Si–Si bonds requires determining the registry of the methyl overlayer structure with that of the underlying Si lattice. The manufacturer of the Si wafers indicated that the flat supplied with the Si wafer was cut along the $<1\bar{1}0>$ direction, and this description was independently verified by X-ray diffraction measurements on these Si crystals. The physical orientation of the Si samples was controlled during the steps of wafer dicing and sample placement in the STM instrument so that the directions of the low-index planes of the Si crystal were precisely known, and are indicated in Figure 5.3(b).

The Si lattice orientation on such samples was furthermore independently verified by an analysis of the orientation of the triangular etch pits, such as those at the lower left corner of Figure 5.2(a), observed in STM images of the mounted sample. The step edges of such pits on the H-terminated Si(111) have been identified as the $<11\bar{2}>$ family, with termination by Si monohydride groups.[11] STM studies indicated that the step edges on such pits in the H-terminated Si(111) surface did not change orientation as a result of the two-

step chlorination/alkylation process. The orientation of the pits in Figure 5.2(a) therefore provided independent confirmation of the direction of the low-index lattice planes. Using these three independent verifications of the orientation of the Si crystal in the STM it was possible to identify the surface unit cell, which is indicated by the parallelogram drawn on Figure 5.3(b). This analysis determined that the C–H bonds of the methyl groups were rotated 7° toward the underlying Si–Si back bond.

5.4 Discussion

During the two-step chlorination/alkylation functionalization route, the Si surface is exposed to several harsh reactants including the Cl· radical and the methylmagnesium halide in hot solvents. As seen in Figure 5.2(b), this results in remarkably little etching or other deformation of the initial flat Si(111) surface. Low energy diffraction patterns of the CH_3-terminated surface, shown in Figure 5.1 confirm the long-range order of the functionalized surface, as well as demonstrating that the surface remains in an unreconstructed (1 x 1) configuration. One of the benefits of H-Si(111) is the low density of step edges along terraces or defect sites, and since that structure appears to be largely preserved on the CH_3-terminated surface, it is possible that the ideal electronic passivity of the H-terminated surface will also be preserved.

Based on prior photoelectron diffraction studies,[2] the topmost Si atoms are assumed to be located directly below the center of each triangular cluster of methyl-derived bright spots in the STM image. The resulting orientation of the Si unit cell relative to the STM bright spots of the sample is indicated by the parallelogram in Figure 5.3(b). Figure 5.4 presents a model for the structure of the CH_3-terminated surface that is consistent with the STM and crystal orientation data. This analysis indicates that the C–H bonds in the overlayer are rotated slightly toward the nearest Si–Si bonds in the underlying Si crystal, producing ∠ A–B–D in Figure 5.4 of 23°.

In order to understand the origin of the H–C–Si–Si torsional angle of 23°, calculations were performed by Santiago Solares of the California Institute of Technology. Small organic molecules such as $H_3C–CH_3$, $H_3C–SiH_3$, $H_3Si–SiH_3$, $CH_3–C(CH_3)_3$, and $SiH_3–$

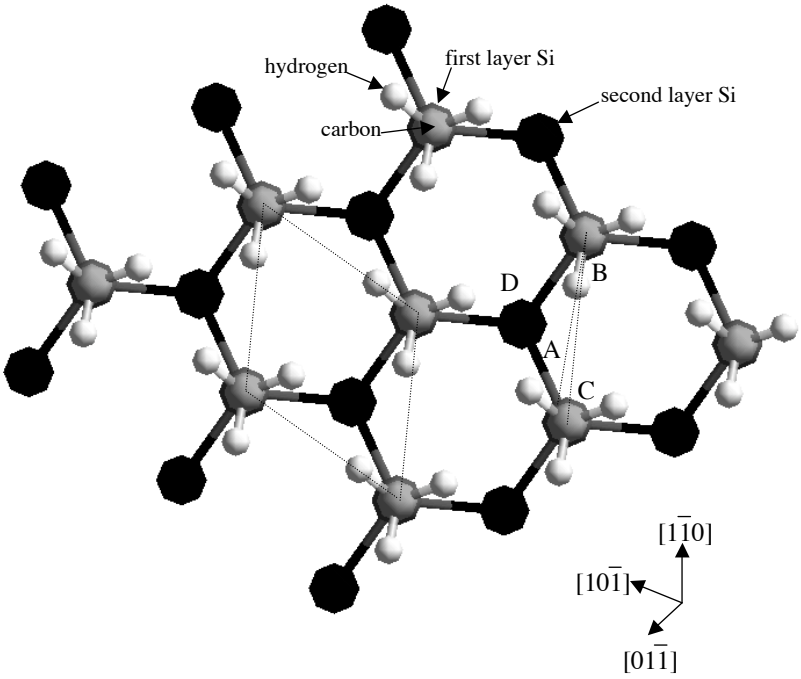

Figure 5.4: Proposed structural model of the CH_3-terminated Si(111) surface, viewed normal to the <111>plane. Light gray atoms are the carbons of the methyl group, white atoms are the hydrogens of the methyl groups, dark gray atoms are the first layer Si atoms (directly beneath the carbons), and black atoms are the second layer Si atoms. Crystallographic orientations are shown. A surface unit cell is outlined by the parallelogram. $\angle$ A–B–C is 7° and $\angle$ A–B–D is 23°. Figure adapted from Yu, *et al*.[9]

$Si(SiH_3)_3$ prefer the staggered conformation (by 2.68, 1.40, 0.94, 3.66, and 0.73 kcal/mol, respectively, at the B3LYP level with a 6311G**++ basis set). This type of interaction would be expected to yield an angle ∠ A–B–D of 60° for an isolated methyl group bonded to a Si(111) surface. This orientation, however, would place hydrogen atoms on adjacent methyl groups directly against one another, which a simple steric model suggests is highly unfavorable. Molecular mechanics calculations were performed in which the Si–C bond length was artifically increased to 1.0 nm to minimize interactions between the C–H and Si–Si bonds. The minimum-energy structure for such a surface was calculated to have an angle ∠ A–B–D of 30°, close to the 23° angle measured from the STM data, and confirming that the interactions that determine the packing of the CH_3-terminated Si surface are primarily the repulsions between hydrogen atoms on adjacent methyl groups in the functionalized organic overlayer. This is contrast with the conclusions of previous researchers in this field, whose model neglected to consider interactions between neighboring methyl groups.[6]

The repulsive methyl-methyl interactions are tempered, however, by an attractive preference for the eclipsed conformation of the C–H bonds relative to the underlying Si–Si bonds. This is manifested by a faborable interaction that produces an angle ∠ A–B–D of 23° on the methyl-terminated Si surface, as opposed to a repulsion between C–H methyl bonds and the S–Si bonds leading from the Si bonded to the methyl group, which would be expected to produce an angle ∠ A–B–D $>$30°. The cause of this preference has not yet been identified through calculations and is the subject of extensive ongoing theoretical analysis by Solares and coworkers.[12]

5.5 Conclusion

In summary, the two-step chlorination/alkylation process produced a highly ordered CH_3-terminated Si(111) surface with very few structural defects. Low energy electron diffraction patterns demonstrated the CH_3-terminated surface remains in an unreconstructed (1 x 1) configuration with very few surface defect sites such as etch pits. This observation was confirmed by UHV STM studies of the fully methylated surface at low temperature.

The methyl groups were frozen into discrete structural positions at 4.7 K, with the packing dominated by repulsive interactions between hydrogen atoms on adjacent methyl groups in the organic overlayer. Taken together, the data attest to the high degree of structural perfection obtainable on methylated Si surfaces that are produced through simple wet chemical methods. The structural perfection suggests that these surfaces can provide superior properties in many electrical and chemical applications where the H-terminated Si is too unstable to be used for extended time periods or for which organic functionalization is needed to impart desired chemical properties to the Si surface. While the CH_3-terminated Si(111) surface is the simplest and most ideal functionalized surface available to study, understanding the morphology of surfaces alkylated with longer or bulkier functional groups is important for gaining a complete picture of the alkylated surface. UHV STM studies of the C_2H_5-terminated Si(111) surface are therefore ongoing in our laboratory.

Acknowledgment

L. Henling is thanked for assistance with the X-ray diffraction experiments.

Bibliography

[1] Sieval, A. B.; van den Hout, B.; Zuilhof, H.; Sudholter, E. J. R. *Langmuir* **2001,** *17*, 2172–2181.

[2] Terry, J.; Linford, M. R.; Wigren, C.; Cao, R. Y.; Pianetta, P.; Chidsey, C. E. D. *Appl. Phys. Lett.* **1997,** *71*, 1056–1058.

[3] Linford, M. R.; Fenter, P.; Eisenberger, P. M.; Chidsey, C. E. D. *J. Am. Chem. Soc.* **1995,** *117*, 3145–3155.

[4] Bansal, A.; Li, X.; Yi, S. I.; Weinberg, W. H.; Lewis, N. S. *J. Phys. Chem. B* **2001,** *105*, 10266–10277.

[5] Bent, S. F. *Surf. Sci.* **2002,** *500*, 879–903.

[6] Yamada, T.; Kawai, M.; Wawro, A.; Suto, S.; Kasuya, A. *J. Chem. Phys.* **2004,** *121*, 10660–10667.

[7] Niwa, D.; Inoue, T.; Fukidome, H.; Akasaka, T.; Yamada, T.; Homma, T.; Osaka, T. *Chem. Lett.* **2004,** *33*, 284–285.

[8] Hunger, R.; Fritsche, R.; Jaeckel, B.; Jaegermann, W.; Webb, L. J.; Lewis, N. S. *Phys. Rev. B.* **2004,** in press.

[9] Yu, H.; Webb, L. J.; Ries, R. S.; Solares, S. D.; Goddard, W. A.; Heath, J. R.; Lewis, N. S. *J. Phys. Chem. B* **2005,** *109*, 671–674.

[10] Yu, H. **2005,** Personal communication.

[11] Hines, M. A. *Annu. Rev. Phys. Chem.* **2003,** *54*, 29–56.

[12] Solares, S. D.; Yu, H.; Webb, L. J.; Lewis, N. S.; Heath, J. R.; Goddard, W. A. **2005,** manuscript in preparation.

Chapter 6

High-Resolution Soft X-ray Photoelectron Spectroscopic Studies of the Air Oxidation of Alkylated Silicon(111) Surfaces

6.1 Introduction

Results presented in Chapters 3–5 describe the freshly prepared alkyl-terminated Si(111) surface prepared through a two-step chlorination/alkylation functionalization route before it has been exposed to even a mildly oxidizing environment like ambient air. When only exposed to an inert N_2(g) atmosphere, photoelectron and infrared spectroscopy and scanning tunneling microscopy studies have shown that this surface is cleanly terminated by approximately one monolayer of closely packed alkyl groups in a nearly ideal configuration predicted by the model shown in Figure 1.4. While this is interesting in its own right, if this chemistry is to have practical applications in microelectronics or photovoltaic devices, it is necessary that this ideal surface be maintained even as the sample is exposed to ambient air by preventing the growth of silicon suboxides, in contrast with the behavior of H-terminated silicon. It is therefore necessary to study the chemical activity of the alkyl-terminated surface as it is exposed to air over long time periods.

To address this issue, we have used high-resolution, "soft" X-ray photoelectron spectroscopy (SXPS) to investigate the oxidation of Si(111) surfaces alkylated with CH_3-, C_2H_5-, and $C_6H_5CH_2$- groups. The use of a high intensity beam of low energy photons

allows measurement of Si 2p photoelectrons that have low escape depths and thus provides enhanced surface sensitivity over what is typically possible using traditional X-ray generation sources in laboratory-based XPS instruments. The surface sensitivity of SXPS was used to identify and quantify the oxidation state and chemical environment of surface Si atoms functionalized with alkyl groups. To determine the importance of step edge-mediated oxidation processes, the oxidation of alkylated Si surfaces having varying densities of surface step edges was investigated by increasing the miscut from the (111) orientation, and scanning Auger microscopy (SAM) was used to measure spatial patterns of oxide growth on an alkylated Si(111) surface.

6.2 Experimental

6.2.1 Materials and Methods

For core photoelectron studies, 525 μm thick silicon(111) wafers polished on one side were obtained from Crysteco (Wilmington, OH). These n-type samples were doped with P to a resistivity of 2.0–8.5 Ω cm. To study the effect of step edge density on the air oxidation of alkylated surfaces, Sb-dobed, 0.005–0.02 Ω cm resistivity, flat, n-type Si(111) wafers with a miscut angle of $\pm 0.5^\circ$ were obtained from ITME (Poland). Additionally, stepped P-doped n-type Si(111) wafers with a resistivity of 0.005–0.02 Ω cm and a miscut angle of 7° were obtained from Montco Silicon Technologies (Spring City, PA).

Surface modification of the Si samples followed procedures detailed in Chapter 2. After spectra had been obtained on the freshly prepared surface, the samples were removed from the UHV system and were exposed to ambient air and light conditions to allow growth of Si oxides. The samples were periodically examined by SXPS to follow the growth of such oxides.

6.2.2 Instrumentation

6.2.2.1 SXPS Measurements

SXPS data were collected on Beamline U4A at Brookhaven National Laboratory, which is described extensively in Section 3.2.2.2. Several changes were made to data analysis procedures to accommodate for the presence of silicon oxide species on the surface. First, after background subtraction and spin-orbit stripping, the spectrum was fit to a series of Voigt line shapes[1] that were 5% Lorentzian and 95% Gaussian functions.[2,3] Once optimal fitting parameters for the binding energy and peak width of Si^{+}–Si^{4+} surfaces on the fully oxidized Cl-terminated surface were determined, those parameters were used to fit all other surfaces while only the peak height was allowed to float freely. This was done to determine any differences between samples in the growth of specific oxidation states of Si.

The simple overlayer-substrate model described in Section 3.2.2.2 was employed here to calculate the total monolayer coverage of surface species observed by SPXS.[2–4] The model as described previously was a simplification of a more complicated description that is necessary when analyzing a silicon surface covered with oxides. In this method, the number density of modified surface Si atoms, $\Gamma_{Si,surf}$, was deduced from the ratio of the integrated area under the Si peak assigned to the surface atoms, $I_{Si,surf}$, to the integrated area of the Si peak assigned to bulk Si atoms $I_{Si,bulk}$:

$$\frac{I_{Si,surf}}{I_{Si,bulk}} = \frac{\Gamma_{Si,surf}\sigma_{Si,surf}}{n_{Si,bulk}\sigma_{Si,bulk}l_{Si} - \Gamma_{Si,surf}\sigma_{Si,surf}} \tag{6.1}$$

In this expression, $n_{Si,bulk}$ is the atom density of bulk crystalline Si (5.0 x 10^{22} cm^{-3}),[5] $\sigma_{Si,surf}$ and $\sigma_{Si,bulk}$ are the photoinonization cross-sections of the surface and bulk species, respectively, and l_{Si} is the electron escape depth, which was 3.5 Å for the data presented herein. The photoionization cross-sections of Si^{0}–Si^{4+} species have been studied extensively by SXPS on surfaces with well-ordered SiO_2 layers of known thicknesses.[4] Near the photon excitation energy used in this work (140 eV), $\sigma_{SiO_2}/\sigma_{Si}$ ~2, while Γ_{SiO_2}/n_{Si} ~0.5, thus approximately canceling out of the surface intensity factor.[4] For the highly amorphous suboxides grown in air in these studies, $n_{Si^{n+}}$ values are not known, cannot be accurately

estimated, and would have to be measured from studies of the thickness of the disordered layer. Therefore, throughout the analysis presented here, $\sigma_{Si^{n+}}$ was approximated as constant for Si^{+}–Si^{4+}, simplifying Eq. 6.1 to:

$$\frac{I_{Si,surf}}{I_{Si,bulk}} = \frac{\Gamma_{Si,surf}}{n_{Si,bulk}l_{Si} - \Gamma_{Si,surf}} \tag{6.2}$$

Substituting $I = I_{Si,surf}/I_{Si,bulk}$ and $\Gamma_{Si,bulk} = n_{Si,bulk}l_{Si}$ into Eq. 6.2 and rearranging yields:

$$\Gamma_{Si,surf} = \frac{I}{1+I}\Gamma_{Si,bulk} \tag{6.3}$$

which was previously seen as Eq. 3.7 in Section 3.2.2.2. Dividing the calculated value of $\Gamma_{Si,surf}$ by the number density of atop sites on the Si(111) surface, $n_{Si,surf}$ = 7.8 x 10^{14} cm^{-2},[4] gives the monolayer coverage of modified Si atoms. The distance between Si layers along a vector perpendicular to the Si(111) crystal face is 1.6 Å, implying that an electron escape depth of 3.5 Å will sample 2.2 monolayers of the Si crystal.

6.2.2.2 XPS Measurements

To determine the influence of step edges on functionalized Si(111) surface oxidation, core photoelectron spectra were collected according to the procedures described in Section 3.2.2.1.

6.2.2.3 SAM Measurements

Spatial resolution of surface oxidation was explored on a Physical Electronics (PHI) 680 Scanning Auger Nanoprobe at the High Temperature Materials Laboratory at Oak Ridge National Laboratory. The sample was introduced through a load lock into a UHV chamber maintained at $\leq 10^{-10}$ Torr. The sample was impinged with an electron beam that was held normal to the surface and maintained at 20 kV and 10 nA for a spatial resolution of 15 nm. Auger electrons were collected by a cylindrical mirror analyzer coaxial to the field emission electron gun. Secondary electron images of the sample were used to identify a debris-free region of the sample surface. Auger electron intensities were then collected

over an area approximately 1 μm square divided into 128 x 128 bins for a pixel width of 7.8 nm. The scan area was periodically calibrated with a scanning electron microscope (SEM) image of a nearby piece of debris in order to account for spatial drift in the image over the scan time. Between 1–5 such scans were added together for the final image. Care was taken to collect data quickly in order to minimize damage to the alkyl overlayer by the impinging electron beam. Because the amount of SiO_2 on the surface of alkylated samples was very small, it was not possible to collect spectra of the SiO_2 signal (72–76 eV) in a short enough amount of time to prevent beam damage. Instead, signal from the Si LVV (90–92 eV)[6–8] and O KLL (510 eV)[9] regions were combined to determine areas of SiO_2 in the SAM image. Spectra were collected with the electron analyzer held in the Si LVV region (92 eV) and the O KLL region (510 eV), which were then superimposed to create a composite image of Si and SiO_2.

6.3 Results

6.3.1 SXPS Analysis of Alkylated Surfaces

6.3.1.1 Cl-Terminated Si(111)

Figure 6.1 shows the SXPS results of a Cl-terminated Si(111) surface immediately after preparation and as it was allowed to oxidize in air for 48 hr. The spectra in Figure 6.1 are shown after subtraction of the Shirley background and after stripping out the Si $2p_{1/2}$ contribution, leaving only the $2p_{3/2}$ component of the Si peak. The freshly prepared surface, which was described in Chapter 3,[10] displayed a peak 0.83 eV higher in binding energy than the bulk Si $2p_{3/2}$ peak, which represented a surface coverage of 0.99 equivalent monolayers (ML). This peak was assigned to the chlorinated surface Si atoms, which are more positive than the Si atoms in the bulk lattice because of the electron-withdrawing effects of Cl. A small feature 1.37 eV higher in binding energy than the bulk peak and which represented 0.11 equivalent ML was tentatively assigned to dichlorinated Si presumably present along step edges or etch pits. A survey XPS scan of the freshly prepared surface, shown in Figure 6.2(a), revealed some amount of adventitious O 1s signal. This adventitious species could

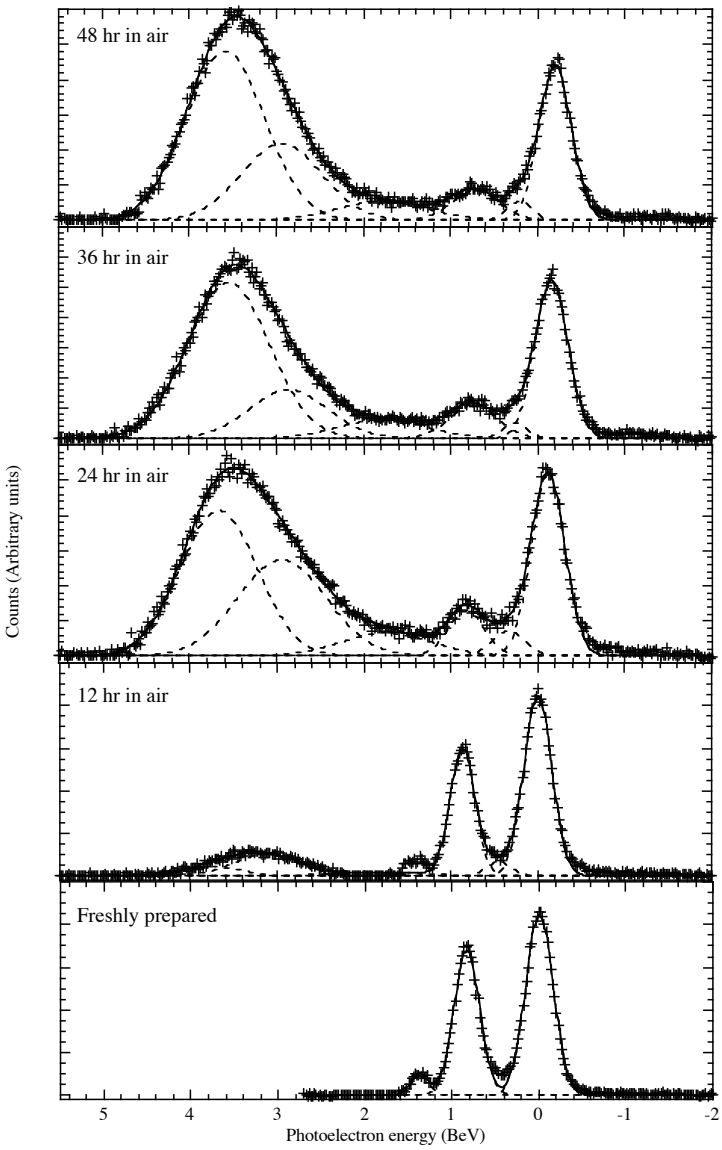

Figure 6.1: Chlorine-terminated Si(111) surface freshly prepared then allowed to sit in air for 12, 24, 36, and 48 hr. The scale is binding energy (BeV) relative to the center of the bulk Si $2p_{3/2}$ peak of the freshly prepared surface. All spectra are shown after background removal, spin-orbit stripping, and peak fitting. In all cases, cross marks are the raw data, dashed lines are the fitted curves, and the solid line is the calculated curve fit. The anomalous break in the pattern of growth of Si suboxides on the sample kept in air for 24 hr was most likely due to some contribution to the signal from the sample holder because of an ill-focused beam.

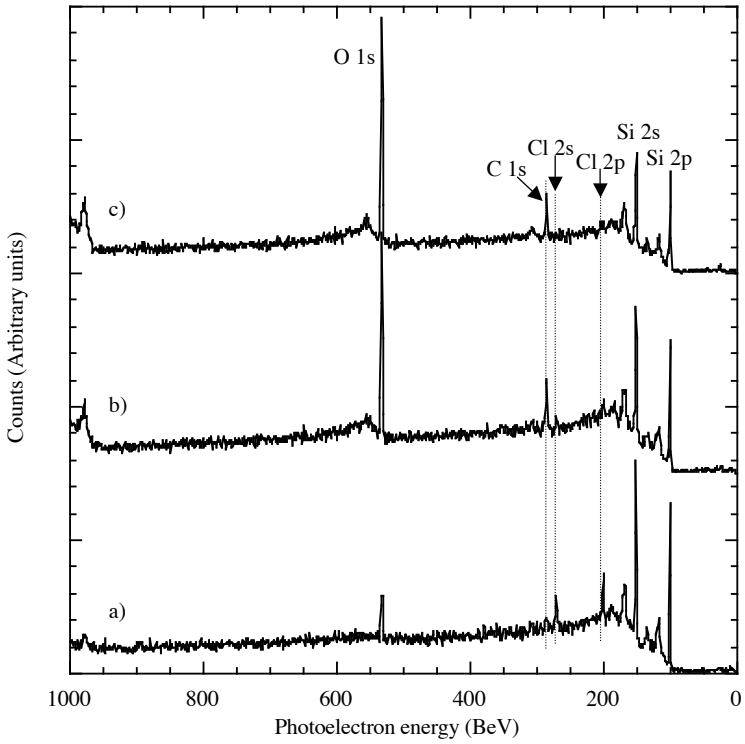

Figure 6.2: XPS of Cl-Si(111) surfaces freshly prepared, then exposed to ambient air for a period of up to 54 hr. a) Freshly prepared surface; b) in air 20 hr; c) in air 54 hr.

be from a number of sources, including absorbed solvent from the wet chemical preparation techniques, absorbed pump oil vapor introduced in the quick-entry load lock, or contaminating dust particles covered with oxygen-containing organic molecules that were not possible to avoid when working in standard laboratory conditions. The principal concern of this study was the growth and characterization of silicon oxides, and because of the uncertainty of the origin of the O 1s signal, this peak was not used to identify the presence of silicon oxides on the surfaces described here. The Si 2p region, which has specific and extensively studied spectroscopic shifts introduced by Si^{+}–Si^{4+} oxides[4,11] was examined instead to address this critical question. The fact that the freshly prepared Cl-terminated surface was free of silicon oxides in the region of higher binding energy above the bulk Si $2p_{3/2}$ peak is clearly demonstrated in Figure 6.1.

When exposed to ambient air, the chlorinated Si surface reacted rapidly, losing the Si–Cl feature and growing silicon oxides at higher binding energy (Table 6.1). After 12 hr in air, the monolayer coverage of the peak approximately 0.8 eV higher in binding energy than the bulk peak, assigned to surface Si bonded to Cl atoms, dropped from 0.99 ML[10] to 0.87 ML, while a large, broad signal of oxide centered at +3.13 eV above the bulk Si $2p_{3/2}$ peak appeared. This feature was accompanied by smaller suboxides at 1.85 eV and 3.74 eV above the bulk Si $2p_{3/2}$ peak, representing a total equivalent monolayer coverage of 1 ML of silicon oxides.

As air exposure of the Cl-Si(111) surface continued, the growth of the surface oxide features correlated qualitatively to loss of the signal from surface Cl-bound Si atoms, ≈0.9 eV above the bulk Si $2p_{3/2}$ peak. As can be seen in Table 6.1 and Figure 6.1, after the surface had been exposed to air for 12 hr, the monolayer coverage of the highest order Si oxide (Si^{4+}, +3.74 eV) grew from below the detection limit of the instrument to 0.21 ML. By the time the sample had been in air for 24 hr, the amount of Cl-bound Si atoms detected on the surface had dropped to only ≈0.5 ML, while the highest order oxide (Si^{4+}, +3.78 eV) grew to 1.45 ML. A XPS survey scan of the Cl-terminated surface collected after the sample had been exposed to air for 20 hr (Figure 6.2(b)) confirmed that the Cl 2s and 2p signals at 200 BeV and 270 BeV, respectively, had dropped significantly from the freshly prepared surface, indicating that most of the Cl present on the surface had disappeared. At

R-	Time in air (hr)	Bulk peak[b] location (eV)	SXPS peak shift and integrated area[a]										Total surface coverage (ML)
			Surface Si-X		"Si^{+}"		"Si^{2+}"		"Si^{3+}"		"Si^{4+}"		
			shift (eV)	coverage (ML)	shift (eV)	coverage (ML)	shift (eV)	coverage (ML)	shift (eV)	coverage (ML)	shift (eV)	coverage (ML)	
			X=Cl		silicon oxides								
Cl-	12	98.64	0.87	0.87	–[c]	–[c]	1.85	0.15	3.13	0.49	3.74	0.21	1.87
	24	98.52	0.94	0.47	–[c]	–[c]	1.86	0.57	3.06	1.30	3.78	1.45	4.06
	36	98.48	0.89	0.53	–[c]	–[c]	1.94	0.53	3.02	0.95	3.71	1.59	3.75
	48	98.44	0.92	0.49	–[c]	–[c]	1.99	0.57	3.15	1.24	3.79	1.62	4.12
			X=C		silicon oxides								
CH_3-	12	98.04	0.30	1.03	0.79	0.08	–	–	–	–	–	–	1.11
	24	98.04	0.31	0.86	0.76	0.06	1.76	$<$0.01	3.11	0.05	3.88	0.04	1.02
	36	98.08	0.30	0.95	0.79	0.08	1.72	$<$0.01	3.07	0.05	3.75	0.09	1.17
	48	98.05	0.31	0.89	0.75	0.07	1.75	$<$0.01	3.10	0.13	3.80	0.07	1.16
C_2H_5-	12	98.19	0.19	0.77	0.61	0.23	1.57	0.04	–	–	–	–	1.04
	24	98.21	0.17	0.66	0.74	0.23	1.78	0.07	3.12	0.06	3.87	0.03	1.05
	36	98.19	0.21	0.76	0.81	0.17	1.85	0.07	3.10	0.13	3.84	0.02	1.15
	48	98.19	0.21	0.71	0.81	0.24	1.85	0.14	3.10	0.15	3.84	0.09	1.33
$C_6H_5CH_2$-	12	98.24	0.18	0.56	0.79	0.33	1.79	0.06	3.16	0.10	3.81	0.03	1.07
	24	98.25	0.17	1.00	0.78	0.27	1.78	0.04	3.19	0.08	3.75	0.03	1.43

Table 6.1: Si $2p_{3/2}$ SXPS data on functionalized Si surfaces oxidized in air for up to 48 hr. [a]Calculated from Eq. 6.3. [b]Absolute energies for the bulk Si $2p_{3/2}$ peak are reported for thoroughness, but are of limited use because the excitation energy was not calibrated. [c]No deconvolution of the shifts of Si–Cl and Si^{+} was attempted.

this point it was difficult to determine if the SXPS peak previously assigned as Cl-bound surface Si atoms was actually cleanly functionalized Cl-Si(111), or rather represented an amorphous Si^{+} substrate.

After the Cl-Si(111) surface had been exposed to air for 48 hr, the XPS survey scan shown in Figure 6.2(c) indicated only a small fraction of any Cl remained on the surface. It is possible that the surface was stabilized to further oxidation with a submonolayer coverage of surficial Cl moieties still present, but SXPS data do not eliminate the possibility that our detection of the Si–Cl peak was hampered as it was convoluted with larger Si^{+} or Si^{2+} oxides. Features representing Si^{2+} (+1.99 eV), Si^{3+} (+3.15 eV), and Si^{4+} (+3.79 eV) oxides dominated the spectrum. The Si^{4+} oxide had a total surface coverage of 3.63 ML. Because a penetration depth of 3.5 Å used in these studies only sampled approximately 2.2 ML perpendicular to the (111) crystal face, this high monolayer coverage is possibly a result of the limitations of the quantitative analysis of surface species described by Eq. 6.3, which might be inadequate for the amorphous surface described here. It is possible to state conclusively, however, that after 48 hr in ambient air the Cl-terminated Si(111) surface had thoroughly reacted to create an amorphous silicon oxide layer that, on the scale of our surface sensitive conditions, was reasonably thick.

6.3.1.2 CH_3-Terminated Si(111)

A CH_3-terminated Si(111) surface prepared through a two-step chlorination/alkylation procedure was exposed to air, and substrate oxide growth was monitored by SXPS. Results of these studies are shown in Figure 6.3. The differences between the behavior of these methylated surfaces and the chlorinated surfaces discussed previously are striking and are described quantitatively in Table 6.1. After 48 hr in air, the peak at 0.3 eV higher binding energy than the bulk Si $2p_{3/2}$ peak, assigned to surface Si atoms bonded to the methyl carbon atom,[10] did not shift substantially in binding energy or representative monolayer coverage.

When the methyl-terminated surface had been exposed to air for 48 hr, a broad feature representing oxidation states of Si^{2+}–Si^{4+} but centered on the Si^{3+} oxidation state at +3.10 eV above the bulk Si $3p_{3/2}$ peak appeared, representing a total of 0.20 ML. Evidence for

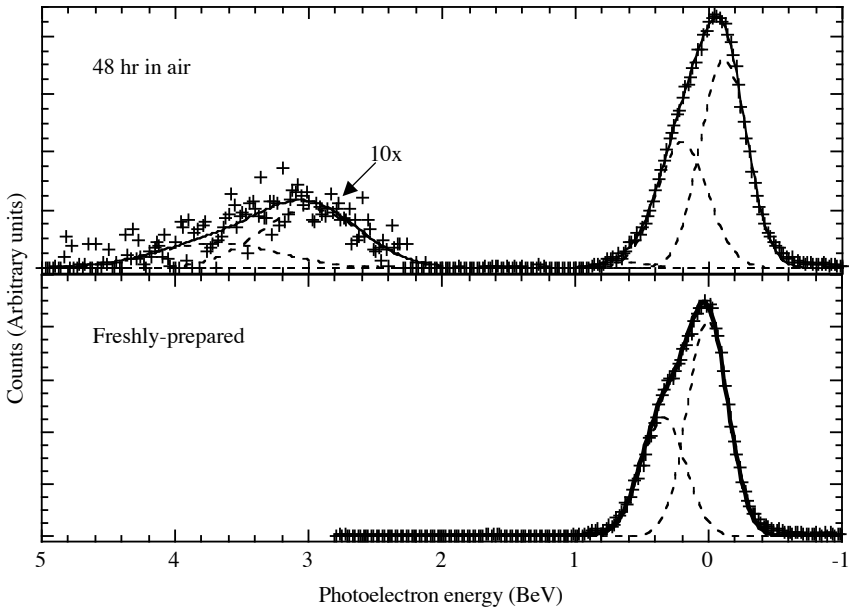

Figure 6.3: CH_3-terminated Si(111) surface freshly prepared then allowed to sit in air for 48 hr. The scale is binding energy (BeV) relative to the center of the Si $2p_{3/2}$ bulk peak of the freshly prepared surface. All spectra are shown after background removal, spin-orbit stripping, and peak fitting. In all cases, cross marks are the raw data, dashed lines are the fitted curves, and the solid line is the calculated curve fit. In the spectrum of the oxidized surface, the region above 2 BeV is shown expanded 10x.

Si^{+}, Si^{3+}, and Si^{4+} species was observed in quantities just above the detection limit of the instrument, and negligible amounts of Si^{2+} were observed. Moreover, when the samples were again examined after 2 months of exposure to ambient air, no increase in suboxide coverage, no peak shifts, nor any other substantial change on the surface was observed (data not shown). While the observation time of silicon oxide formation on these surfaces was limited, it is clear that the CH_3-terminated Si(111) surface was remarkably passivated to chemical oxidation.

6.3.1.3 C_2H_5-Terminated Si(111)

The Si(111) surface was also functionalized with C_2H_5-groups and chemical oxidation was observed as a function of time exposed to ambient air. The SXPS behavior of this surface, shown in Figure 6.4 and described in Table 6.1, was similar to that of the CH_3-terminated Si surface. A feature in the spectrum of the freshly prepared ethyl-terminated surface at 0.19 eV above the bulk Si $2p_{3/2}$ peak, previously identified as surface Si atoms bonded to the C of the ethyl group,[10] did not shift significantly over time, indicating that the Si–C bonds formed in the alkylation procedure were not substantially altered by exposing the surface to ambient air. A peak observed on the freshly prepared surface 0.81 eV higher in binding energy than the silicon bulk peak also did not increase in amplitude with time, comprising only 0.25 ML after 48 hr of air exposure. Small features corresponding to silicon oxides were observed at +1.85 eV, +3.10 eV, and +3.84 eV above the bulk Si $2p_{3/2}$ peak, also at 48 hr of air exposure. These signals together comprised 0.62 equivalent ML of oxide, with the Si^{+} species representing the greatest portion of suboxide present. Taken together, these three peaks on the Si surface after 48 hr of air exposure indicated that a range of silicon suboxides from Si^{+} to Si^{4+} were present, although in significantly reduced quantities relative to the unpassivated Cl-terminated Si(111) surface. Unlike the CH_3-terminated surface, the C_2H_5-terminated surface had significant quantities of both Si^{+} and Si^{3+} suboxides.

6.3.1.4 $C_6H_5CH_2$-Terminated Si(111)

The Si(111) surface was also functionalized with benzyl groups. Such functionalized surfaces (Figure 6.5, Table 6.1) behaved similarly to those alkylated with straight-chain hy-

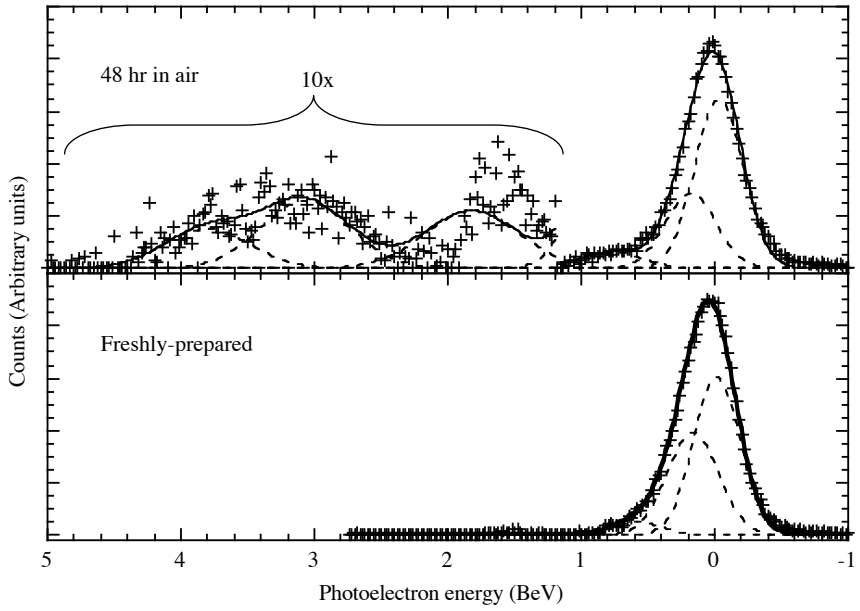

Figure 6.4: C_2H_5-terminated Si(111) surface freshly prepared then allowed to sit in air for 48 hr. The scale is binding energy (BeV) relative to the center of the bulk Si $2p_{3/2}$ peak of the freshly prepared surface. All spectra are shown after background removal, spin-orbit stripping, and peak fitting. In all cases, cross marks are the raw data, dashed lines are the fitted curves, and the solid line is the calculated curve fit. In the spectrum of the oxidized surface, the region above 1 BeV is shown expanded 10x.

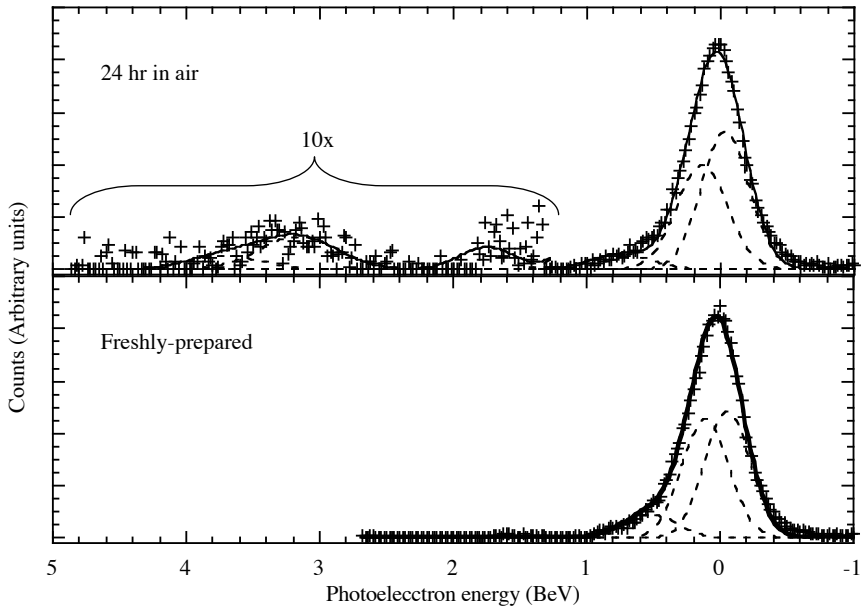

Figure 6.5: $C_6H_5CH_2$-terminated Si(111) surface freshly prepared then allowed to sit in air for 48 hr. The scale is binding energy (BeV) relative to the center of the bulk Si $2p_{3/2}$ peak of the freshly prepared surface. All spectra are shown after background removal, spin-orbit stripping, and peak fitting. In all cases, cross marks are the raw data, dashed lines are the fitted curves, and the solid line is the calculated curve fit. In the spectrum of the oxidized surface, the region above 1 BeV is shown expanded 10x.

drocarbons; after 1 day in air, peaks present on the freshly prepared surface, at $\sim$0.2 eV and $\sim$0.8 eV higher in binding energy than the bulk Si $2p_{3/2}$ peak, changed binding energy and intensity only slightly. During the same period, only small oxide peaks 1.78 eV, 3.19 eV, and 3.75 eV higher than the bulk Si $2p_{3/2}$ peak, together representing $<$0.5 ML, were observed. As on the C_2H_5-terminated surface, the Si^+ and Si^{3+} signal (+0.78 eV and +3.19 eV above the Si $2p_{3/2}$ bulk peak, respectively) comprised the majority of the oxide signal.

6.3.2 Oxidation Rates of Stepped Surfaces

To determine if Si surface alkylation prevented deleterious oxidation by interrupting possible step edge-mediated oxidation mechanisms,[12] alkyl-terminated surfaces of differing step-edge density were prepared and stored in ambient air in the dark for a period of up to 6 weeks. Surfaces with a higher miscut angle have smaller terrace sizes, and thus a higher fraction of the exposed surface lies along step edges instead of on the atomically flat terraces. A small change in miscut angle leads to a dramatic change in the step edge density of the surface. With a 0.5° miscut, 1 in every $\sim$600 surface Si atoms lies along a step edge. Increasing the miscut to 7° increases the step-edge density by two orders of magnitude, resulting in a surface on which 1 in every 7 surface Si atoms lies along a step edge. Figure 6.6(a) compares the oxidation of CH_3-terminated Si(111) surfaces having a miscut angle of either $\leq$0.5° or 7°. Figure 6.6(b) shows such a comparison for C_2H_5-terminated surfaces. In both cases, after normalization for peak intensity, at no time during the course of the air oxidation was any difference observed in native oxide growth on surfaces with different miscut angles, and therefore with different surface step-edge densities. When the spectra were deconvoluted into the characteristic oxidation peaks of Si, contributions from Si^+ and Si^{3+} species were again a larger part of the Si oxidation peak than the other two available oxidation states.

6.3.3 SAM of Alkyl-Terminated Si(111) Samples

Another method of testing if Si surface oxidation begins at step edges is scanning Auger microscopy, which can spatially resolve any chemical inhomogeneity on the Si surface.

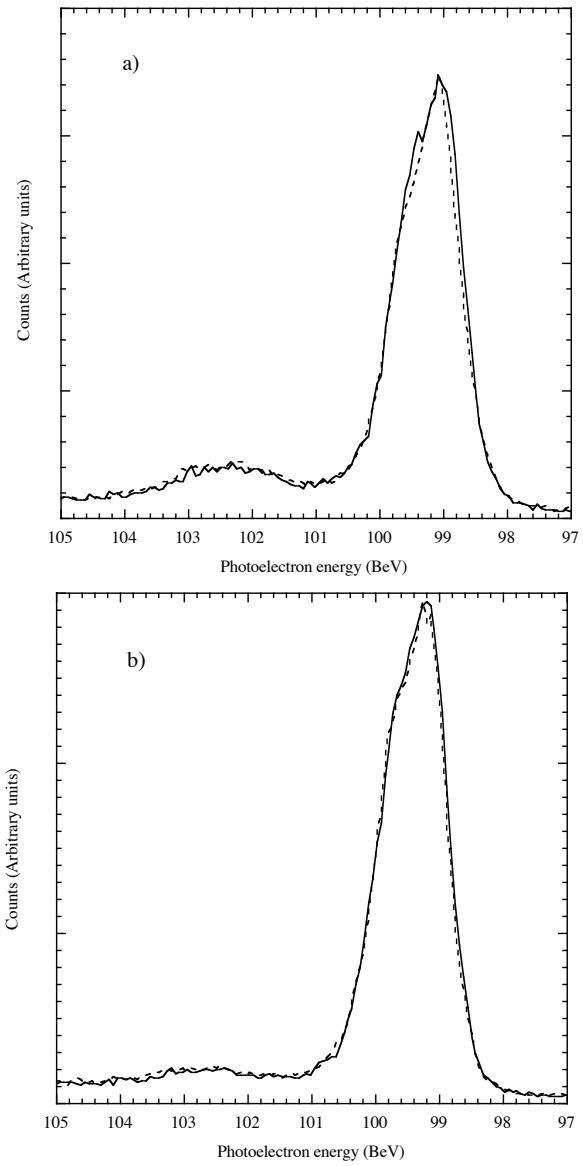

Figure 6.6: XPS of the Si 2p region of alkyl-terminated Si(111) surfaces at different miscut angles. The spectra have been normalized for intensity. a) CH_3-Si(111) stored in ambient air in the dark for 39 days. Solid line: surface miscut $\leq 0.5^\circ$; dashed line: surface miscut 7°. b) C_2H_5-Si(111) stored in ambient air in the dark for 19 days. Solid line: surface miscut $\leq 0.5^\circ$; dashed line: surface miscut 7°.

There is a well-documented shift in the Si LVV Auger electron peak from 92 eV for Si^0 to 75 eV for Si^{4+} in SiO_2,[6–8] which could be used to map regions of SiO_2 on an otherwise clean Si surface. When SAM was conducted on the C_2H_5-terminated surface, the impinging electron beam was found to damage the alkyl overlayer on the surface before sufficient data could be collected on the low signal from any existing SiO_2 regions on the surface. To overcome this problem, two spectral maps of the surface were collected: one of the Si LVV region at 92 eV, and one of the O KLL region at 510 eV. These spectra were then superimposed to create a composite image in which areas of Si could be distinguished from areas of Si + O due to silicon oxides.

On a freshly prepared C_2H_5-Si(111) sample, SAM images revealed a homogeneous surface when scanning in both the Si LVV and O KLL energy regions (Figure 6.7). When an identically prepared C_2H_5-Si(111) sample that had been exposed to air and light for 8 days was investigated with SAM, discrete chemically altered regions of the surface were clearly visible. In a regular SEM image (Figure 6.8(a)) discolored portions of the Si surface appeared in patches running approximately parallel to each other. The Auger electron spectra of these patches versus the background surface are shown in Figure 6.8(b). The lightly colored patches showed a decreased concentration of Si^0 but an increased concentration of O when compared to the otherwise clean Si background. In the SAM image of the same area scanning in the Si LVV energy region (Figure 6.8(a)), these patches appeared as areas deficient in Si LVV signal at 92 eV, while in the O KLL energy region SAM image these patches appeared to have higher concentrations of O. These two images are also presented overlayed in Figure 6.8(a). Although XPS data presented above indicates that even freshly prepared alkyl-terminated surfaces contained some amount of non-oxide O 1s (Figure 3.1(c)–(d)), SAM studies presented here found that on the oxidized alkyl surface, the O KLL signal was concentrated in specific regions of the Si surface.

6.4 Discussion

There have been several examples of the ability of chemical functionalization of the Si single crystal surface to reduce and in some cases halt the formation of active surface charge

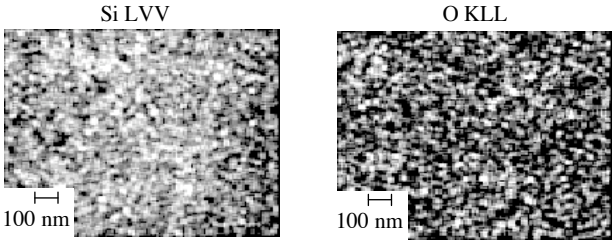

Figure 6.7: SAM image of a freshly prepared C_2H_5-terminated Si(111) surface investigated in both the Si LVV (92 eV, left) and the O KLL energy regions (510 eV, right). Both images were collected in 128 x 128 point scans with an electron beam held at 20 kV and 10 nA with spatial resolution of 15 nm. The individual pixel scans were combined to form an image map.

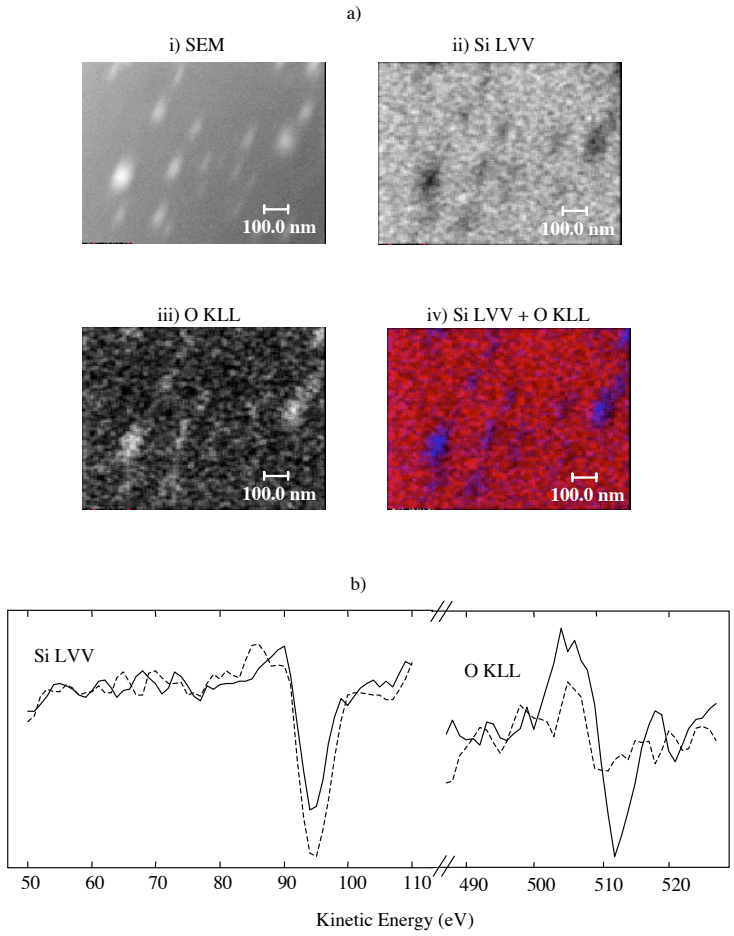

Figure 6.8: Auger electron spectroscopy of a C_2H_5-terminated Si(111) surface exposed to air for 8 days. a) SAM images of a $\sim$1 μm^2 area of the surface: i) SEM image of the surface; ii) SAM image collected by scanning in the Si LVV energy region (92 eV). Lighter gray indicates greater Si signal; iii) SAM image collected by scanning in the O KLL energy region (510 eV). Lighter gray indicates greater O signal; iv) composite SAM image of the overlayed maps of the Si LVV (red) and O KLL (blue) energy regions. SAM images were collected in 128 x 128 point scans with an electron beam held at 20 kV and 10 nA with a spatial resolution of 15 nm. The individual pixels were then combined to form an image map. b) Auger electron spectroscopy of a point on an isolated white discolored region in the SEM image (solid line) and on the dark background in the SEM image (dashed line).

carrier recombination trap sites.[2,13] This remarkable electrical pssivation has been correlated experimentally to the absence of large amounts of deleterious native silicon oxides, which can provide numerous defect sites at the disordered Si/SiO_x interface.[2,14] The relationship between low rates of surface electron-hole recombination and lack of native silicon oxides appears to be a complicated one, however, as shown in detail in the data presented here. Alkylated surfaces of single crystal Si(111) were investigated by SXPS under high surface sensitivity conditions to measure both the amount and oxidation state of native oxides introduced when exposed to air. We found that although the rate of silicon oxidation was dramatically slowed, some amount of silicon oxide did in fact appear. The native oxide on an unpassivated Cl-terminated Si(111) surface covered all available oxidation states of Si, from Si^{+} to Si^{4+}, with the majority of the oxide signal from Si^{4+} species. This is similar to what has been observed previously on unpassivated H-terminated Si surfaces.[15–18] In contrast, the submonolayer of native oxide observed on the alkyl-terminated surfaces described here appeared to correspond principally to Si^{+} and Si^{3+}, albeit with small contributions from Si^{2+} and Si^{4+} oxidation states.

The difference in Si oxidation states on the passivated versus unpassivated surfaces could be useful in determining the structure of the native oxide developing on those surfaces. The structure of the Si/SiO_2 interface has been the subject of prolonged interest because of its importance in integrated circuit fabrication.[4,16,19–26] Although the structure of the Si/SiO_2 interface depends on crystal face and growth conditions, it is generally agreed that the junction is not abrupt, but contains an amorphous region $\geq$3 Å thick where all five oxidation states of Si (Si^{0}–Si^{4+}) are found.[19,25] Previous core photoelectron spectroscopic studies of the Si(111)/SiO_2 interface have shown that Si^{+} and Si^{3+} are more abundant than Si^{2+} because disrupting an atomically flat (111) surface through layer-by-layer oxidation will cleave either 1 or 3 tetrahedral Si bonds.[4,16,19,24,25] To have periodic Si^{+}, however, it is necessary also to have some concentration of Si^{4+}, which our data suggests is present only in very small quantities. Two Si bonds will be cleaved only at step edges and etch defects, which are a minor component of Si(111) surfaces prepared in this manner (Chapter 5). The SXPS data alone, therefore, suggest that the slow oxidation of alkyl-terminated Si(111) surfaces creates discrete patches of amorphous oxide that are spatially isolated from each

other.

Another difference between the unpassivated and passivated surfaces studied here was the behavior of surface-bound species as the sample was exposed to oxidizing conditions. Studies of native oxidation growth of H-Si(111) surfaces at room temperature have previously shown that the first oxidation step is insertion of O into a Si–Si backbound, not attack of the stronger Si–H bond.[22,23,26] The data presented here on alkylated Si surfaces show the same behavior, in that Si–C features remain largely unchanged during the first several days of surface oxidation. On the Cl-terminated surface, the monolayer coverage of Cl atoms dropped precipitously after the sample had been in air for only 12 hr during the initial oxidation events. On alkylated surfaces, however, features in the spectra of the freshly prepared sample that have been previously identified as surface Si atoms bonded to carbon[10] did not shift significantly either in binding energy or in monolayer coverage. This indicates that the surface Si–C bonds are not altered by the oxidizing environment.

It has been suggested that oxidation of the Si(111) surface proceeds fastest at step edges, rather than along the atomically flat terraces.[12] One possible explanation for the remarkable surface passivation reported here for alkylated Si(111), even when protected by bulky alkyl groups, is that the role of the surface-bound moieties is to passivate step edges, thereby preventing the initial oxidation events that quickly destroy the unpassivated H- or Cl-terminated Si(111) surface. If the bulky alkyl group only must bond to step-edge Si atoms and not to every surface Si atom in order to achieve adequate passivation, even large functional groups would work reasonably well. One test of this hypothesis is to observe the rate of oxidation on identically functionalized Si surfaces with differing step-edge densities, which can be obtained easily by increasing the miscut of the sample away from the (111) surface. When CH_3- and C_2H_5-terminated Si(111) surfaces of different miscut angles were exposed to air for long time periods, however, no difference in oxidation rate or total amount of oxide of these surfaces was observed, indicating that any step-edge effects of alkylation are negligible. SAM studies, however, do confirm that oxide is growing on the C_2H_5-Si(111) surface in a non-uniform manner that suggests that the alkyl-terminated surfaces does prevent a continuous, general oxide from growing on the surface. Further investigation is required to determine if this oxide is nucleating specifically at step-edge or

other defect sites, or if its growth is initiated by some other mechanism.

6.5 Conclusion

Surface sensitive SXPS of Si(111) surfaces alkylated through a two-step chlorination/ alkylation technique has been used to investigate the growth of native oxides on samples kept in ambient air. We have found that this alkylation technique drastically reduces the growth of silicon oxides over a time period of at least 2 months, allowing $<$0.40 ML of silicon oxides to form. The oxide that is observed is principally Si^{+} and Si^{3+}, with very limited contributions from the other silicon suboxides that are seen on unpassivated Si surfaces exposed to the same ambient conditions. This effect was, to first order, identical for surfaces alkylated with both small CH_3- groups and larger, bulkier C_2H_5- and $C_6H_5CH_2$- moieties that are not sterically able to fit on every surface Si atom. Furthermore, SAM investigations of the freshly prepared and oxidized C_2H_5-terminated Si(111) surface demonstrated that silicon oxides do not grow uniformly on the surface, but instead appear in small patches, leaving the rest of the Si surface clean. This observation is surprising, and one possible explanation is that surface alkylation is important only by protecting the step edges from oxidation, leaving the terraces to oxidize at the same slow rate.[12] When the oxidation behavior of two surfaces of differing step-edge density were compared, however, no difference in Si oxide growth was seen over a period of several weeks. This result indicates that oxidation on these alkylated Si surfaces is a complex process that requires significant further investigation before the goal of understanding Si surfaces and manipulating them at will can be realized.

Acknowledgment

This research was carried out in part at the National Synchrotron Light Source, Brookhaven National Laboratory, which is supported by the U.S. Department of Energy, Division of Materials Sciences and Division of Chemical Sciences, under Contract DE-AC02-98CH-10886. This research was sponsored in part by the Assistant Secretary for Energy Efficiency

and Renewable Energy, Office of Freedom CAR and Vehicle Technologies, as part of the High Temperature Materials Laboratory User Program, Oak Ridge National Laboratory, managed by UT-Battelle, LLC, for the U.S. Department of Energy under contract number DE-AC05-00OR22725.

Bibliography

[1] Sherwood, P. M. A. Data Analysis in XPS and AES. In *Practical Surface Analysis*, Vol. 1; Briggs, D.; Seah, M. P., Eds.; John Wiley & Sons Ltd: New York, 1990.

[2] Webb, L. J.; Lewis, N. S. *J. Phys. Chem. B* **2003,** *107*, 5404–5412.

[3] Haber, J. A.; Lewis, N. S. *J. Phys. Chem. B* **2002,** *106*, 3639–3656.

[4] Himpsel, F. J.; McFeeley, F. R.; Taleb-Ibrahimi, A.; Yarmoff, J. A.; Hollinger, G. *Phys. Rev. B.* **1988,** *38*, 6084–6096.

[5] Sze, S. M. *The Physics of Semiconductor Devices;* Wiley: New York, 2nd ed.; 1981.

[6] Kanashima, T.; Maida, O.; Kohma, N.; Agata, M.; Yudate, S.; Ueno, M.; Okuyama, M.; Ohashi, H. *Jpn. J. Appl. Phys.* **2001,** *40*, 4195–4196.

[7] Hwang, D. S.; Yasuda, T.; Ikuta, K.; Yamasaki, S.; Tanaka, K. *Jpn. J. Appl. Phys.* **1998,** *37*, 4204–4208.

[8] Helms, C. R.; Poindexter, E. H. *Rep. Prog. Phys.* **1994,** *57*, 791–852.

[9] van Oostrom, A.; Augustus, L.; Habraken, F. H. P. M.; Kuiper, A. E. T. *J. Vac. Sci. Technol.* **1982,** *20*, 953–956.

[10] Webb, L. J.; Nemanick, E. J.; Biteen, J. S.; Knapp, D. W.; Michalak, D. J.; Traub, M. C.; Chan, A. S. Y.; Brunschwig, B. S.; Lewis, N. S. *J. Phys. Chem. B* **2005,** *109*, 3930–3937.

[11] Himpsel, F. J.; Meyerson, B. S.; McFeeley, F. R.; Morar, J. F.; Taleb-Ibrahimi, A.; Yarmoff, J. A. Core Level Spectroscopy at Silicon Surfaces and Interfaces. In *Proceedings of the 1988 Enrico Fermi School on Photoemission and Absorption Spectroscopy of Solids and Interfaces with Synchrotron Radiation*; Varenna: North Holland, 1988.

[12] Garcia, S. P.; Bao, H.; Manimaran, M.; Hines, M. A. *J. Phys. Chem. B* **2002,** *106*, 8258–8264.

[13] Royea, W. J.; Juang, A.; Lewis, N. S. *Appl. Phys. Lett.* **2000,** *77*, 1988–1990.

[14] Yablonovitch, E.; Allara, D. L.; Chang, C. C.; Gmitter, T.; Bright, T. B. *Phys. Rev. Lett.* **1986,** *57*, 249–252.

[15] Yamamoto, K.; Hasegawa, M. *J. Vac. Sci. Technol. B* **1994,** *12*, 2493–2499.

[16] Takahasi, K.; Nohira, H.; Nakamura, T.; Ohmi, T.; Hattori, T. *Jpn. J. Appl. Phys.* **2001,** *40*, L68–L70.

[17] Sugiyama, K.; Igarashi, T.; Moriki, K.; Nagasawa, Y.; Aoyama, T.; Sugino, R.; Ito, T.; Hattori, T. *Jpn. J. Appl. Phys.* **1990,** *29*, L2401–L2404.

[18] Hattori, T.; Aiba, T.; Iijima, E.; Okube, Y.; Nohira, H.; Tate, N.; Katayama, M. *Appl. Surf. Sci*. **1996,** *104/105*, 323–328.

[19] Keister, J. W.; Rowe, J. E.; Kolodziej, J. J.; Niimi, H.; Tao, H. S.; Madey, T. E.; Lucovsky, G. *J. Vac. Sci. Technol. A* **1999,** *17*, 1250–1257.

[20] Chabal, Y. J., Ed.; *Fundamental Aspects of Silicon Oxidation;* Springer-Verlag: Berlin, 2001.

[21] Ohishi, K.; Hattori, T. *Jpn. J. Appl. Phys.* **1994,** *33*, L675–L678.

[22] Tachibana, A.; Sakata, K.; Sato, T. *Jpn. J. Appl. Phys.* **1998,** *37*, 4493–4504.

[23] Ogawa, H.; Ishikawa, K.; Inomata, C.; Fujimura, S. *J. Appl. Phys.* **1996,** *79*, 472–477.

[24] Niwano, M.; Kageyama, J.; Kurita, K.; Kinashi, K.; Takahashi, I.; Miyamoto, N. *J. Appl. Phys.* **1994,** *76*, 2157–2163.

[25] Grunthaner, P. J.; Hecht, M. H.; Grunthaner, F. J.; Johnson, N. M. *J. Appl. Phys.* **1987,** *61*, 629–638.

[26] Yasaka, T.; Takakura, M.; Sawara, K.; Uenaga, S.; Yasutake, H.; Miyazaki, S.; Hirose, M. *IEICE Trans. Electron.* **1992,** *E75-C*, 764–769.

Chapter 7

Electronic Properties of Si(111) Surfaces Functionalized with Saturated Unbranched Hydrocarbons

7.1 Introduction

Freshly prepared H-terminated Si(111) surfaces have low surface recombination velocities (S) but rapidly form a disordered oxide layer when exposed to air. This silicon/native silicon oxide interface displays high rates of surface charge carrier recombination, reflecting a significant density of electrically active trap sites.[1] These surfaces are of great importance because as electronic devices fabricated from Si become smaller in size, the properties of the semiconductor surface begin to dominate the properties of the device as a whole. Hence, there has been considerable interest in learning how to control surface electronic properties through chemical methods, including protecting the surface from unwanted activity. These protection strategies should prevent extensive oxidation of the Si(111) surface while preserving the low surface recombination rate of the H-terminated Si(111) surface.

The formation of surficial Si–C bonds has been pursued as a possible solution to the problem of uncontrolled Si surface oxidation.[2] Previous work in our laboratory attempted to correlate the chemical and electronic stability of the functionalized Si surface prepared through the two-step chlorination/alkylation route. This has been done primarily through measurement of surface recombination rates and current-voltage (I–V) behavior on Si(111) surfaces modified with a variety of alkyl groups. Surface charge carrier recombination

velocities were measured on Si(111) surfaces terminated with either CH_3- or C_8H_{17}- groups and were found to be low even as the sample was exposed to air.[1] Methyl-terminated Si surfaces were used as electrodes in contact with a $Fe(CN)_6^{3-/4-}$(aq) solution and I–V curves were collected while the sample was illuminated for up to an hour. Unlike the H-terminated surface, the CH_3-terminated photoanode suffered only a small reduction in ideal rectifying behavior at the electrode surface.[3]

Detailed investigation of the oxidation of functionalized Si(111) surfaces in air was described in Chapter 6. This work demonstrated that alkylation of the Si(111) surface through a two-step chlorination/alkylation route is largely successful at preventing uncontrolled oxidation of the Si surface in air. Before further conclusions can be drawn about the capability of this functionalization technique to passivate the Si(111) surface it is necessary to correlate observed oxidation behavior directly to the rate at which charge carrier pairs on the alkylated surface recombine. Surface charge carrier recombination velocities are our most sensitive measurement of the electronic quality of a surface and must be the standard by which surface passivation is judged. In the work described here, surface charge carrier recombination rates on H-, Cl-, and alkyl-terminated Si(111) surfaces were measured using a radio frequency (rf) photoconductivity decay technique. These measurements were made when the sample was maintained under N_2(g) and then as they were exposed to air for up to 1 month. Furthermore, a detailed electron band description of the CH_3-Si(111) surface was assembled from photoelectron spectroscopy measurements. The observed surface charge carrier recombination dynamics were correlated to the chemical and band structure measurements in an attempt to explain any apparent electronic passivation of the alkyl-terminated Si(111) surface.

7.2 Experimental

7.2.1 Materials and Methods

7.2.1.1 Materials

Two different types of Si(111) wafers were used in this study. The n-type Si(111) wafers used for X-ray photoelectron spectroscopy (XPS) measurements were polished only on one side and were obtained from Crysteco (Wilmington, OH). These samples were 525 μm thick and P-doped, with a resistivity of 2.0–8.5 Ω cm. Samples for surface recombination velocity measurements were obtained from Topsil Inc. (Frederikssund, Denmark). These wafers were float-zone grown n-type, P-doped, Si(111), 280 μm thick, with resistivities of 3500–4600 Ω cm, and were polished on both sides. The manufacturer reported a bulk charge carrier lifetime, τ_b, of 2 ms.

All solvents used in functionalization reactions were anhydrous, stored under N_2(g), and, apart from occasionally pouring over molecular sieves, were used as received from Aldrich Chemical Corp. Solvents were only exposed to the atmosphere of a N_2(g)-purged flush box. Nanopure 18 MΩ cm resistivity H_2O was used at all times. All other chemicals were used as received unless otherwise specified.

7.2.1.2 Sample Preparation

Several modifications were made to the process of Si functionalization described in Chapter 2 and so sample preparation methods will be described in detail here. Before use, all wafers were chemically oxidized in 3:1 (v/v) concentrated H_2SO_4:30% H_2O_2(aq) at 100°C for 1 hr, rinsed in H_2O, and dried under a stream of N_2(g). Oxidized samples of approximately 1 cm^2 were cleaned by sonicating for 5 min in H_2O, rinsing with CH_3OH and acetone, sonicating for an additional 5 min in H_2O, and drying under a stream of N_2(g). Samples were etched for 20 min in 40% NH_4F(aq) (Transene Inc.) to produce a H-terminated Si surface. During the etching process the wafers were occasionally agitated to remove bubbles that formed on the surface. The samples were removed from the etching solution, rinsed in H_2O, dried under a stream of N_2(g), and immediately inserted via a quick-entry

load lock into an ultra-high vacuum (UHV) system for XPS measurements. The UHV chamber was connected via a second quick-entry load lock into a N_2(g)-purged flush box in which further surface modification reactions were conducted. Once a sample entered the UHV system it was not exposed to ambient air until after surface modification. Occasionally wafers were inserted directly into the vacuum-sealed antechamber of the N_2(g)-purged flush box to prevent scratches on the surface that arose from contact with the XPS sample holder.

7.2.1.3 Functionalization by Chlorination/Alkylation

Chorinated Si(111) surfaces were prepared by two different methods. In the first chlorination method, a H-terminated sample was immersed into a saturated solution of PCl_5 in C_6H_5Cl that contained a few grains of benzoyl peroxide to act as a radical initiator.[4,5] The reaction solution was heated to 90–100°C for 45 min. Samples were then removed from the reaction solution and rinsed in tetrahydrofuran (THF) followed by a rinse in CH_3OH and were then dried under a stream of N_2(g). Samples were occasionally also rinsed in 1,1,1-trichloroethane (TCE) before drying under N_2(g).

In the second chlorination method, a H-terminated sample was placed into a quartz Schlenk reaction tube and transported to a vacuum line. After thoroughly evacuating the sample vessel, approximately 50–200 Torr of Cl_2(g) (Matheson, 99.999%) was introduced through the vacuum line into the reaction tube, and the sample was illuminated for 30 s with 366 nm ultraviolet light from a UVP-type multiband lamp to generate a reactive Cl· radical.[6,7] Rigorous exclusion of ambient air from the reaction tube was required to produce oxide-free surfaces. Excess Cl_2(g) was then removed under vacuum, and the flask was transported to the N_2(g)-purged flush box. XP spectra and surface charge carrier recombination velocities were collected for Cl-terminated samples that had been prepared through both chlorination routes.

The chlorine-terminated Si surfaces were alkylated by immersing the sample in 1.0–3.0 M $C_nH_{2n+1}MgX$, where n = 1, 2, 6, and 8 and X = Cl or Br, in either diethyl ether or THF (Aldrich). The reaction was performed for 1.5–16 hr at 70–80°C with longer alkyl chain lengths requiring longer reaction times. Excess THF was added to all reaction so-

lutions for solvent replacement. At the end of the reaction time, samples were removed from the reaction solution and were then rinsed in THF, CH_3OH, and occasionally TCE. Samples were then sonicated for 5 min each in CH_3OH and CH_3CN and were dried under a stream of N_2(g). Occasionally a small Mg signal that presumably arose from the Grignard reagent appeared in the initial XP spectrum. When this peak was observed, the sample was sonicated in CH_3OH for an additional 10 min to remove any remaining Mg. The samples were then exposed to laboratory air, and XPS and rf photoconductivity data were collected periodically during air exposures of $>$600 hr.

7.2.2 Instrumentation

7.2.2.1 XPS

XP spectra were collected in the UHV M-Probe system described in Section 3.2.2.1. Several differences in data collection and handling are described here. Data were collected with the M-Probe ESCA Software version S-Probe 1.36.00. An initial survey scan was run from 0–900 or from 0–1000 BeV (binding electron volts) to identify all chemical species on the surface. A second scan was collected at the Si 2p region at approximately 98.5–105.5 BeV to measure the presence of any SiO_2 species at $\approx$104 BeV. Wafers were fixed to the XPS sample holder at their edges, and XPS data were collected near the middle of the wafer to prevent interference from any surface oxide growth that might be promoted by scratches caused by contact with the sample fixture during handling of the sample.

The surface coverages of species of interest were compared between different samples by referencing all peaks to the Si 2p peak at 99.4 BeV. The area under the peaks obtained in the initial survey scan was determined by the XPS software. The detailed scan of the Si 2p region was used to determine the amount of Si oxides present. The Si $2p_{1/2}$ and Si $2p_{3/2}$ peaks were fitted with two peaks held 0.60 BeV apart and with the Si $2p_{1/2}$: Si $2p_{3/2}$ peak area ratio maintained at 0.51, as has been described previously.[4,8] Any peak detected between 100 and 104 BeV, where Si^{+}–Si^{4+} oxides would be located, was fitted to a third peak.[9] Peak line shapes were set at 95% Gaussian and 5% Lorentzian, with a 15% asymmetry. The SiO_x : Si 2p peak area ratio was then obtained from the area under

the third curve divided by the total area of the Si $2p_{1/2}$ and Si $2p_{3/2}$ peaks. This peak area corresponds to the coverage of Si^{+}, Si^{2+}, Si^{3+}, and Si^{4+} oxides on the surface.

The equivalent fractional monolayer coverage of SiO_x on the Si(111) substrate was determined from the SiO_x:Si 2p peak area ratio using a substrate-overlayer model.[8,10] The overlayer thickness, d_{ov}, was computed using

$$d_{ov} = \lambda_{ov} \sin\theta \left\{ \ln \left[1 + \left(\frac{I^0_{Si}}{I^0_{ov}} \right) \left(\frac{I_{ov}}{I_{Si}} \right] \right\} \tag{7.1}$$

where λ_{ov} is the attenuation factor of the overlayer (2.6 nm), θ is the electron takeoff angle relative to the sample surface (35° for this instrument), I^0_{Si}/I^0_{ov} is an instrument normalization factor related to the sensitivity and abundance of the substrate and overlayer species, determined to be 1.3 for this instrument for a SiO_2 overlayer on a Si substrate, and I_{ov}/I_{Si} is the measured SiO_2 : Si 2p peak area ratio. Assuming that the oxide is composed entirely of SiO_2, the computed overlayer thickness, d_{ov}, was divided by the thickness of a monolayer of SiO_2, 0.35 nm, to determine the equivalent fractional monolayer of SiO_2 present.[8]

For very thin oxide overlayers, the monolayer coverage of oxidized Si can also be calculated directly from the SiO_2:Si 2p peak area ratio.[8] This approach directly determines the amount of oxidized Si present on the surface regardless of whether it is SiO_2 or it is composed of other oxides of Si. The total observed Si 2p signal is

$$I_{si} \approx n_{Si}\sigma_{Si} \int_0 \exp(-z/l_{Si}) dz = n_{Si}\sigma_{Si} l_{Si} \tag{7.2}$$

where n_{Si} is the atomic number density of Si atoms (5.0 x 10^{22} atoms cm^{-3}), σ_{Si} is the atomic photoionization cross-section of Si, and the escape depth, l_{Si}, is given by

$$l_{Si} = \lambda_{Si} \sin\theta \tag{7.3}$$

with λ_{Si} = 1.6 nm. The measured signal arising from the oxidized surface Si atoms at higher binding energies than the bulk Si 2p peak is given by

$$I_{Si,surf} = \Gamma_{Si,surf}\sigma_{Si} \tag{7.4}$$

where $\Gamma_{Si,surf}$ is the surface density of Si atoms, 7.8 x 10^{14} atoms cm^{-2} for Si(111). If every surface Si atom is oxidized and σ_{Si} remains constant for every Si species, then the relative intensity of the oxidized Si peak to bulk Si peak can be found by combining Eqs. 7.2 and 7.4:

$$\frac{I_{Si,surf}}{I_{Si,bulk}} = \frac{\Gamma_{Si,surf}\sigma_{Si}}{n_{Si}\sigma_{Si}l_{Si} - n_{Si,surf}\sigma_{Si}} = \frac{\Gamma_{Si,surf}}{n_{Si}l_{Si} - n_{Si,surf}} \tag{7.5}$$

As can be seen in Eq. 7.5, the SiO_x:Si 2p peak area ratio is independent of the photoionization cross-section of all species present in the scan. Substituting into Eq. 7.5 yields a ratio of 0.21 for a Si(111) surface on which 100% of the surface Si atoms are oxidized. The observed oxidized/bulk Si 2p peak area ratios were therefore divided by this normalization constant to estimate the fraction of surface atoms that were oxidized.

7.2.2.2 Surface Recombination Velocity Measurements

Charge carrier lifetimes were measured using a contactless time-resolved rf conductivity apparatus.[1] Samples were illuminated at 1064 nm with 10 nm pulses from a Nd:YAG laser operating at a repetition rate of 10 Hz. To ensure high-level injection conditions, the pulse power was 7 x 10^{-4} mJ pulse^{-1} cm^{-2}, which resulted in an injected carrier concentration in the semiconductor immediately after the light pulse of 4 x 10^{13} carriers cm^{-3}. The sample was placed over a coil emitting a 450 MHz signal that was reflected back from the sample. The difference in intensity between the initial and reflected signal was proportional to the rf absorbed by the sample. Signals were averaged over 128 decays, plotted on a digital oscilloscope (Tektronix, TDS210), and captured by the PC data acquisition program WaveStar. Data were fitted to a single exponential decay to determine τ, the lifetime of charge carriers in the semiconductor. Once samples were set in the rf conductivity sample holder, they were not handled again for the duration of the experiment to prevent scratching of the surface.

The fundamental charge carrier decay lifetime, τ, is dependent on the lifetime of the charge carriers both in the bulk and at the surfaces of the sample. The surface recombination

velocity, S, can be related to the measured lifetime using

$$S = \frac{d}{2}\left(\frac{1}{\tau} - \frac{1}{\tau_b}\right) \tag{7.6}$$

where d is the sample thickness, τ_b is the lifetime of a charge carrier in the bulk of the semiconductor,[1] and the factor of 2 is required for recombination on both sides of a double-polished Si wafer. For the samples used here, $\tau_b \gg \tau$, and the expression for S reduces to

$$S = d/2\tau \tag{7.7}$$

7.2.2.3 High-Resolution Core Level Photoelectron Spectroscopy

Further photoelectron spectroscopy to elucidate the electronic structure of the CH_3-Si(111) surface was collected by Dr. Ralf Hunger of the Institute of Materials Science at the Technische Universität Darmstadt in Darmstadt, Germany.[11] Silicon wafers doped with Sb to a resistivity of 0.005–0.02 Ω cm were used for these experiments. The silicon surface was CH_3-terminated following a procedure described in Chapter 2; only the PCl_5 chlorination route was employed. Core-level spectroscopy was collected on beamline U49/2-PGM2 at the BESSY II synchrotron facility in Berlin at excitation energies between 115–650 eV. Core photoelectrons were collected by an analyzer positioned normal to the sample surface.

7.3 Results

7.3.1 XPS Results

Figure 7.1 presents representative XPS data for the functionalization of Si(111) surfaces using a two-step chlorination/alkylation route. As expected,[4,6,7] on a freshly etched Si(111) surface (Figure 7.1(a)), only Si 2p and Si 2s peaks, at 100 BeV and 150 BeV, respectively, were observed. After chlorinating the surface in a solution of PCl_5, Cl 2p (200 BeV) and Cl 2s (270 BeV) peaks became visible (Figure 7.1(b)). After alkylation, the Cl peaks disappeared and a significant C 1s peak appeared at 285 BeV (Figure 7.1(c)). Table 7.1 presents the peak area ratios of C, Cl, and O that were detected in these XPS scans.

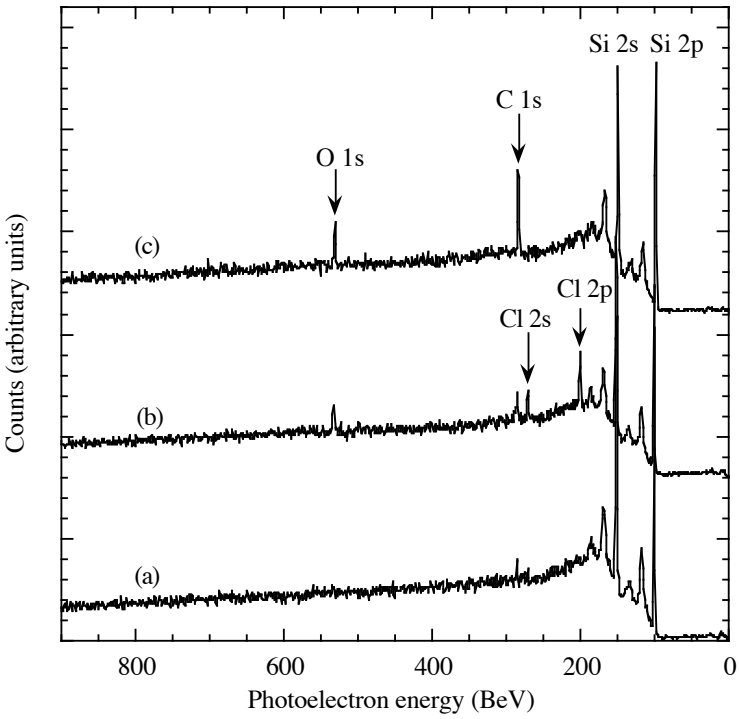

Figure 7.1: Survey scan XP spectra of a Si(111) surface (a) cleaned and etched in 40% NH_3F(aq) for 20 min, (b) chlorinated with saturated PCl_5 in chlorobenzene with benzoyl peroxide at 90–100°C for 45 min, and (c) then alkylated with $C_8H_{17}MgCl$ for 16 hr.

surface preparation route	-R	XPS peak area ratio[a]		
		C 1s	O 1s	Cl 2p
$PCl_5/C_nH_{2n+1}MgX$	-Cl	0.3±0.2	0.5±0.2	0.45±0.06
	$-CH_3$	0.52±0.03	0.459±0.003	
	$-C_2H_5$	0.40±0.004	0.27±0.07	
	$-C_6H_{13}$	0.68±0.08	0.4±0.01	
	$-C_8H_{17}$	0.6±0.1	0.3±0.2	
$Cl_2/C_nH_{2n+1}MgX$	-Cl	0.3±0.2	0.2±0.1	0.8±0.4
	$-CH_3$	0.62±0.9	0.75±0.8	
	$-C_2H_5$	0.36±0.06	0.3±0.1	
	$-C_8H_{17}$	0.75±0.03	0.48±0.04	

Table 7.1: Normalized peak area ratios for species present on the functionalized Si(111) surface prepared through two different chlorination/alkylation procedures. [a]Values are normalized to the Si 2p peak area.

The XPS peak for the Si^{4+} in SiO_2 appears at 4.3 BeV higher in energy than Si^0, so oxidation of the surface Si atoms is accompanied by the appearance of Si 2p peaks having energies >100 BeV. No SiO_2 was observed in the high-resolution Si 2p XPS scans at any step in the alkylation process, indicating that the O 1s peak at 532 BeV shown in Figure 7.1 was due to the presence of small amounts of adventitious O on the surface.

Figure 7.2 presents high-resolution XPS scans of the Si 2p region during the air oxidation of H-terminated Si(111) surfaces. A freshly etched H-terminated Si(111) surface (Figure 7.2(a)) oxidized rapidly and displayed a prominent silicon oxide peak after only 4 hr of exposure (Figure 7.2(b)). The oxide grew further upon extended exposure to air (Figure 7.2(c),(d)). The SiO_x:Si 2p peak area ratio for H-terminated Si(111) is plotted in Figure 7.3. The ratio was used to compute the monolayer equivalents of SiO_2 on the surface, which is given in Table 7.2. After 216 hr of exposure to ambient air, the H-terminated Si surface displayed 1.4 equivalent monolayers (ML) of SiO_2. Similar oxidation behavior was observed for Cl-terminated surfaces that had been prepared using either chlorination procedure (Figure 7.3, Table 7.2). In contrast, CH_3-terminated surfaces displayed less oxide growth than was observed after a few minutes of air exposure of the H- or Cl-terminated Si(111) surfaces (Figure 7.3).

Similar behavior was observed for C_2H_5-terminated surfaces, shown in Figure 7.4. Oxidation was suppressed on alkylated surfaces that had been prepared through use of either PCl_5 or Cl_2(g) as the chlorination agent (Table 7.2). On all alkylated surfaces, silicon oxide growth was negligible for the first ≈30 hr of the experiment, and after 200 hr in air, only <0.9 equiv monolayers of SiO_2 were observed. As shown in Table 7.2, no clear difference in the growth rate or accumulated amount of surface oxide was observed as the chain length of the alkyl group increased.

7.3.2 Surface Recombination Velocity Results

Results of the rf photoconductivity decay studies for the various surfaces of interest are summarized in Table 7.3. Silicon surfaces that had been functionalized through the chlorination/alkylation route displayed long surface charge carrier lifetimes and low surface

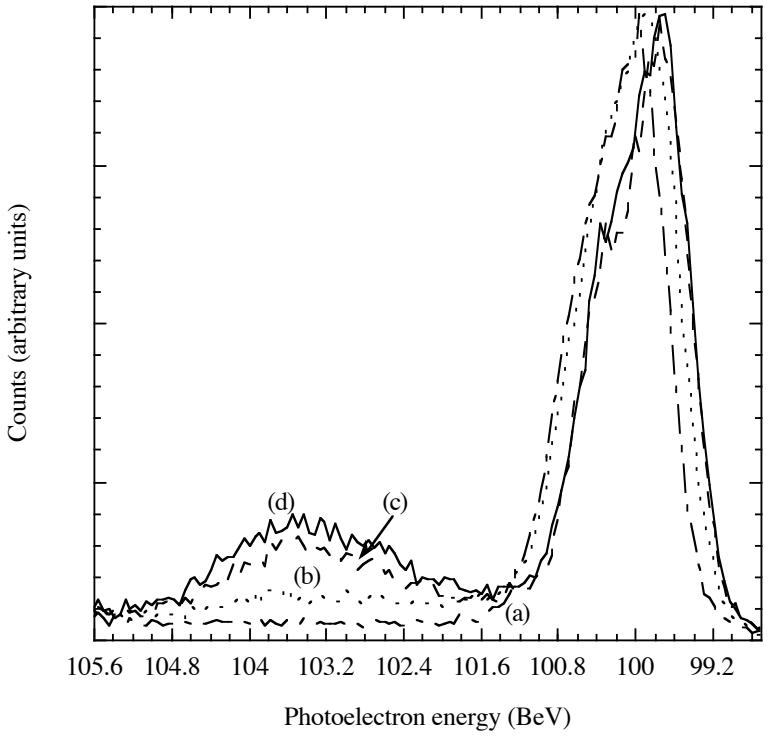

Figure 7.2: High-resolution XP spectra of the Si 2p region of a H-terminated Si(111) surface that was (a) freshly etched (dashed-dotted line) and then exposed to ambient laboratory air for (b) 4 hr (dotted line), (c) 72 hr (dashed line), and (d) 216 hr (solid line).

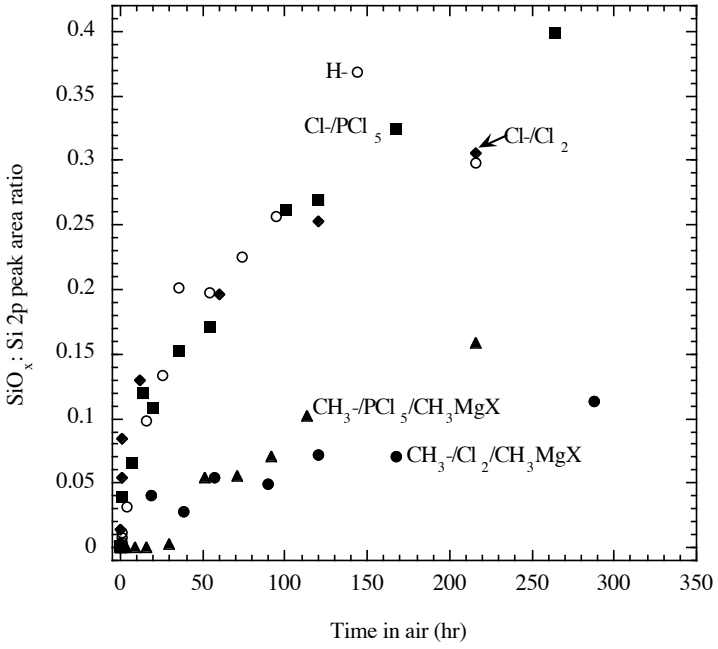

Figure 7.3: Ratio of the oxidized Si 2p peak area to the bulk Si 2p peak area for various Si(111) surfaces exposed to ambient air over extended time periods: open circles, H-terminated Si; squares, Cl-terminated Si prepared using PCl_5; diamonds, Cl-terminated Si prepared using Cl_2(g); triangles, CH_3-terminated surface prepared through PCl_5/CH_3MgCl; closed circles, CH_3-terminated surface prepared through Cl_2(g)/CH_3MgBr. Standard deviation is not shown for clarity. Although the standard deviation of oxide growth was sometimes large, occasionally as much as 50% of the value, no overlap of the standard deviation of H- and Cl-terminated surfaces and the CH_3-terminated surfaces was observed after 30 hr in air.

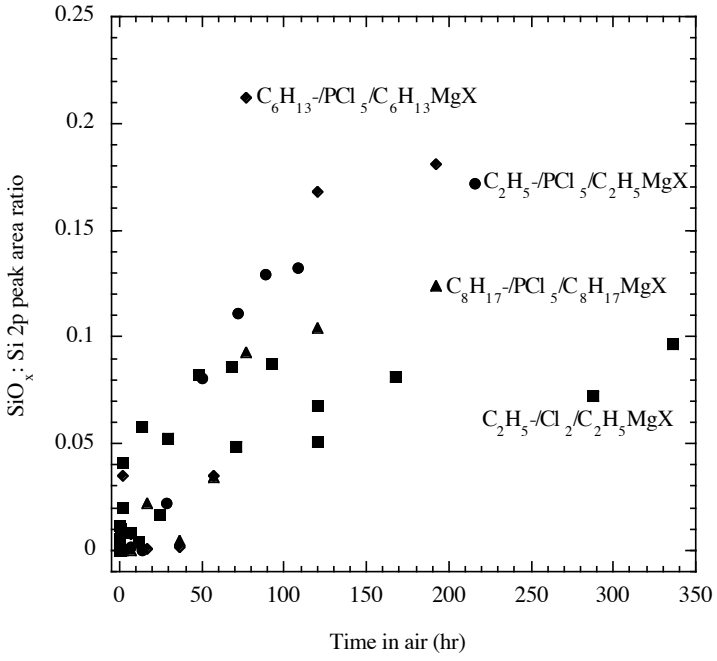

Figure 7.4: Ratio of the oxidized Si 2p peak area to the bulk Si 2p peak area for alkylated Si(111) prepared through chlorination/alkylation while exposed to ambient air over extended time periods: circles, C_2H_5-terminated Si prepared through PCl_5/C_2H_5MgBr; squares, C_2H_5-terminated Si prepared through Cl_2(g)/C_2H_5MgBr; diamonds, C_6H_{13}-terminated Si prepared through PCl_5/C_6H_5MgBr; triangles, C_8H_{17}-terminated Si prepared through $PCl_5/C_8H_{17}MgCl$. Standard deviations were large ($\sim$50%), and no significant difference was observed for different chain lengths.

Surface preparation route	-R	time in air (hr)	SiO_x equivalent monolayer coverage: SiO_x:Si 2p peak area ratio	SiO_2^a (ML)	SiO_2^b (ML)
NH_4F etch	-H	216	0.3	1.4	1.4
$PCl_5/C_nH_{2n+1}MgX$	-Cl	264	0.40±0.09	1.8±0.3	1.9±0.4
	$-CH_3$	216	0.16±0.08	0.8±0.4	0.8±0.4
	$-C_2H_5$	216	0.17±0.03	0.9±0.1	0.8±0.1
	$-C_6H_{13}$	192	0.18±0.02	0.90±0.07	0.86±0.07
	$-C_8H_{17}$	192	0.12	∼0.6	∼0.6
$Cl_2/C_nH_{2n+1}MgX$	-Cl	215	0.306±0.009	1.43±0.04	1.46±0.04
	$-CH_3$	288	0.11	∼0.6	∼0.5
	$-C_2H_5$	312	0.08±0.02	0.44±0.09	0.40±0.08

Table 7.2: Normalized SiO_x:Si 2p peak area ratio and fractional monolayer coverage of SiO_x on the functionalized Si(111) surface prepared through two different chlorination/alkylation procedures. [a]Calculated from Eq. 7.1 and then divided by 0.35 nm. [b]Calculated by dividing the SiO_x:Si 2p peak area ratio by 0.21, a normalization constant representing 1 fractional monolayer of SiO_x calculated from Eq. 7.5.

surface preparation route	-R	time in air					
		0 min (under N_2(g))		10 min		>24 hr	
		τ (μs)	S (cm s^{-1})	τ (μs)	S (cm s^{-1})	τ (μs)	S (cm s^{-1})
NH_4F(aq)	-H, control[a]	11.8±0.6	1180±60	<10	>1400	<10	>1400
	-H, control[b]	10±1	1350±10	<10	>1400	<10	>1400
	-H, control[c]	21.5±0.4	650±10			<10	>1400
PCl_5/$C_nH_{2n+1}MgX$	-Cl	510±140	28±8	300±30	46±4	<10	>1400
	-Cl, control[d]	70±6	200±20	40±20	370±140	<10	>1400
	-CH_3	130±60	130±50	140±30	100±20	200±70	80±30
	-C_2H_5	40±20	450±180	70±50	260±100	200±90	80±30
	-C_6H_{13}	80±50	260±140	60±30	270±110	120±20	120±20
	-C_8H_{17}	80±20	190±50	50±10	280±60	150±7	93±4
Cl_2(g)/$C_nH_{2n+1}MgX$	-Cl	460±110	31±7	370±70	39±7	<10	>1400
	-CH_3	70±20	250±150	50±20	330±230	110±30	150±60
	-C_2H_5	31±7	470±100	37±8	400±100	80±30	200±80

Table 7.3: Charge carrier lifetimes and recombination velocities of functionalized Si(111) surfaces prepared through two different chlorination/alkylation procedures. [a]Control surfaces prepared by immersing a H-terminated surface in chlorobenzene and heating for the appropriate reaction time. [b]Control surfaces prepared by immersing a H-terminated surface in chlorobenzene, followed by immersion in THF and heating for the appropriate reaction times in each solvent. [c]Control surfaces prepared by immersing a H-terminated surface in chlorobenzene with benzoyl peroxide and heating for the appropriate reaction time. [d]Control surfaces prepared by immersing a Cl-terminated surface in THF at 70–80°C for 3.5 hr.

recombination velocities.[1] Methyl-terminated Si surfaces that were prepared using either chlorination method displayed the lowest charge carrier recombination velocity of the chain lengths included in this study. After methyl-terminated surfaces were exposed to laboratory air, the carrier lifetime increased over a period of ≈24 hr, after which it remained stable for the duration of the experiment (150 – 700 hr). The CH_3-terminated surfaces prepared from a PCl_5-chlorinated surface exhibited a stabilized S value of 80 ± 30 cm s^{-1}, and surfaces prepared from Cl_2(g) followed by treatment with CH_3MgBr exhibited a stabilized S value of 150 ± 60 cm s^{-1}. Ethyl-terminated Si surfaces functionalized through both chlorination techniques behaved similarly, with stabilized S values of 80 ± 20 and 200 ± 80 cm s^{-1} for the PCl_5/C_2H_5MgBr- and Cl_2(g)/C_2H_5MgBr-treated surfaces, respectively. These values of S indicate that these two alkylation techniques produced passivated surfaces that maintained low electrically active trap densities for extended periods of time in air.

In general, the S values of all the alkylated surfaces were similar to each other. However, somewhat more complex behavior was observed on surfaces prepared using PCl_5/ $C_6H_{13}MgBr$ or $PCl_5/C_8H_{17}MgCl$, as shown in Figure 7.5. Under N_2(g), the rf photoconductivity decay lifetimes were 80 ± 50 and 80 ± 20 μs for the C_6H_{13}- and C_8H_{17}-terminated surfaces, respectively. After 24 hr of exposure to air, the lifetimes decreased to 60 ± 30 and 50 ± 10 μs, respectively. Upon extended air exposure, however, the lifetimes gradually rose over a period of 600–700 hr to 120 ± 20 and 150 ± 7 μs, at which point the experiment was terminated.

A series of controls was run to determine if the observed lifetimes were the result of experimental conditions and not bonded alkane chains. Freshly etched, H-terminated Si(111) samples that were immersed in either chlorobenzene, chlorobenzene and benzoyl peroxide, or chlorobenzene followed by THF and heated for identical reaction times as the functionalized surfaces displayed short charge carrier lifetimes indicative of highly defective surfaces (Table 7.3). Charge carrier lifetimes for these control surfaces were <22 μs (S = 650 cm s^{-1}) under N_2(g) and decreased to <10 μs after 1–3 hr of exposure to laboratory air. Chlorine-terminated Si(111) surfaces prepared by either chlorination method displayed charge carrier lifetimes of ≈500 μs (S = 30 cm s^{-1}) under N_2(g), but τ decreased to ≈300 μs after only 10 min in air, and surface-limited carrier lifetimes, with τ <10 μs (S >1400

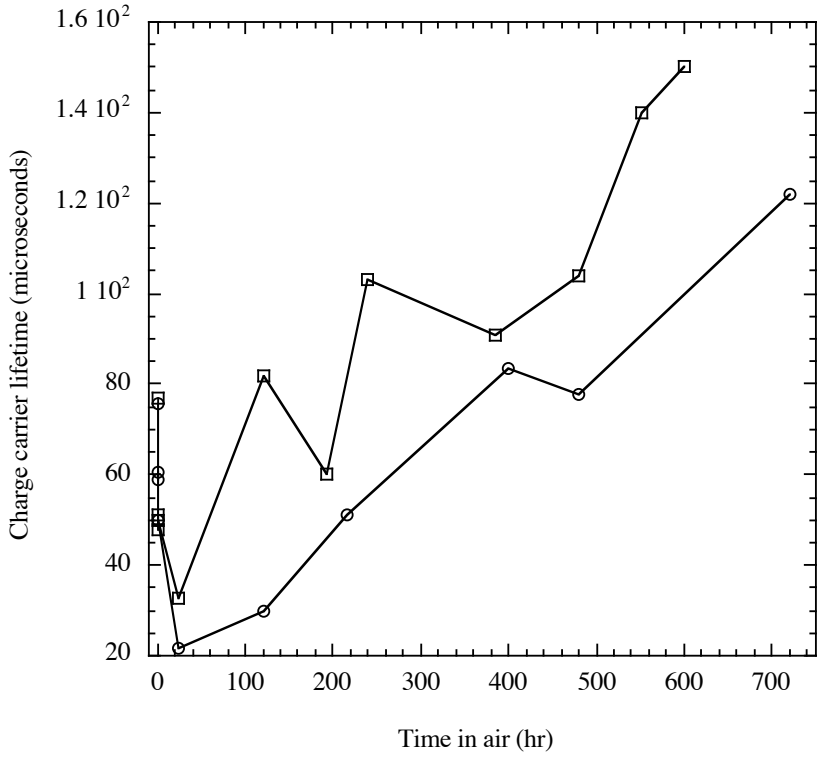

Figure 7.5: Charge carrier lifetimes of C_6H_{13}- and C_8H_{17}-terminated Si(111) prepared by exposure to PCl_5 followed by reaction with alkylmagnesium halide: circles, C_6H_{13}-terminated Si(111); squares, C_8H_{17}-terminated Si(111).

cm s^{-1}), were observed after 24 hr in air. Surface recombination velocities of Cl-terminated Si(111) samples prepared by chlorination with PCl_5 that had been immersed in THF at 70–80°C for 3.5 hr were 200 $\pm$ 20 cm s^{-1} under N_2(g) but increased to S >1400 cm s^{-1} after 24 hr of exposure to ambient air.

7.3.3 High-Resolution Core Level Photoelectron Spectroscopy Results

High-resolution soft XPS was used to determine the electronic band structure of the CH_3-terminated Si(111) surface. These results are described extensively in Hunger, *et al*.[11] and are summarized here. The amount of band bending, qV_{bb}, at the functionalized surface was determined from a comparison between the positions of the Fermi level, E_F, at the surface versus the bulk material. The absolute Si 2p binding energy, which is the energy difference between the 2p orbital and E_F, was found to be 99.68 eV.[11] The binding energy of the Si 2p signal, E_{Si2p}, with respect to the valence band maximum, E_{VB}, is known to be 98.74 eV in the bulk material.[12] Comparison of these two values implies a difference of 0.94 eV from the top of the valence band to the Fermi level, E_F at the surface. Because the bulk Fermi level defined by the dopant density of the sample was 1.04 eV above E_{VB} in the bulk material, and assuming that the location of E_F does not change, this implies that the valence band maximum at the surface is 0.10 eV higher in energy than in the bulk material. This value is an approximation of the extent of band bending at the CH_3-terminated Si(111) surface.

The electron affinity, χ, of the CH_3-terminated Si(111) surface was determined according to:

$$\chi = E_{vac} - E_{CB} = E_{vac} - E_F + E_F - E_{CB} = W_f - (E_g - E_F - E_{VB}) \qquad (7.8)$$

where E_{CB} is the energy of the conduction band edges, E_g is the band gap of the sample, E_{vac} is the vacuum level, and W_f is the work function of the material ($E_{vac} - E_F$). The dopant density of the Si samples used in these experiments set E_F 1.04 eV above E_{VB} (i.e., $E_F - E_{VB}$ = 1.04 eV). The secondary electron cutoff was used to estimate W_f = 3.86 eV. The bandgap of Si is well-known to be 1.12 eV. From these values, the electron affinity

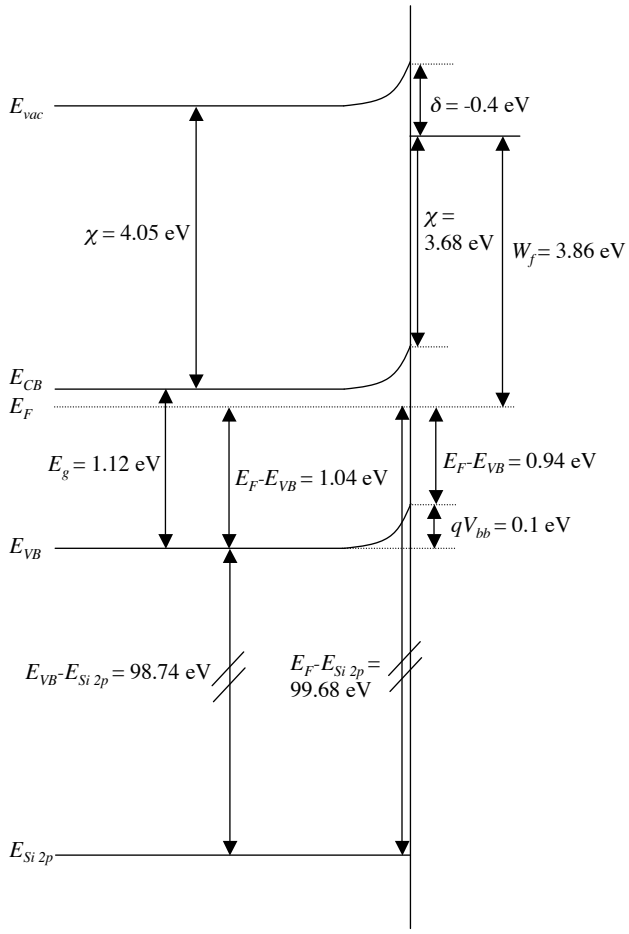

Figure 7.6: Surface energy band diagram of the CH_3-terminated Si(111) surface. Known quantities of the bulk material are χ, E_F, $E_F - E - VB$, and $E_{VB} - E_{Si2p}$. Surface properties $E_F - E_{Si2p}$ and W_f were measured (99.86 eV and 3.86 eV, respectively), implying a surface band bending, qV_{bb} = 0.10 eV. Eq. 7.8 was used to calculate surface properties χ = 3.68 eV and δ = -0.40 eV. Figure adapted from Hunger, *et al.*[11]

of the Si surface was calculated to be 3.68 eV. If the electron affinity of bulk silicon is estimated at 4.05 eV,[13] this indicates the presence of a surface dipole, δ, with a magnitude of -0.4 eV. The degree of surface band bending and electron affinity of the CH_3-terminated Si(111) surface are summarized in Figure 7.6.

7.4 Discussion

Alkylation using both of the chlorination/alkylation routes significantly reduced the rate of air oxidation and concomitantly preserved the electrical properties of the H-terminated Si surface. Although the two chlorination routes produced differing levels of Cl on the Si(111) surface, subsequent alkylation resulted in very similar coverages of alkyl groups on the Si surface as determined by XPS (Table 7.1). The degree of electrical passivation obtained through either chlorination/alkylation method is notable. The surface electronic trap density, N_t, may be related to S through

$$S = N_t \sigma \nu_{th} \tag{7.9}$$

where σ is the cross-section for carrier capture on the surface, typically 10^{-15} cm^2, and ν_{th} is the thermal charge carrier velocity, which is 5.2 x 10^6 cm s^{-1} in n-type Si(111) at room temperature.[1,13,14] Hence the observed S value for such surfaces, 200 cm s^{-1}, corresponds to N_t = 4 x 10^{10} cm^{-2}. Assuming a surface atom density of $\sim 10^{15}$ cm^{-2},[13] this corresponds to an electrically active defect density of only 1 atom in every 10^5 surface sites.

It is interesting to compare the behavior of CH_3-terminated Si(111) surfaces to surfaces functionalized with longer alkyl chains. Because the distance between atop atoms on the unreconstructed Si(111) surface (3.8 Å)[13] is larger than the van der Waals radius of a methyl group (2.5 Å),[15] methyl groups are the only alkyl group that can terminate every Si atop atom site, and thus are unique among the straight-chain alkyls.[1] It therefore would be expected that methylated Si(111) surfaces would have the lowest incidence of defects and would display the lowest surface recombination velocities. This behavior was in fact observed experimentally, although surprisingly the other alkyl groups produced surfaces

with S values that were only a factor of $\sim$2 higher than those of the methylated Si(111) surface.

The chemical stability of the functionalized surfaces will reflect not only the degree of surface termination but also the nature of the alkylation agent, the ability of the overlayer to prevent oxidants from reaching the surface, the level of surface defects, electronic passivation through induced band bending or surface dipoles, and possibly other factors. For short term exposure to air, all of the surfaces prepared by the chlorination/alkylation routes were much more chemically inert to oxidation than the H-terminated or Cl-terminated Si(111) surfaces. Longer term exposure to air did produce some evidence for oxidation, although the levels of oxide never exceeded the equivalent of 1 monolayer of SiO_2 even after up to 300 hr of air exposure. The CH_3-terminated surfaces appeared to be somewhat more resistant to oxidation than surfaces alkylated with longer alkyl chains, which is consistent with the notion that CH_3- groups can terminate more Si atop sites with Si–C bonds and with the hypothesis that Si–C bonds are more kinetically or thermodynamically inert to oxidative processes than are the unalkylated Si atop sites. It is possible that the greater incidence of pinhole defects in surfaces functionalized with longer alkyl chains is offset by the greater hydrophobicity of these chains, so that the overall rate of oxidation is similar for the surfaces functionalized with alkyl chains ranging from one to eight carbons in length.[16]

In some cases, the changes in surface composition correlated well with changes in the electrical properties of the surface, while in other cases the growth of oxide, surprisingly, did not degrade the electrical properties of the Si surface. The rapid oxide growth seen upon air exposure of the H- and Cl-terminated surfaces correlated with a precipitous drop in surface charge carrier lifetimes. This was contrasted with the slower, yet still significant, oxide growth on the alkylated surfaces prepared through chlorination/alkylation techniques that did not deleteriously affect the charge carrier lifetimes of such surfaces. In fact all of the samples that were functionalized using the chlorination/alkylation route showed an increased lifetime with longer exposure to air. A similar effect on stabilizing the photoluminescent behavior of porous Si modified with surface-bound organic functional groups has been described previously.[16,17] It is possible that slower growth of the oxide allows it to form in a more ordered fashion than that caused by rapid growth seen on the unpassi-

vated surfaces, and that this ordered oxide does not introduce electron-hole energy traps that promote extensive recombination. This is supported by the well-documented observation that high-quality SiO_2 layers grown by thermal annealing have low surface charge carrier recombination rates but that the native oxide, grown in an uncontrolled fashion in air, supports high charge carrier recombination velocities.[16–18]

A second possible reason that surface alkylation electronically passivates the surface is that the functionalized Si surface is stabilized by band bending induced by the alkylation layer. If the passivated surface is protected by a reasonably large near-surface space-charge region, then an energy barrier will prevent one of the charge carriers from reaching the surface. The surface could have large numbers of trap states, but with a low concentration of one of the charge carriers, recombination rates will still be low. This can be seen in Eq. 1.1, where the rejection of one charge carrier, and hence the accumulation of the other charge carrier, at the surface will increase the denominator of the rate equation, thus decreasing the overall recombination rate. This effect has been measured in our laboratory at the Si surface/liquid interface in the presence of strongly oxidizing molecules like ferrocenium and molecular iodine in methanolic solutions.[19,20] Although the Si surfaces used in these experiments had high defect densities, strong band bending produced an interface that supported exceptionally low rates of charge carrier recombination. To test if this effect might also be occurring on the alkylated Si surface, high-resolution core level photoelectron spectroscopy was used to determine the extent of any band bending on the CH_3-Si(111) surface in vacuum. This revealed that the bands were bent downward slightly by 0.10 eV. While not insignificant, this value is approximately $3k_bT$ at room temperature (k_bT = 26 mV at 300 K), and it is unlikely that this is a large enough barrier to prevent the majority carrier from accessing the surface, and hence to cause the low charge carrier recombination rates observed on this surface. Connecting surface alkylation to electronic passivation must await further studies in our laboratory.

7.5 Conclusion

One hypothesis driving the study of Si surface modification is that replacing the surface H atom on the freshly etched surface with some other surface-bound moiety with a stronger Si–R bond will prevent the large extent of Si surface oxidation, thus passivating the surface to harmful electron-hole recombination activity. The two-step chlorination/alkylation route has been found to slow surface oxidation substantially, but it does not stop it entirely. Measurable silicon suboxides appear on surfaces alkylated with unbranched saturated hydrocarbons within a few days, thus indicating that the surface has not been fully chemically passivated. This is contradicted, however, by the surface electron-hole pair recombination behavior. Even as small oxides grow on the alkylated surface, it remains electronically passivated, and charge carrier recombination rates remain low. Indeed, in the first $\sim$24 hr the alkylated surface is exposed to air, surface recombination velocities drop before stabilizing at a low value for extended periods of time.

One possible explanation of low charge carrier recombination rates, electronic passivation from the presence of a large amount of band bending, has been shown here to be improbable, based on observed band bending of only 0.10 eV, a relatively small barrier at room temperature. Another possible explanation is that the oxide growing on the alkylated surface more closely resembles the high-quality, annealed oxide grown on Si microelectronic devices, which does not place orbital trap states near the middle of the Si bandgap and thus does not cause extensive electron-hole surface recombination. This hypothesis is somewhat supported by the results given in Chapter 6, which showed a difference in the chemical state of the oxide growing on passivated versus unpassivated Si. Further measurements of the location of possible surface trap states are required to determine if this is correct.

Bibliography

[1] Royea, W. J.; Juang, A.; Lewis, N. S. *Appl. Phys. Lett.* **2000,** *77*, 1988–1990.

[2] Bent, S. F. *Surf. Sci.* **2002,** *500*, 879–903.

[3] Bansal, A.; Lewis, N. S. *J. Phys. Chem. B* **1998,** *102*, 4058–4060.

[4] Bansal, A.; Li, X.; Yi, S. I.; Weinberg, W. H.; Lewis, N. S. *J. Phys. Chem. B* **2001,** *105*, 10266–10277.

[5] Bansal, A.; Li, X. L.; Lauermann, I.; Lewis, N. S.; Yi, S. I.; Weinberg, W. H. *J. Am. Chem. Soc.* **1996,** *118*, 7225–7226.

[6] Terry, J.; Linford, M. R.; Wigren, C.; Cao, R. Y.; Pianetta, P.; Chidsey, C. E. D. *Appl. Phys. Lett.* **1997,** *71*, 1056–1058.

[7] Terry, J.; Linford, M. R.; Wigren, C.; Cao, R. Y.; Pianetta, P.; Chidsey, C. E. D. *J. Appl. Phys.* **1999,** *85*, 213–221.

[8] Haber, J. A.; Lewis, N. S. *J. Phys. Chem. B* **2002,** *106*, 3639–3656.

[9] Himpsel, F. J.; McFeeley, F. R.; Taleb-Ibrahimi, A.; Yarmoff, J. A.; Hollinger, G. *Phys. Rev. B.* **1988,** *38*, 6084–6096.

[10] Seah, M. P. Quantification of AES and XPS. In *Practical Surface Analysis*, Vol. 1, 2nd ed.; Briggs, D.; Seah, M. P., Eds.; John Wiley & Sons: Chichester, 1990.

[11] Hunger, R.; Fritsche, R.; Jaeckel, B.; Jaegermann, W.; Webb, L. J.; Lewis, N. S. *Phys. Rev. B.* **2004,** in press.

[12] Himpsel, F. J.; Hollinger, G.; Pollak, R. A. *Phys. Rev. B.* **1983,** *28*, 7014–7018.

[13] Sze, S. M. *The Physics of Semiconductor Devices;* Wiley: New York, 2nd ed.; 1981.

[14] Sturzenegger, M.; Prokopuk, N.; Kenyon, C. N.; Royea, W. J.; Lewis, N. S. *J. Phys. Chem. B* **1999,** *103*, 10838–10849.

[15] Fidelis, A.; Ozanam, F.; Chazalviel, J. N. *Surf. Sci.* **2000,** *444*, L7–L10.

[16] Boukherroub, R.; Wayner, D. D. M.; Sproule, G. I.; Lockwood, D. J.; Canham, L. T. *Nano Letters* **2001,** *1*, 713–717.

[17] Boukherroub, R.; Wayner, D. D. M.; Lockwood, D. J.; Canham, L. T. *J. Electrochem. Soc.* **2001,** *148*, H91–H97.

[18] Yablonovitch, E.; Gmitter, T. J. *Solid-State Electron.* **1992,** *35*, 261–267.

[19] Royea, W. J.; Michalak, D. J.; Lewis, N. S. *Appl. Phys. Lett.* **2000,** *77*, 2566–2568.

[20] Gstrein, F.; Michalak, D. J.; Royea, W. J.; Lewis, N. S. *J. Phys. Chem. B* **2002,** *106*, 2950–2961.

Chapter 8

Comparison of the Electrical Properties and Chemical Stability of Crystalline Silicon(111) Surfaces Alkylated Using Grignard Reagents or Olefins with Lewis Acid Catalysts

8.1 Introduction

Results presented in Chapters 6 and 7 make clear how important the production of high-quality, oxide-free surfaces is to the success of surface functionalization techniques at preventing harmful surface charge carrier recombination behavior. As described extensively in Section 1.2, numerous research groups have examined a number of functionalization methods for alkylating silicon surfaces.[1] These techniques fall generally into the categories of nucleophilic substitution with electron-rich functional groups such as alkylmagnesium or alkyllithium reagents,[2–10] hydrosilation of a terminal alkene through a radical intermediate,[8,11–28] and electrochemical grafting of a functional group onto the Si surface.[29–36] The work in this field has been pursued on Si(111) and (100) surfaces, as well as on porous Si, and has been analyzed by numerous analytical methods appropriate for each surface. There has been very little comparison of the quality of the surface generated by these various methods based on a consistent, clean, well-defined model, which makes it difficult to evaluate the relative strengths or weaknesses of each functionalization route or to make

a quantitative assessment of the most promising or useful functionalization methods. In order for this promising field to develop further, some direct comparisons of the chemical and electrical stability of different modification techniques must be made.

In the work described here, Si(111) surfaces were modified with straight-chain alkyl groups by four functionalization techniques: (i) chlorination/alkylation with PCl_5 as the chlorinating agent or (ii) chlorination/alkylation with Cl_2(g) as the chlorinating agent, (iii) Lewis acid-mediated reduction of a terminal alkene, and (iv) electrochemical oxidation of CH_3MgI. The functionalized surfaces were initially characterized by X-ray photoelectron spectroscopy (XPS) while time-resolved radio frequency (rf) photoconductivity methods were used to determine the recombination velocities of charge carriers on the functionalized surfaces while the sample was maintained under N_2(g). XP spectra and surface charge carrier recombination velocities (S) were then measured periodically, while the functionalized surfaces were exposed to air for over 600 hr. The chemical oxidation of the surface due to air exposure, determined by XPS, was correlated to the *S* values of the surface to determine if changes in the surface recombination velocity could be linked to changes in the chemical composition of the functionalized Si surfaces.

8.2 Experimental

8.2.1 Materials and Methods

8.2.1.1 Materials

Two different types of Si(111) wafers were used in this study. The n-type Si(111) wafers used for XPS measurements were polished only on one side and were obtained from Crysteco (Wilmington, OH). These samples were 525 μm thick and P-doped, with a resistivity of 2.0–8.5 Ω cm. Samples for surface recombination velocity measurements were obtained from Topsil Inc. (Frederikssund, Denmark). These wafers were float-zone grown n-type, P-doped, Si(111), 280 μm thick, with resistivities of 3500–4600 Ω cm, and were polished on both sides. The manufacturer reported a bulk charge carrier lifetime, τ_b, of 2 ms.

All solvents used in functionalization reactions were anhydrous, stored under N_2(g),

and, apart from occasionally pouring over molecular sieves to ensure solvent dryness, were used as received from Aldrich Chemical Corp. Solvents were only exposed to the atmosphere of a N_2(g)-purged flush box. Nanopure 18 MΩ cm resistivity H_2O was used at all times. All other chemicals were used as received unless otherwise specified.

8.2.1.2 Sample Preparation

Because there were substantial variations in sample preparation from what was described in Chapter 2, experimental procedures used in surface preparation will be described here in detail. Before use, all wafers were chemically oxidized, cleaned, and etched as described in Section 7.2.1.2. After etching, the samples were immediately inserted via a quick-entry load lock into an ultra-high vacuum (UHV) system for XPS measurements. The UHV chamber was connected via a second quick-entry load lock into a N_2(g)-purged flush box in which further surface modification reactions were conducted. Once a sample entered the UHV system it was not exposed to ambient air until after surface modification. Occasionally wafers were inserted directly into the vacuum-sealed antechamber of the N_2(g)-purged flush box to prevent scratches on the surface that arose from contact with the XPS sample holder.

8.2.1.3 Functionalization by Chlorination/Alkylation

Chlorinated Si(111) surfaces were prepared by two chlorination agents, PCl_5 and Cl_2(g), as described in Section 7.2.1.3. Subsequent alkylation of the Cl-terminated Si surface was then conducted as described also in Section 7.2.1.3.

8.2.1.4 Lewis Acid-Mediated Terminal Alkene Reduction

A third functionalization route employed in this study was the Lewis acid-catalyzed reduction of a terminal alkene directly on the H-terminated Si(111) surface. The alkenes 1-hexene and 1-octene ($>$94%, Aldrich) were filtered over activated alumnia and dried by refluxing over sodium/benzophenone. The alkenes were then transferred into the N_2(g)-purged flush box. Freshly etched, H-terminated Si(111) samples were functionalized by

immersion in approximately equal volumes of the alkene and 1.0 M $C_2H_5AlCl_2$ in hexanes (Aldrich) at room temperature for 12 hr.[25,26] Samples were then removed from solution and were rinsed in tetrahydrofuran (THF), CH_2Cl_2, and CH_3OH, and dried under a stream of N_2(g). XP spectra and surface recombination velocities were then recorded on the functionalized surfaces under a N_2(g) ambient. Samples were then exposed to air for extended periods of time during which XP spectra and rf photoconductivity decay data were periodically collected.

8.2.1.5 Electrochemical Reduction of CH_3MgI

Hydrogen-terminated Si(111) surfaces were also functionalized through the electrochemical oxidation of CH_3MgI.[32,33] Samples that were polished and functionalized on both sides were used to obtain both XP spectra and surface charge carrier recombination velocities for this system. These samples were treated slightly differently from those functionalized through the methods described above because of the need to protect the electrical contacts from the methylmagnesium iodide solution. A Teflon two-chambered cell was fabricated so that both sides of the double-polished wafer could be exposed to the electrolysis solution. Oxidized wafers were cleaned by sequential rinsing with H_2O, CH_3OH, acetone, CH_3OH, and H_2O, and the samples were then dried under a stream of N_2(g). Dried samples were mounted into the cell to perform the surface functionalization reactions. Ohmic contacts were made with a Ga/In eutectic on the regions of the wafer that were exposed above and below the cell body. The contacts were shorted together using a tinned Cu wire.

The sample was etched by filling both sides of the cell with 40% NH_4F(aq). After 20 min, the etching solution was removed and the cell was filled with H_2O to rinse the sample surface. The H_2O was then removed from the cell, and the sample was dried under a stream of N_2(g). The surface and interior of the cell could not be dried completely in a short period of time, so the partially dried sample was immediately placed into the antechamber of a N_2(g)-purged flush box and vacuum was applied to remove any remaining H_2O. The cell was then moved into the N_2(g)-purged flush box for electrochemical modification. Each chamber of the electrochemical cell contained a section of Cu gauze that served as a counter electrode. The pieces of Cu gauze were connected together using a Cu wire,

thereby forming a single counter electrode.

Alkylation was performed in a solution of 3.0 M CH_3MgI in diethyl ether (Aldrich) by applying 0.1 mA cm^{-2} of constant anodic current density for 5 min with continuous stirring of the solution. After surface modification, the cell was rinsed with CH_2Cl_2 and CH_3OH, respectively. The cell was then dismantled, and the top and bottom ohmic contacts were scribed off to leave behind only the portion of the wafer that had been exposed to the reaction solution. This wafer was rinsed again in CH_3OH, sonicated in CH_3OH, further sonicated in CH_3CN, and dried with a stream of N_2(g). XP spectra and rf photoconductivity decay data were measured on the functionalized surface under a N_2(g) ambient atmosphere, and the sample was then exposed to air and the surface composition and electrical properties were monitored periodically .

8.2.2 Instrumentation

XPS and SRV data were collected as previously described in Section 7.2.2.

8.3 Results

8.3.1 Surfaces Functionalized by Chlorination/Alkylation Methods

Results for Si(111) surfaces alkylated through two different chlorination methods, exposure to PCl_5 with a chemical radical initiator and Cl_2(g) homolytically cleaved with UV light, are described in detail in Section 7.3.1. To aid in comparison of the chemical and electronic properties of alkylated surfaces prepared through different chemical techniques, data described in Section 7.3.1 are repeated in Tables 8.1–8.3.

8.3.2 Lewis Acid-Mediated Terminal Alkene Reduction

8.3.2.1 XPS Results

The XP spectrum of a freshly prepared C_6H_{13}-terminated surface prepared through the Lewis acid-catalyzed reduction of 1-hexene is displayed in Figure 8.1. The C 1s peak area

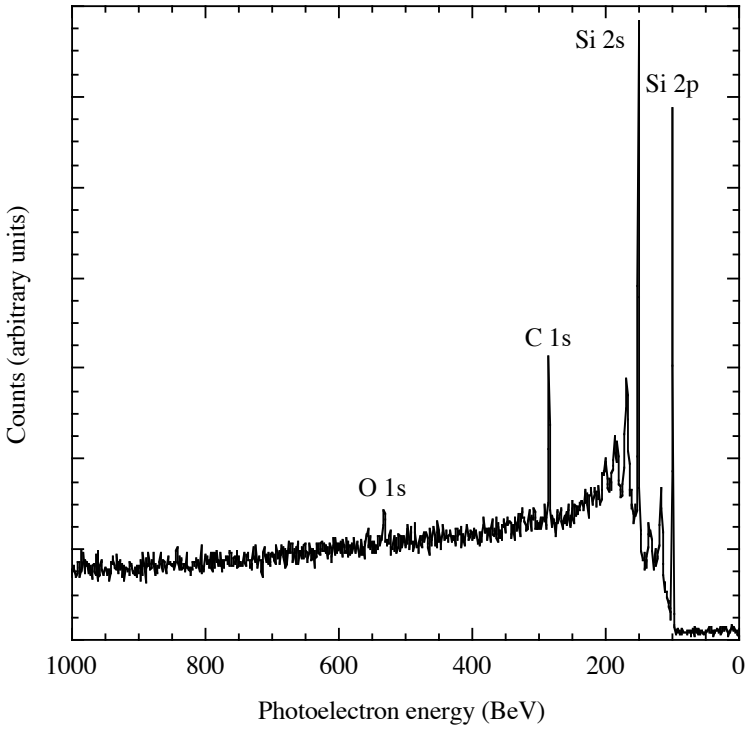

Figure 8.1: Survey scan XP spectrum of C_6H_{13}-terminated Si(111) prepared by reduction of 1-hexene catalyzed by $C_2H_5AlCl_2$.

surface preparation route	-R	XPS peak area ratio[d]		
		C 1s	O 1s	Cl 2p
$PCl_5/C_nH_{2n+1}MgX$[a]	-Cl	0.3±0.2	0.5±0.2	0.45±0.06
	$-CH_3$	0.52±0.03	0.459±0.003	
	$-C_2H_5$	0.40±0.004	0.27±0.07	
	$-C_6H_{13}$	0.68±0.08	0.4±0.01	
	$-C_8H_{17}$	0.6±0.1	0.3±0.2	
$Cl_2/C_nH_{2n+1}MgX$[a]	-Cl	0.3±0.2	0.2±0.1	0.8±0.4
	$-CH_3$	0.62±0.9	0.75±0.8	
	$-C_2H_5$	0.36±0.06	0.3±0.1	
	$-C_8H_{17}$	0.75±0.03	0.48±0.04	
C_nH_{2n+1}-CH=$CH_2/C_2H_5AlCl_2$[b]	$-C_6H_{13}$ control[e]	0.17±0.01	0.21±0.002	
	$-C_8H_{17}$ control[e]	0.26±0.01	∼1	
	$-C_6H_{13}$	0.26±0.01	∼1	
	$-C_8H_{17}$	0.6±0.1	0.247±0.002	
CH_3MgI/h^+[c]	$-CH_3$	1.4±0.9	13.±0.7	

Table 8.1: Normalized peak area ratios for species present on the functionalized Si(111) surface. [a]Preparation described in Section 7.2.1.3. [b]Preparation described in Section 8.2.1.4. [c]Preparation described in Section 8.2.1.5. [d]Values are normalized to the Si 2p peak area. [e]Surface prepared by immersing the sample in alkene without $C_2H_5AlCl_2$.

surface preparation route	-R	XPS SiO_x:Si equivalent monolayer coverage			
		time in air (hr)	SiO_x:Si 2p peak area ratio	equiv ML SiO_2[a]	equiv ML SiO_2[b]
NH_4F etch	-H	216	0.3	1.4	1.4
$PCl_5/C_nH_{2n+1}MgX$	-Cl	264	0.40±0.09	1.8±0.3	1.9±0.4
	$-CH_3$	216	0.16±0.08	0.8±0.4	0.8±0.4
	$-C_2H_5$	216	0.17±0.03	0.9±0.1	0.8±0.1
	$-C_6H_{13}$	192	0.18±0.02	0.90±0.07	0.86±0.07
	$-C_8H_{17}$	192	0.12	∼0.6	∼0.6
$Cl_2/C_nH_{2n+1}MgX$	-Cl	215	0.306±0.009	1.43±0.04	1.46±0.04
	$-CH_3$	288	0.11	∼0.6	∼0.5
	$-C_2H_5$	312	0.08±0.02	0.44±0.09	0.40±0.08
$C_nH_{2n+1}CH{=}CH_2/CH_2H_5AlCl_2$	$-C_6H_{13}$ control[c]	192	0.281±0.008	1.33±0.03	1.34±0.04
	$-C_8H_{17}$ control[c]	192	0.24±0.01	1.17±0.05	1.16±0.06
	$-C_6H_{13}$	168	0.4±0.2	1.6±0.7	1.7±0.9
	$-C_8H_{17}$	360	0.21±0.02	1.01±0.07	0.98±0.07

Table 8.2: Normalized SiO_x:Si 2p peak area ratio and fractional monolayer coverage of SiO_x on the functionalized Si(111) surface. [a]Calculated from Eq. 7.1 and then divided by 0.35 nm. [b]Calculated by dividing the SiO_x:Si 2p peak area ratio by 0.21, a normalization constant representing 1 fractional monolayer of SiP_x caluclated from Eq. 7.5. [c]Surface prepared by immersing the sample in alkene without $C_2H_5AlCl_2$.

surface preparation route	-R	time in air					
		0 min (under N_2(g))		10 min		>24 hr	
		τ (μs)	S (cm s^{-1})	τ (μs)	S (cm s^{-1})	τ (μs)	S (cm s^{-1})
NH_4F(aq)	-H, control[a]	11.8±0.6	1180±60	<10	>1400	<10	>1400
	-H, control[b]	10±1	1350±10	<10	>1400	<10	>1400
	-H, control[c]	21.5±0.4	650±10			<10	>1400
$PCl_5/C_nH_{2n+1}MgX$	-Cl	510±140	28±8	300±30	46±4	<10	>1400
	-Cl, control[d]	70±6	200±20	40±20	370±140	<10	>1400
	-CH_3	130±60	130±50	140±30	100±20	200±70	80±30
	-C_2H_5	40±20	450±180	70±50	260±100	200±90	80±30
	-C_6H_{13}	80±50	260±140	60±30	270±110	120±20	120±20
	-C_8H_{17}	80±20	190±50	50±10	280±60	150±7	93±4
Cl_2(g)/$C_nH_{2n+1}MgX$	-Cl	460±110	31±7	370±70	39±7	<10	>1400
	-CH_3	70±20	250±150	50±20	330±230	110±30	150±60
	-C_2H_5	31±7	470±100	37±8	400±100	80±30	200±80
$C_nH_{2n+1}CH{=}CH_2/C_2H_5AlCl_2$	-C_6H_{13}	40±10	410±120	23±7	660±190	<15	>1200
	-C_6H_{13}, control[e]	<10	>1400			<10	>1400
	-C_8H_{17}	20±10	690±270	18±4	790±160	<15	>1200
	-C_8H_{17}, control[e]	<10	>1400			<10	>1400
CH_3MgI/h^+	-CH_3	18±6	860±200			40±20	460±200
	-CH_3, control[f]	<10	>1400			<10	>1400

Table 8.3: Charge carrier lifetimes and recombination velocities of functionalized Si(111) surfaces. [a]Control surfaces prepared by immersing a H-terminated surface in chlorobenzene and heating for the appropriate reaction time. [b]Control surfaces prepared by immersing a H-terminated surface in chlorobenzene, followed by immersion in THF and heating for the appropriate reaction times in each solvent. [c]Control surfaces prepared by immersing a H-terminated surface in chlorobenzene with benzoyl peroxide and heating for the appropriate reaction time. [d]Control surfaces prepared by immersing a Cl-terminated surface in THF at 70–80°C for 3.5 hr. [e]Control surfaces prepared by immersing a H-terminated surface in alkene without $C_2H_5AlCl_2$ for 12 hr at room temperature. [f]Control surface prepared by immersing a H-terminated surface in CH_3MgI without passing current.

was somewhat lower than that observed for hexyl-terminated surfaces prepared through the PCl_5 chlorination/$C_6H_{13}MgBr$ alkylation route (0.46 $\pm$ 0.08 vs. 0.68 $\pm$ 0.08, Table 8.1). Octyl-terminated surfaces, however, displayed the same C 1s surface coverages for this method as for the chlorination/alkylation route. Control surfaces prepared by immersing Si(111) samples in either 1-hexene or 1-octene for 12 hr without addition of the Lewis acid catalyst showed much lower normalized C 1s and O 1s peak area ratios (Table 8.1), indicating that the functionalization did not occur readily in the absence of the catalyst.

Figure 8.2 summarizes the Si 2p high-resolution XPS oxidation data for C_6H_{13}- and C_8H_{17}-terminated Si(111) surfaces prepared through this functionalization route, and also displays the results for surfaces that were prepared by immersing a sample into the terminal olefin without addition of the $C_2H_5AlCl_2$ catalyst. The C_6H_{13}-terminated surface behaved identically to both of the controls and to the H-terminated surface, indicating that this functionalization technique did not suppress the rate of oxidation of the Si. While all of the surfaces functionalized through a two-step chlorination/alkylation process fully resisted oxidation for the first 30 hr in air, the C_6H_{13}- and C_8H_{17}-terminated surfaces prepared through reduction of a terminal olefin displayed rapid oxidation behavior identical to the H-terminated Si(111) surfaces. Functionalization with C_8H_{17}- groups provided some improved long-term resistance to oxidation. After 200 hr in air, the C_8H_{17}-functionalized surface displayed a normalized SiO_x:Si 2p peak area ratio of 0.21, as compared to a SiO_x : Si 2p peak area ratio of 0.12 observed for an C_8H_{17}-terminated surface prepared by PCl_5 chlorination/C_8H_{17} alkylation.

8.3.2.2 Surface Recombination Velocity Results

Table 8.3 presents the S values of C_6H_{13}- and C_8H_{17}-terminated Si(111) that had been functionalized by the Lewis acid-catalyzed reduction of the terminal alkene. Under a N_2(g) ambient, the initial charge carrier lifetimes of these surfaces were 20–40 μs, but the lifetimes decayed rapidly upon exposure to air, with τ $<$15 μs after 24 hr of air exposure. Unlike the lifetimes of hexyl- and octyl-terminated Si(111) surfaces prepared through the $PCl_5/C_nH_{2n+1}MgX$ route, which dropped upon exposure to air but recovered their initial values over a period of 600–700 hr, the lifetimes of hexyl- and octyl-functionalized Si(111)

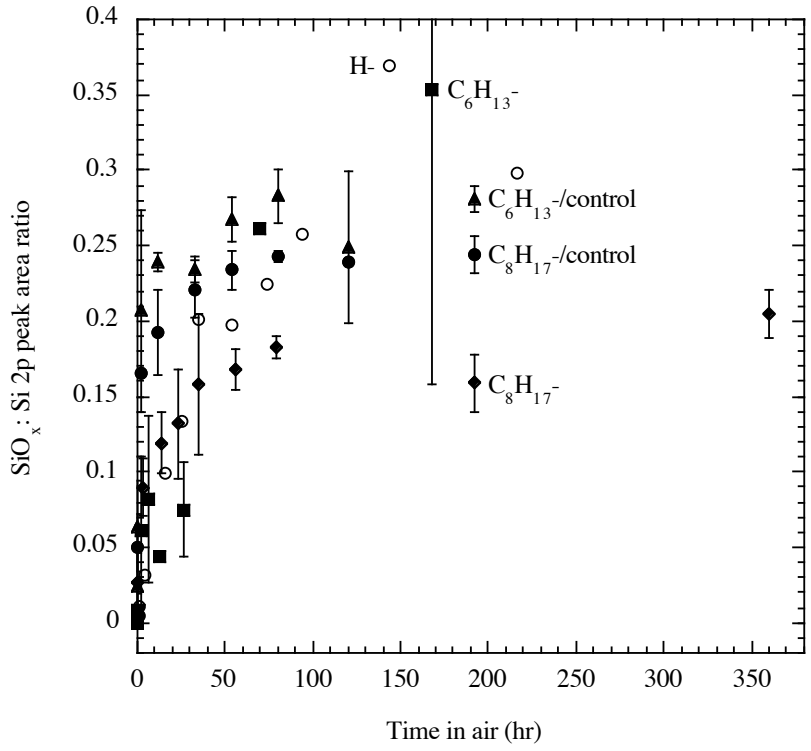

Figure 8.2: Ratio of the oxidized Si 2p peak area (SiO_x) to the bulk Si 2p peak area (Si^0) for Si(111) surfaces prepared by terminal olefin reduction catalyzed by $C_2H_5AlCl_2$ and exposed to ambient air over extended time periods: open circles, H-terminated Si; squares, C_6H_{13}-terminated Si; diamonds, C_8H_{17}-terminated Si; triangles, control surface immersed in 1-hexene with no Lewis acid; closed circles, control surface immersed in 1-octene with no Lewis acid.

surfaces prepared through the reduction of a terminal olefin did not recover and remained $<$15 μs until the experiment was terminated ($\approx$500 hr). Surface recombination velocities on control surfaces prepared by immersion in terminal alkene without the catalyst were $>$1400 cm s^{-1} (Table 8.3), indicative of a highly defective surface containing a large number of electrical recombination sites.

8.3.3 Electrochemical Reduction of CH_3MgI

8.3.3.1 XPS Results

Figure 8.3 displays the XP spectrum of a functionalized Si(111) surface prepared by anodization in 3.0 M CH_3MgI in diethyl ether. A large C 1s peak was observed at 285.5 BeV with a C 1s : Si 2p peak area ratio of 1.4 $\pm$ 0.9. Large peaks were also observed at 532 and 980 BeV, corresponding to O 1s and O $K_1L_{23}L_{23}$ (Auger) peaks, respectively. Peaks at 620 and 631 BeV, identified as I $3d_{5/2}$ and I $3d_{3/2}$, respectively, were also observed periodically. Occasionally a peak at 307 BeV, tentatively identified as the Mg $K_1L_{23}L_{23}$ peak, was also observed, even after the samples had been sonicated extensively in CH_3OH and CH_3CN.

The magnitude of the C 1s : Si 2p peak area ratio was larger than that expected for alkyl chains of at least 12 carbon atoms in length,[5] indicating that the C 1s signal was not due entirely to surface-bound methyl groups. The O 1s : Si 2p peak area ratio (Table 8.1) was substantially larger than that observed for any other alkylation method studied in this work, although no SiO_x signals were observed in the spectra of freshly prepared CH_3-terminated surfaces.

Methylated samples were kept in air for up to 150 hr, and XPS data were again collected on the surfaces. All surfaces showed a SiO_x:Si 2p normalized peak area ratio of $>$0.1, although the peak areas varied widely and were occasionally in excess of 0.4. This latter value corresponds to an equivalent SiO_2 coverage of at least 2 monolayers.

8.3.3.2 Surface Recombination Velocity Results

After an extended period of time in air, τ values for these surfaces were 40 $\pm$ 20 μs (S = 460 $\pm$ 200 cm s^{-1}, Table 8.3). A control surface was formed by immersing the Si electrode and

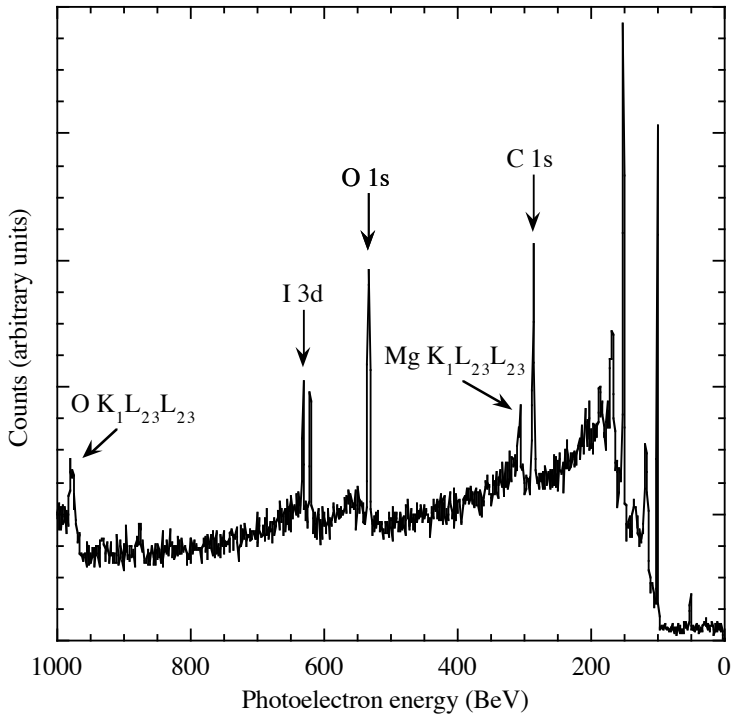

Figure 8.3: Survey scan XPS spectrum of CH_3-terminated Si(111) prepared by anodic grafting in CH_3MgI in diethyl ether.

the Cu counter electrode into the CH_3MgI solution while no current was passed through the cell. The resulting surface exhibited $\tau \leq 10$ μs over a period of 100 hr in air, after which time the sample was discarded. The electrochemical functionalization method therefore produced a surface that was moderately more passivated electrically than a H-terminated Si(111) surface but which still possessed significant levels of electrically active surface recombination sites.

8.4 Discussion

The contrast between alkyl-terminated surfaces prepared through both two-step chlorination/ alkylation functionalization routes that were examined in Chapter 7 and other, nominally similar, alkyl surfaces prepared through other wet-chemical techniques is striking. Surface coverage of the alkyl group on the freshly prepared surface, estimated by the normalized peak area ratio of the C 1s:Si 2p regions determined by XPS, are roughly similar for C_6H_{13}- and C_8H_{17}-terminated Si(111) surfaces (Table 8.1). After approximately 1 week of exposure to ambient air, only somewhat higher amounts of silicon oxides had grown on C_6H_{13}- and C_8H_{17}-terminated Si(111) surfaces prepared through the Lewis acid-catalyzed reduction of a terminal olefin than on identically terminated surfaces prepared through the two-step chlorination/alkylation routes (Table 8.2). Yet alkylated surfaces produced by the Lewis acid-catalyzed reduction of a terminal alkene directly on the H-terminated surface showed significantly higher surface charge carrier recombination rates than those produced through the chlorination/alkylation processes. This observation can be understood when the probable mechanism of alkylation, shown in Figure 8.4, is considered.[26,37,38] Because alkylation involves coupling between an alkyl bonded to the negatively charged Lewis acid catalyst and a hindered surface-localized cation, it is likely that steric constraints will prevent alkylation from occurring at all possible surface sites. This could result in a surface with substantial pinhole defects that would not be detected by the XPS analytical technique used here because of inevitable contamination from adventitious hydrocarbon sources. If the terminal olefin reduction functionalization route does indeed leave behind any great number of pinhole defects at the Si(111) surface, it will be less likely to prevent substantial

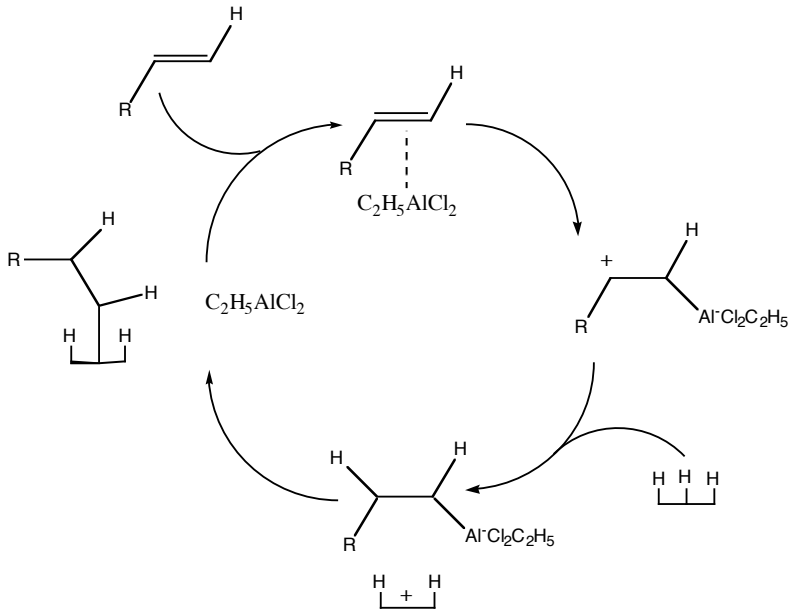

Figure 8.4: Proposed mechanism of Si surface alkylation through the Lewis acid-catalyzed reduction of a terminal olefin.

rates of surface electron-hole recombination.

Functionalization through the Lewis acid-catalyzed reduction of a terminal olefin on the H-terminated Si surface, as well as transition metal-catalyzed terminal alkene reductions, have been employed successfully on porous Si surfaces.[25,26,39] Differences in behavior of single-crystal and porous Si substrates may arise in part from the greater surface area of porous Si, which will present less steric resistance to coupling between the surface and the catalyst, as well as the distribution of chemically different silicon hydride sites that are present on porous Si surfaces relative to that of atomically flat H-terminated Si(111) crystals. Clearly, the reaction chemistry of crystalline Si(111) is quite sensitive to the method of preparation of the alkyl overlayer on the functionalized Si surface.

Data from XPS and rf conductivity decay methods indicate that alkylated Si(111) surfaces formed by an electrochemical treatment are not as passivated chemically or electrically as surfaces that were prepared through the chlorination/alkylation routes. Infrared spectroscopic studies have indicated that the electrochemical anodization method produces some degree of methylation of the Si(111) surface.[33] The XPS data described above indicate however that this surface also has a large O 1s XPS signal, as well as signals from other elements used in the functionalization step. Accordingly, these surfaces displayed chemical and electrical properties inferior to any of the alkylated surfaces that were prepared by either of the chlorination/alkylation routes. Clearly, although all four of the Si surfaces studied in this work nominally had alkyl groups introduced onto the Si surface, subtle changes in the extent and quality of the alkyl termination are significant factors in determining the magnitude and degree of chemical and electrical passivation of the resulting functionalized Si surfaces.

8.5 Conclusion

Significant differences were observed in the chemical and electrical properties of Si(111) surfaces that were functionalized to introduce alkyl groups on the surface. A two-step functionalization route involving chlorination of a freshly etched H-terminated surface followed by alkylation with a Grignard reagent resulted in surfaces that resisted oxidation in

air for a period of ≈50 hr and subsequently oxidized only slowly in air. These surfaces also displayed long charge carrier lifetimes and low surface recombination velocities, demonstrating that they are well-passivated electrically even during native oxide growth. Similar behavior was observed for surfaces that were functionalized using Cl_2(g) as the chlorinating agent. Methylation using the chlorination/alkylation routes produced the lowest surface recombination velocities of all the alkyl groups studied, although good chemical stability and a high degree of electrical passivation was also observed for the other alkyl overlayers on the Si(111) surface. In contrast, surfaces functionalized by the Lewis acid-mediated reduction of a terminal alkene directly on the H-terminated Si(111) oxidized rapidly in air and exhibited higher surface recombination velocities. Methyl-terminated Si(111) surfaces prepared by electrochemical anodization of the Si in diethyl ether solutions of CH_3MgI displayed extensive oxidation in air and exhibited significantly higher surface recombination velocities than the other alkylated surfaces.

Bibliography

[1] Bent, S. F. *Surf. Sci.* **2002,** *500,* 879–903.

[2] Mitchell, S. A.; Boukherroub, R.; Anderson, S. *J. Phys. Chem. B* **2000,** *104,* 7668–7676.

[3] Yu, H. Z.; Boukherroub, R.; Morin, S.; Wayner, D. D. M. *Electrochem. Commun.* **2000,** *2,* 562–566.

[4] Bansal, A.; Li, X. L.; Lauermann, I.; Lewis, N. S.; Yi, S. I.; Weinberg, W. H. *J. Am. Chem. Soc.* **1996,** *118,* 7225–7226.

[5] Bansal, A.; Li, X.; Yi, S. I.; Weinberg, W. H.; Lewis, N. S. *J. Phys. Chem. B* **2001,** *105,* 10266–10277.

[6] He, J.; Patitsas, S. N.; Preston, K. F.; Wolkow, R. A.; Wayner, D. D. M. *Chem. Phys. Lett.* **1998,** *286,* 508–514.

[7] Okubo, T.; Tsuchiya, H.; Sadakata, M.; Yasuda, T.; Tanaka, K. *Appl. Surf. Sci.* **2001,** *171,* 252–256.

[8] Terry, J.; Linford, M. R.; Wigren, C.; Cao, R. Y.; Pianetta, P.; Chidsey, C. E. D. *Appl. Phys. Lett.* **1997,** *71,* 1056–1058.

[9] Terry, J.; Linford, M. R.; Wigren, C.; Cao, R. Y.; Pianetta, P.; Chidsey, C. E. D. *J. Appl. Phys.* **1999,** *85,* 213–221.

[10] Webb, L. J.; Lewis, N. S. *J. Phys. Chem. B* **2003,** *107,* 5404–5412.

[11] Boukherroub, R.; Wayner, D. D. M. *J. Am. Chem. Soc.* **1999,** *121,* 11513–11515.

[12] Cicero, R. L.; Linford, M. R.; Chidsey, C. E. D. *Langmuir* **2000,** *16,* 5688–5695.

[13] Effenberger, F.; Gotz, G.; Bidlingmaier, B.; Wezstein, M. *Angew. Chem.-Int. Edit.* **1998,** *37,* 2462–2464.

[14] Terry, J.; Mo, R.; Wigren, C.; Cao, R. Y.; Mount, G.; Pianetta, P.; Linford, M. R.; Chidsey, C. E. D. *Nucl. Instr. Methods Phys. Res. Sect. B* **1997,** *133*, 94–101.

[15] Linford, M. R.; Chidsey, C. E. D. *J. Am. Chem. Soc.* **1993,** *115*, 12631–12632.

[16] Linford, M. R.; Fenter, P.; Eisenberger, P. M.; Chidsey, C. E. D. *J. Am. Chem. Soc.* **1995,** *117*, 3145–3155.

[17] Sieval, A. B.; Demirel, A. L.; Nissink, J. W. M.; Linford, M. R.; van der Maas, J. H.; de Jeu, W. H.; Zuilhof, H.; Sudholter, E. J. R. *Langmuir* **1998,** *14*, 1759–1768.

[18] Sieval, A. B.; Linke, R.; Heij, G.; Meijer, G.; Zuilhof, H.; Sudholter, E. J. R. *Langmuir* **2001,** *17*, 7554–7559.

[19] Sung, M. M.; Kluth, G. J.; Yauw, O. W.; Maboudian, R. *Langmuir* **1997,** *13*, 6164–6168.

[20] Boukherroub, R.; Wojtyk, J. T. C.; Wayner, D. D. M.; Lockwood, D. J. *J. Electrochem. Soc.* **2002,** *149*, H59–H63.

[21] Boukherroub, R.; Wayner, D. D. M.; Sproule, G. I.; Lockwood, D. J.; Canham, L. T. *Nano Letters* **2001,** *1*, 713–717.

[22] Boukherroub, R.; Wayner, D. D. M.; Lockwood, D. J.; Canham, L. T. *J. Electrochem. Soc.* **2001,** *148*, H91–H97.

[23] Gelloz, B.; Sano, H.; Boukherroub, R.; Wayner, D. D. M.; Lockwood, D. J.; Koshida, N. *Appl. Phys. Lett.* **2003,** *83*, 2342–2344.

[24] Boukherroub, R.; Morin, S.; Bensebaa, F.; Wayner, D. D. M. *Langmuir* **1999,** *15*, 3831–3835.

[25] Buriak, J. M.; Allen, M. J. *J. Am. Chem. Soc.* **1998,** *120*, 1339–1340.

[26] Buriak, J. M.; Stewart, M. P.; Geders, T. W.; Allen, M. J.; Choi, H. C.; Smith, J.; Raftery, D.; Canham, L. T. *J. Am. Chem. Soc.* **1999,** *121*, 11491–11502.

[27] Zazzera, L. A.; Evans, J. F.; Deruelle, M.; Tirrell, M.; Kessel, C. R.; McKeown, P. *J. Electrochem. Soc.* **1997,** *144*, 2184–2189.

[28] Schmeltzer, J. M.; Porter, L. A.; Stewart, M. P.; Buriak, J. M. *Langmuir* **2002,** *18*, 2971–2974.

[29] Allongue, P.; de Villeneuve, C. H.; Pinson, J.; Ozanam, F.; Chazalviel, J. N.; Wallart, X. *Electrochimica Acta* **1998,** *43*, 2791–2798.

[30] Allongue, P.; de Villeneuve, C. H.; Pinson, J. *Electrochimica Acta* **2000,** *45*, 3241–3248.

[31] Allongue, P.; de Villeneuve, C. H.; Cherouvrier, G.; Cortes, R.; Bernard, M. C. *J. Electroanal. Chem.* **2003,** *550*, 161–174.

[32] Dubois, T.; Ozanam, F.; Chazalviel, J.-N. *Electrochem. Soc. Proc.* **1997,** *97–7*, 296 – 310.

[33] Fidelis, A.; Ozanam, F.; Chazalviel, J. N. *Surf. Sci.* **2000,** *444*, L7–L10.

[34] Gros-Jean, M.; Herino, R.; Chazalviel, J. N.; Ozanam, F.; Lincot, D. *Mat. Sci. Eng. B* **2000,** *69*, 77–80.

[35] Henry de Villeneuve, C.; Pinson, J.; Bernard, M. C.; Allongue, P. *J. Phys. Chem. B* **1997,** *101*, 2415–2420.

[36] Lees, I. N.; Lin, H. H.; Canaria, C. A.; Gurtner, C.; Sailor, M. J.; Miskelly, G. M. *Langmuir* **2003,** *19*, 9812–9817.

[37] Asao, N.; Sudo, T.; Yamamoto, Y. *J. Org. Chem.* **1996,** *61*, 7654–7655.

[38] Sudo, T.; Asao, N.; Gevorgyan, V.; Yamamoto, Y. *J. Org. Chem.* **1999,** *64*, 2494–2499.

[39] Saghatelian, A.; Buriak, J. M.; Lin, V. S. Y.; Ghadiri, M. R. *Tetrahedron* **2001,** *57*, 5131–5136.

Chapter 9

Summary of Current Understanding of the Chemistry and Electrochemical Characteristics of the Alkyl-Terminated Si(111) Surface Prepared Through a Chlorination/Alkylation Route

9.1 General Conclusion

The most important aspect of the work described here has been to demonstrate that a two-step chlorination/alkylation functionalization route of the Si(111) surface produces a surface-bound alkyl layer that is highly chemically and morphologically homogeneous. Both high-resolution soft X-ray photoelectron spectroscopy (SXPS) and surface-sensitive transmission infrared spectroscopy (TIRS) have shown the sequential formation of a H-terminated and Cl-terminated surface on which very nearly 1 monolayer (ML) of surface Si atoms are chemically bonded to the overlayer molecule. SXPS studies have shown that when the Cl-Si(111) surface is exposed to an alkylmagnesium halide solution, all of the Cl is replaced with an alkyl moiety linked to the surface with a Si–C bond. The most direct evidence of this surface Si–C bond has not yet been observed using TIRS. Polarization-type TIRS was used, however, to characterize the CH_3- symmetrical bending motion on the methyl-terminated surface located at a frequency of 1257 cm^{-1}, and to demonstrate that the methyl group is perpendicular to the Si surface, as predicted by tetrahedral geome-

tries of both C and Si. At all points in the surface functionalization chemistry described herein, the level of contamination of the Si surface by either silicon oxides or adventitious hydrocarbon species was low.

A question that has been consistently addressed in this work is the chemical bonding to an Si(111) surface functionalized with an alkyl group, such as C_2H_5-, that is sterically prevented from bonding to every surface Si(111) atop atom because of the restrictive distance between Si atop atoms (3.8 Å).[1] SXPS and standard laboratory-based XPS found that any remaining unalkylated Si sites could not be functionalized with Cl, O, or Mg. The only other atom that would be readily available to bond to the surface during the functionalization reaction is H, which cannot be seen by survey scan XPS. Close investigation of the Si 2p region, however, revealed that the Si–C peak of a C_2H_5-terminated surface was shifted +0.19 eV above the Si $2p_{3/2}$ bulk peak, which is between the photoelectron shifts from Si–H surface bonds (+0.15 eV) and Si–C bonds on the CH_3-terminated surface (+0.34 eV). It was also broader than that seen on the CH_3-terminated surface. These two observations could be explained if this peak were actually a convolution of contributions from Si–C and Si–H features. TIRS of the C_2H_5-terminated surface identified peaks that could be ascribed to the Si–H stretching and bending motions, confirming that a Si–H species is present on the alkylated surface. The peak corresponding to the Si–H stretching mode was centered at 2080 cm^{-1}, slightly lower than the well-known value of 2083 cm^{-1} on the Si(111) surface,[2] and was much broader than the sharp feature seen on the ideally flat Si(111) surface. This indicates that any hydrogen bonded to atop Si atoms is exposed to a number of different chemical environments, as expected for a surface that is sterically less ordered than either the freshly prepared H- or CH_3-modified surfaces.

These clean, alkylated Si(111) surfaces prepared through the two-step preparation technique were found to have a very high degree of morphological order. Low energy electron diffraction (LEED) and scanning tunneling microscopy (STM) both demonstrated that the CH_3-terminated Si(111) surface retains an unreconstructed (1 x 1) structure over very long length scales. Furthermore, a low density of surface defects or etch pits emerges on the surface even after being exposed at high temperature to the harsh chemical reaction conditions containing Cl· radicals and alkylmagnesium halide reagents. This has demonstrated

that the nearly ideal, flat H-terminated Si(111) template provided by the freshly etched surface[2] is not significantly degraded, and the alkylated Si(111) surface can be considered flat and defect-free on a long length scale. Moreover, the microscopic structure of the CH_3-terminated surface is ordered enough that at 4.7 K, it was possible for STM to resolve the image of individual methyl hydrogen atoms for the first time. To date, STM studies of the C_2H_5-terminated surface have not been able to determine if any comparable microscopic order is present with the larger alkyl group, or to determine how the bulky C_2H_5- group packs on the Si(111) surface. Such studies are ongoing in our laboratory.

The structural regularity of this surface becomes important when considering the electronic properties and chemical stability of the alkyl-terminated Si(111) surface when exposed to oxidizing conditions for long periods of time. On an ideal surface, electron-hole recombination would occur only at structural or chemical defects that have molecular orbitals inserted into the bandgap, where they would be accessible to charge carrier pairs present at the surface, shown schematically in Figure 1.2. Measuring the rate at which these charge carrier pairs recombine using radio frequency (rf) photoconductivity decay methods provides a sensitive handle to determine the chemical perfection of the surface. These measurements have shown that alkyl-terminated surfaces prepared through the two-step chlorination/alkylation functionalization route have surface charge carrier recombination velocities (S) of $\approx$100 cm s^{-1}, similar to the freshly prepared ideal H-terminated Si(111) surface ($\approx$0.25 cm s^{-1}),[3] and much lower than S of an unpassivated surface ($>$1400 cm s^{-1}).

Unlike the H-terminated surface, however, the alkyl-terminated surfaces studied here maintained those low rates of electron-hole recombination over a period of time of at least 1 month that the sample was exposed to an air ambient. This suggests the alkyl layer imparted a level of chemical stability to the surface that prevented carrier trap states from forming in the bandgap of the crystal in any measurable extent. It was also seen that the method of surface functionalization was important. When surfaces prepared through different functionalization routes were seen to be very similar by XPS, they still could display vastly different rates of surface charge carrier pair recombination. This is possibly a result of the high sensitivity of radio frequency (rf) photoconductivity decay methods in

determining the quality of surface trap states. Surfaces alkylated through a two-step chlorination/alkylation route displayed S values that corresponded to a surface charge carrier pair trap density, (N_t, Eq. 7.9) of 1 in 10^5 surface atoms (Chapter 7). An increase in surface electron hole recombination velocity of 1 order of magnitude, the difference seen in "passivated" versus "unpassivated" surfaces here, corresponds to an increase in surface charge carrier trap states, N_t, also of 1 order of magnitude, to 1 atom in 10^4. It is unlikely that this difference could be measured using chemical characterization techniques, even under the highly surface sensitive conditions employed herein. This difference, however, has been shown to be easy to measure through rf photoconductivity decay methods. This underscores the importance of rigorous chemical characterization of the functionalized surface combined with methods to determine electronic qualities of the surface, to assemble a complete, detailed picture of the surface-overlayer interaction.

Given the extraordinary electronic passivity of alkyl-terminated Si(111) surfaces that maintain low surface charge carrier recombination rates in air, it is reasonable to hypothesize that this is caused by a corresponding chemical passivity that prevents the surface from oxidizing in air. This was found not to be the case, however, as low surface charge carrier recombination rates were correlated to the appearance of a small amount of silicon suboxide, largely Si^{3+}, on alkyl-terminated Si(111) surfaces. A second obvious hypothesis for the low rates of surface electron-hole recombination is the presence of a significant amount of band bending at the Si/alkyl interface that would prevent one of the charge carrier pairs from reaching the surface. This was measured with surface-sensitive SXPS, but the extent of band bending was found to be only 0.1 eV, which is not a significant barrier for either charge carrier at room temperature. The work presented here was unfortunately not able to determine the reason that this suboxide did not contribute to large electron-hole recombination velocities as it appears to do on H- and Cl-terminated Si(111) surfaces, but this puzzling observation provides the motivation for much future work.

Bibliography

[1] Sze, S. M. *The Physics of Semiconductor Devices;* Wiley: New York, 2nd ed.; 1981.

[2] Higashi, G. S.; Chabal, Y. J.; Trucks, G. W.; Raghavachari, K. *Appl. Phys. Lett.* **1990,** *56,* 656–658.

[3] Yablonovitch, E.; Allara, D. L.; Chang, C. C.; Gmitter, T.; Bright, T. B. *Phys. Rev. Lett.* **1986,** *57,* 249–252.

Appendix A

X-ray Photoelectron Spectroscopy Peak Fitting Program

A.1 Introduction

To fit high-resolution soft X-ray photoelectron spectroscopy (SXPS) data collected at the National Synchrotron Light Source (NSLS) at Brookhaven National Laboratory, it was necessary to write a peak fitting program to fit the spectra to a series of doublets (for peaks from the Si^0 signal) and singlets (for peaks from the Si^+–Si^{4+} signals) of Voigt functions after subtraction of an appropriate background spectrum. The general description of the peak fitting strategy as well as the specific program files are reproduced here. This peak fitting program was written specifically for SXPS data collected in the energy range 30.02–39.00 eV in 0.02 eV steps, for a total of 450 data points. For silicon SXPS data the Si $2p_{1/2}$ and $2p_{3/2}$ peak energy difference is well-known to be 0.6 eV and the relative area of the Si $2p_{1/2}$ to $2p_{3/2}$ peaks is known to be 0.51.[1–4] Voigt functions of 95% Gaussian and 5% Lorentzian[4–6] are also well-known to be appropriate for the Si 2p region under high-resolution SXPS conditions. All of these parameters are included in the data fitting programs described below, but can be easily modified to fit other samples or data collection conditions. All programs were written as ".m" files in Matlab v. 6.0 (R13).

A.2 Data Entry and Manipulation

A.2.1 Description

Data from NSLS was stored in text files as a 2-column matrix of the measured kinetic energy in eV, E_{KE}, and intensity of the ejected photoelectrons in counts, I_E. The measured kinetic energy E_{KE} increased down the column of the matrix. Programs for background subtraction and spin-orbit stripping, described below, required the electron intensity to be expressed as a function of binding energy, E_{BE}. The relationship between E_{KE} and E_{BE} is defined by:

$$E_{KE} = h\nu - E_{BE} - \phi \tag{A.1}$$

where $h\nu$ is the excitation energy of the beam (140 eV at NSLS) and ϕ is the work function of the instrument ($\approx$4.64 eV,[7] although it was not calibrated). Once E_{KE} data was converted to E_{BE}, the data set was "flipped" so that E_{BE} decreased down a column. The height of the electron intensity was normalized to 1. The high E_{BE} region of the spectra were often featureless, and peak fitting was easier if large regions of the flat background were eliminated. Therefore a high E_{BE} end point (ept) was designated, and the rest of the data were ignored. Finally, a and b were defined as the mean of the 20 highest and lowest E_{BE} electron intensity points, repsectively. The final data set was defined as $x1 = E_{BE}$ and $y1 = I_E$.

A.2.2 Program File “loaddata_bnl.m”

% start

filename=input(‘filename = ’); % enter file name in format “filepath/filename.txt” and

% hit Enter

g=filename(:,1)

g1=140-g-4.64; % hν and ϕ should be changed depending on the data collection conditions

gnew=flipud(g1);

h=filename(:,2);

hnew=flipud(h);

hrealnew=hnew/max(hnew); % normalizes maximum peak height to 1

ept=input(‘high BE endpoint = ’); % select the data index number of the desired

% high binding energy endpoint and hit Enter

y1=hrealnew(1:ept); % this is the y-axis data

blast=y1(1:20);

b=mean(blast);

last=y1(ept-20:ept);

a=mean(last);

x1=gnew(1:ept); % this is the x-axis data

plot(x1,y1) % the normalized counts are plotted as a function of E_{BE} increasing

% from left to right

% end

A.3 Background Subtraction

A.3.1 Description

The background of all SXPS data were assumed to be a Shirley-type background,[8–10] following extensive precedent in the literature of XPS on the Si 2p core level.[11] This background is caused by inelastically scattered photoelectrons of higher kinetic energy than the energy being measured at any given point on the E_{KE} axis. The background is thus proportional to the integrated area above the high E_{KE} side of the peak.[8] The process for determining this background is described in Figure A.1 in which the background, $B(x)$, at any point along the energy axis x in a spectrum composed of k points of energy separation h, is proportional to the total area of the curve above the background at that point[11] and is defined by:[8]

$$B(x) = \frac{(a-b)Q}{(P+Q)} + b \tag{A.2}$$

In this formulation, a and b are the high and low E_{BE} end points, respectively, $(P+Q)$ is the total integrated area of the curve less the background (called the "background-subtracted," or BS, spectrum), and Q is the total integrated area of the BS spectrum from any point x to point k. The area Q is defined by a simple trapazoidal rule:[8]

$$Q = h\left[\left(\sum_{i=x}^{k} y_i\right) - 0.5(y_x + y_k)\right] \tag{A.3}$$

The background is determined in an iterative procedure in which the first background is estimated as $B_1(x) = b$, the BS spectrum is calculated, and the quantities Q and $(P+Q)$ are used in Eq. A.2 to determine the new background $B_2(x)$. This is then used as the starting point for the next step.[8] The procedure for this is summarized as follows:[10]

(1) choose $B_1(x) = b$;

(2) calculate the BS spectrum, $BS = I_E(x) - B_1(x)$;

(3) determine Q through Eq. A.3 and $(P+Q)$ through a simple trapazoidal rule;

(4) calculate $B_2(x)$ through Eq. A.2;

(5) repeat steps (2) and (3) for the new background;

(6) compare $(P+Q)_{B_2(x)}$ and $(P+Q)_{B_1(x)}$. If the difference is greater than a given toler-

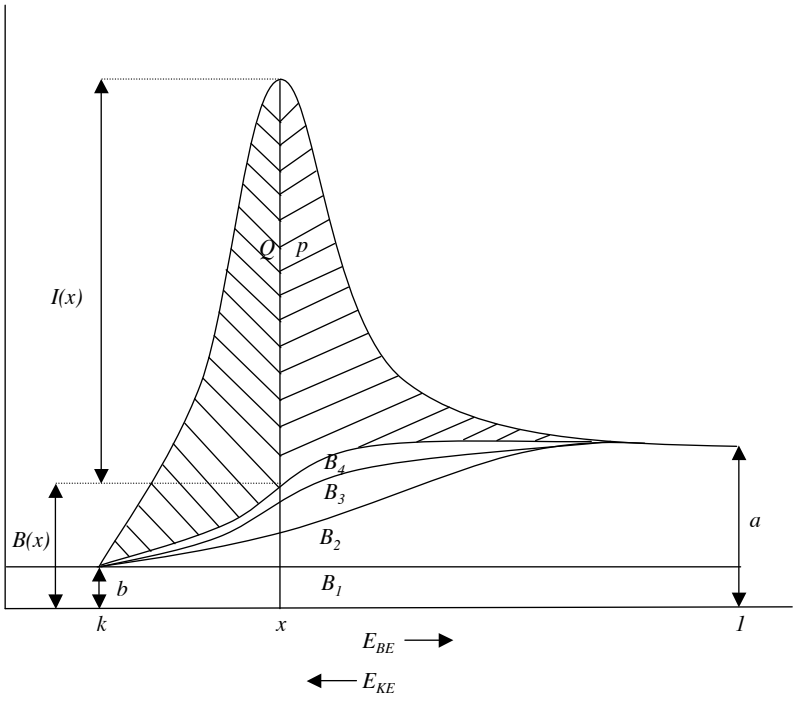

Figure A.1: Schematic representation of background parameters for X-ray photoelectron spectra. A total of k number of x data points evenly dispersed along the x-axis between a and b are shown as E_{BE} increasing from left to right, and E_{KE} decreasing from left to right. $(P + Q)$ is the total area under the background subtracted (BS) spectrum, while Q is the area under the curve between point x and point k. $B_1(x)$–$B_4(x)$ are successive background approximations. Figure adapted from Proctor and Sherwood.[8]

ance, repeat steps (4) and (5).

Data were read in by the file “loaddata_bnl.m” and used without further manipulation. Area under the curve was calculated using a simple trapazoidal command in Matlab. The tolerance was defined as a difference in $(P + Q)$ of 1 x 10^{-5} between two sequential background approximations. The program paused between each iteration of fitting the background to aid the user in following the calculation procedure. Occasionally the high binding energy trailing background could not be fully cut out and would cause the background fitting program to fluctuate wildly after the first few iterations. If this happened, the program was stopped after the last appropriate iteration, and that approximation of the background was used as the final background.

A.3.2 Program File “shirley_bk450.m”

```
% start
% estimate first background:
BS1=y1-b;
Atot=trapz(x1,BS1);
BS1b=cumsum(BS1);
Axk=0.02*((BS1b)-(BS1+BS1(1))/2); % x-axis data step width collected at
% NSLS was 0.02 eV
B2=(a-b)*Axk/Atot+b;
plot(x1,y1,x1,B2); % plot of peak and calculated background
pause; % pause to allow inspection of the calculated background;
% to continue, hit any key
BS2=y1-B2;
Atotnew=trapz(x1,BS2);
Adiff=abs(Atotnew-Atot);
% begin iterations:
while Adiff>1e-5;
BS2b=cumsum(BS2);
Axk2=0.02*((BS2b)-(BS2+BS2(1))/2);
B3=(a-b)*Axk2/Atotnew+b;
plot(x1,y1,x1,B3);
BS3=y1-B3;
Atot=trapz(x1,BS3);
Adiff=abs(Atotnew-Atot);
pause; % to continue, hit any key
BS2=BS3;
Atotnew=trapz(x1,BS2);
end
% end
```

A.4 Spin-Orbit Stripping

A.4.1 Description

Throughout the literature of Si 2p high-resolution SXPS it is common to analyze data after the Si $2p_{1/2}$ portion of the peak has been removed from the data, converting the Si 2p spin-orbit doublet into a single peak.[1,2] When initial attempts were made to fit doublets in the spectra collected at NSLS to a series of Voigt functions, it was observed that the peak-fitting program would not adequately fit the full doublet peak, while the singlet could be fit comparatively easily. Therefore all data was spin-orbit stripped prior to peak fitting, assuming that the Si $2p_{1/2}$–Si $2p_{3/2}$ peak difference remained constant at 0.6 eV and relative area at 0.51, as has been reported.[1–4] To do this, the data was used as defined from the previous program file "shirley_bk450.m" without further modification. At each point in the spectrum the peak intensity was measured, then 0.51 of that value was subtracted from the spectrum 0.6 eV higher in binding energy.[1,2]

A.4.2 Program File “remove.m”

```
% start
r=x1;
s=BS3;
top=ept-31; % skips the last 30 points, which do not have a point in the spectrum 0.6 eV
% higher up the x-axis
for n=[1:1:top];
P1=n;
P2=n+31;
I1=s(P1);
I2old=s(P2);
I2new=I2old-I1*0.51;
if I2new>0
s(P2)=I2new;
else s(P2)=0;
end
end
plot(r,s);
% end
```

A.5 Peak Fitting

A.5.1 Description

Peak fits were based on a Voigt function described in the literature:[5]

$$f = \frac{h}{\left(1 + \frac{M(x-c)^2}{\beta^2}\right) \exp\left(\frac{(1-M)\log 2(x-c)^2}{\beta^2}\right)} \tag{A.4}$$

where h is the peak height, c is the position of the peak center, β is a factor related to the full width at half maximum (fwhm), and M is the Lorentzian:Gaussian ratio, equal to 1 for a pure Lorentzian peak and 0 for a pure Gaussian peak. To fit the data described here, M=0.05. To fit data to multiple peaks, multiple functions were added together as many times as necessary to describe every peak to be fit, for example:

$$f = \sum_{i=1}^{n} \frac{h_i}{\left(1 + \frac{M(x-c_i)^2}{\beta_i^2}\right) \exp\left(\frac{(1-M)\log 2(x-c_i)^2}{\beta_i^2}\right)} \tag{A.5}$$

In Matlab, the Voigt function was written as a ".m" function file, which was then called by the peak-fitting file, described here as "prtc_new_xx.m" where xx represents a file number. Once the "function.m" file was created and checked, it was not altered. When actual fitting was carried out, changes in starting conditions were entered into the "prtc_new_xx.m" file only. Initial conditions given in the "prtc_new_xx.m" program files below are representative of values used to fit Si 2p core level spectra collected at NSLS, but obviously can be altered to fit the needs of any data set.

The peak-fitting programs output the values of h, c, β, χ-squared, y-axis data of the curve fit results and residuals, and peak areas. This data could be written separately into a data file using the program files "print_dataxx.m" and "print_paramxx.m." The "function.m" and "prtc_new_xx.m" files for spectra from 1 to 6 peaks are given below. Detailed explanations for each step will only be given for the first files. Data was input into the program file directly from "remove.m" without further alteration.

A.5.2 Program File “laurenvoigt14.m”

```
function yvoigt14=laurenvoigt14(c,xdata);
% in Matlab, the first line of a “function.m” file must name the function
% function.m file for 1 peak
% f=c(1)/(((1+M*(x-c(2))^2)/c(3)^2)*exp((1-M)*(log(2)*(x-c(2))^2)/c(3)^2))
% c(1)=height (h), c(2)=center (c), c(3)=beta (β)
% M=Lorentzian:Gaussian = 0.05 (1 for pure Lorenzian)
yvoigt14=c(1)./(((1+0.05*(xdata-c(2)).^2)/c(3).^2).*exp((1-0.05)*(log(2)*
(xdata-c(2)).^2)/c(3).^2));
% end
```

A.5.3 Program File “prtc_new_16.m”

```
% start
% laurenvoigt14 has 1 Voigt peak for any data with two peaks defined
% as a spin-orbit doublet
g=r;
h=s;
funstr=‘laurenvoigt14’; % define function to use
c0=[10,98.2,0.2]; % define starting values for peak fitting variables in format
% c0=[c(1),c(2),c(3)]
lb=[0,97.5,0.1]; % define lower bound of peak fitting variables
ub=[2000,102,2]; % define upper bound of peak fitting variables
c=lsqcurvefit(funstr,c0,g,h,lb,ub); % define initial conditions and x and y data
% for least squares curve fit
yvoigt14=laurenvoigt14(c,g); % call function to determine c(1) – c(3)
d=c(1)./(((1+0.05*(g-c(2)).^2)/c(3)^2).*exp((1-0.05)*(log(2)*(g-c(2)).^2)/c(3).^2));
% define curve with values found in curve fit
f=h-yvoigt14; % difference spectrum
plot(g,h,g,d,g,yvoigt14,‘x’,g,f,‘:’); % plot results
fprintf(1,‘height1 =%10.5f\n center1 = %10.5f\n beta1 = %10.5f\n’,c);
% print the values of c(1), c(2), and c(3) to the screen
darea=trapz(g,d); % calculate area defined by curve d
fprintf(‘curve 1 area =%10.5f\n’,darea); % print the value of the area under
% curve d to the screen
chisquared=(sum(0.5*(BS3-yvoigt14).^2))/(ept-3); % goodness of fit
fprintf(‘chi^2 =%10.5f’,chisquared); % print the value of chi^2 to the screen
% end
```

A.5.4 Program File “laurenvoigt15.m”

```
function yvoigt15=laurenvoigt15(c,xdata);
% function.m file for 2 peaks
% f=c(1)/(((1+M*(x-c(2))^2)/c(3)^2)*exp((1-M)*(log(2)*(x-c(2))^2)/c(3)^2))
% c(1)=height (h), c(2)=center (c), c(3)=beta (β),
% c(4)=height2 (h2), c(5)=center2 (c2), c(6)=beta2 (β2)
yvoigt15=c(1)./(((1+0.05*(xdata-c(2)).^2)/c(3).^2).*exp((1-0.05)*(log(2)*
(xdata-c(2)).^2)/c(3).^2))+...
c(4)./(((1+0.05*(xdata-c(5)).^2)/c(6).^2).*exp((1-0.05)*(log(2)*(xdata-c(5)).^2)/
c(6).^2));
% end
```

A.5.5 Program File “prtc_new_17.m”

```
% start
% laurenvoigt15 has 2 Voigt singlets
g=r;
h=s;
funstr=‘laurenvoigt15’;
c0=[10,98.4,0.17,3,98.8,0.17];
lb=[1,98.12,0.18,0.5,98.7,0.18];
ub=[2000,98.6,0.22,1000,99.3,0.22];
c=lsqcurvefit(funstr,c0,g,h,lb,ub);
yvoigt15=laurenvoigt15(c,g);
d=c(1)./(((1+0.05*(g-c(2)).^2)/c(3)^2).*exp((1-0.05)*(log(2)*(g-c(2)).^2)/c(3).^2));
j=c(4)./(((1+0.05*(g-c(5)).^2)/c(6).^2).*exp((1-0.05)*(log(2)*(g-c(5)).^2)/c(6).^2));
f=h-yvoigt15;
plot(g,h,‘b’,g,d,‘g’,g,j,‘r’,g,yvoigt15,‘x’,g,f,‘:’);
fprintf(1,‘height1 =%10.5f\n center1 =%10.5f\n beta1 =%10.5f\n
height2 =%10.5f\n center2 =%10.5f\n beta2 =%10.5f\n’,c);
darea=trapz(g,d);
jarea=trapz(g,j);
fprintf(‘curve 1 area =%10.5f\n curve 2 area =%10.5f\n’,darea,jarea);
chisquared=(sum(0.5*(BS3-yvoigt15).^2))/(ept-6);
fprintf(‘chi^2 =%10.7f’,chisquared);
% end
```

A.5.6 Program File “laurenvoigt16.m”

```
function yvoigt16=laurenvoigt16(c,xdata);
% function.m file for 3 peaks
% f=c(1)/(((1+M*(x-c(2))^2)/c(3)^2)*exp((1-M)*(log(2)*(x-c(2))^2)/c(3)^2))
% c(1)=height (h), c(2)=center (c), c(3)=beta (β),
% c(4)=height2 (h2), c(5)=center2 (c2), c(6)=beta2 (β2),
% c(7)=height3 (h3), c(8)=center3 (c3), c(9)=beta3 (β3)
yvoigt16=c(1)./(((1+0.05*(xdata-c(2)).^2)/c(3).^2).*exp((1-0.05)*(log(2)*
(xdata-c(2)).^2)/c(3).^2))+...
c(4)./(((1+0.05*(xdata-c(5)).^2)/c(6).^2).*exp((1-0.05)*(log(2)*(xdata-c(5)).^2)/
c(6).^2))+...
c(7)./(((1+0.05*(xdata-c(8)).^2)/c(9).^2).*exp((1-0.05)*(log(2)*(xdata-c(8)).^2)/
c(9).^2));
% end
```

A.5.7 Program File “prtc_new_18.m”

```
% start % laurenvoigt16 has 3 Voigt singlets
g=r;
h=s;
funstr=‘laurenvoigt16’;
c0=[14,98.8,0.2,8,99.5,0.18,8,100,0.2];
lb=[0.5,98.5,0.18,0.5,99.2,0.18,0.1,99.8,0.1];
ub=[50,99,0.22,50,100,0.22,25,100.2,0.4];
c=lsqcurvefit(funstr,c0,g,h,lb,ub);
yvoigt16=laurenvoigt16(c,g);
d=c(1)./(((1+0.05*(g-c(2)).^2)/c(3)^2).*exp((1-0.05)*(log(2)*(g-c(2)).^2)/c(3).^2));
j=c(4)./(((1+0.05*(g-c(5)).^2)/c(6).^2).*exp((1-0.05)*(log(2)*(g-c(5)).^2)/c(6).^2));
m=c(7)./(((1+0.05*(g-c(8)).^2)/c(9).^2).*exp((1-0.05)*(log(2)*(g-c(8)).^2)/c(9).^2));
f=h-yvoigt16;
plot(g,h,‘b’,g,d,‘g’,g,j,‘r’,g,m,‘c’,g,yvoigt16,‘x’,g,f,‘:’);
fprintf(1,‘height1 =%10.5f\n center1 =%10.5f\n beta1 =%10.5f\n
height2 =%10.5f\n center2 =%10.5f\n beta2 =%10.5f\n height3 =%10.5f\n
center3 =%10.5f\n beta3 =%10.5f\n’,c);
darea=trapz(g,d);
jarea=trapz(g,j);
marea=trapz(g,m);
fprintf(‘curve 1 area =%10.5f\n curve 2 area =%10.5f\n curve 3 area =%10.5f\n’,
darea,jarea,marea);
chisquared=(sum(0.5*(BS3-yvoigt16).^2))/(ept-9);
fprintf(‘chi^2 =%10.7f’,chisquared);
% end
```

A.5.8 Program File “laurenvoigt17.m”

```
function yvoigt17=laurenvoigt17(c,xdata);
% function.m file for 4 peaks
% f=c(1)/(((1+M*(x-c(2))^2)/c(3)^2)*exp((1-M)*(log(2)*(x-c(2))^2)/c(3)^2))
% c(1)=height (h), c(2)=center (c), c(3)=beta (β),
% c(4)=height2 (h2), c(5)=center2 (c2), c(6)=beta2 (β2),
% c(7)=height3 (h3), c(8)=center3 (c3), c(9)=beta3 (β3),
% c(10)=height4 (h4), c(11)=center4 (c4), c(12)=beta4 (β4)
yvoigt17=c(1)./(((1+0.05*(xdata-c(2)).^2)/c(3).^2).*exp((1-0.05)*(log(2)*
(xdata-c(2)).^2)/c(3).^2))+...
c(4)./(((1+0.05*(xdata-c(5)).^2)/c(6).^2).*exp((1-0.05)*(log(2)*(xdata-c(5)).^2)/
c(6).^2))+...
c(7)./(((1+0.05*(xdata-c(8)).^2)/c(9).^2).*exp((1-0.05)*(log(2)*(xdata-c(8)).^2)/
c(9).^2))+...
c(10)./(((1+0.05*(xdata-c(11)).^2)/c(12).^2).*exp((1-0.05)*(log(2)*(xdata-c(11)).^2)/
c(12).^2));
% end
```

A.5.9 Program File “prtc_new_19.m”

```
% start
% laurenvoigt17 has 4 Voigt singlets
g=r;
h=s;
funstr=‘laurenvoigt17’;
c0=[14,98.1,0.2,8,98.5,0.2,8,100,0.2,1,101,0.2];
lb=[0.5,98.0,0.18,0.5,98.8,0.21,0.05,99.7,0.16,0.05,101,0.16];
ub=[50,98.5,0.20,50,99.2,0.22,25,100.1,0.3,50,102,0.8];
c=lsqcurvefit(funstr,c0,g,h,lb,ub);
yvoigt17=laurenvoigt17(c,g);
d=c(1)./(((1+0.05*(g-c(2)).^2)/c(3)^2).*exp((1-0.05)*(log(2)*(g-c(2)).^2)/c(3).^2));
j=c(4)./(((1+0.05*(g-c(5)).^2)/c(6).^2).*exp((1-0.05)*(log(2)*(g-c(5)).^2)/c(6).^2));
m=c(7)./(((1+0.05*(g-c(8)).^2)/c(9).^2).*exp((1-0.05)*(log(2)*(g-c(8)).^2)/c(9).^2));
n=c(10)./(((1+0.05*(g-c(11)).^2)/c(12).^2).*exp((1-0.05)*(log(2)*(g-c(11)).^2)/
c(12).^2));
f=h-yvoigt17;
plot(g,h,‘b’,g,d,‘g’,g,j,‘r’,g,m,‘c’,g,n,‘k’,g,yvoigt17,‘x’,g,f,‘:’);
fprintf(1,‘height1 =%10.5f\n center1 =%10.5f\n beta1 =%10.5f\n height2 =%10.5f\n cen-
ter2 =%10.5f\n beta2 =%10.5f\n height3 =%10.5f\n center3 =%10.5f\n beta3 =%10.5f\n
height4 =%10.5f\n center4 =%10.5f\n beta4 =%10.5f\n’,c);
darea=trapz(g,d);
jarea=trapz(g,j);
marea=trapz(g,m);
narea=trapz(g,n);
fprintf(‘curve 1 area =%10.5f\n curve 2 area =%10.5f\n curve 3 area =%10.5f\n curve 4
area =%10.5f\n’,darea,jarea,marea,narea);
chisquared=(sum(0.5*(BS3-yvoigt17).^2))/(ept-9);
fprintf(‘chi^2 =%10.7f’,chisquared);
```

```
% end
```

A.5.10 Program File “laurenvoigt18.m”

```
function yvoigt18=laurenvoigt18(c,xdata);
% function.m file for 5 peaks
% f=c(1)/(((1+M*(x-c(2))^2)/c(3)^2)*exp((1-M)*(log(2)*(x-c(2))^2)/c(3)^2))
% c(1)=height (h), c(2)=center (c), c(3)=beta (β),
% c(4)=height2 (h_2), c(5)=center2 (c_2), c(6)=beta2 (β_2),
% c(7)=height3 (h_3), c(8)=center3 (c_3), c(9)=beta3 (β_3),
% c(10)=height4 (h_4), c(11)=center4 (c_4), c(12)=beta4 (β_4),
% c(13)=height5 (h_5), c(14)=center5 (c_5), c(15)=beta5 (β_5)
yvoigt18=c(1)./(((1+0.05*(xdata-c(2)).^2)/c(3).^2).*exp((1-0.05)*(log(2)*
(xdata-c(2)).^2)/c(3).^2))+...
c(4)./(((1+0.05*(xdata-c(5)).^2)/c(6).^2).*exp((1-0.05)*(log(2)*(xdata-c(5)).^2)/
c(6).^2))+...
c(7)./(((1+0.05*(xdata-c(8)).^2)/c(9).^2).*exp((1-0.05)*(log(2)*(xdata-c(8)).^2)/
c(9).^2))+...
c(10)./(((1+0.05*(xdata-c(11)).^2)/c(12).^2).*exp((1-0.05)*(log(2)*(xdata-c(11)).^2)/
c(12).^2))+...
c(13)./(((1+0.05*(xdata-c(14)).^2)/c(15).^2).*exp((1-0.05)*(log(2)*(xdata-c(14)).^2)/
c(15).^2));
% end
```

A.5.11 Program File “prtc_new_20.m”

```
% start
% laurenvoigt18 has 5 Voigt singlets
g=r;
h=s;
funstr=‘laurenvoigt18’;
c0=[14,98.6,0.2,8,99.4,0.2,8,100.1,0.2,1,101,0.2,1,102,0.2];
lb=[0.5,98.4,0.16,0.5,99.1,0.16,0.1,100,0.16,0.05,100.6,0.16,0.02,101.5,0.1];
ub=[50,98.8,0.22,50,99.6,0.22,25,100.5,0.5,50,101.5,0.6,50,102.5,0.8];
c=lsqcurvefit(funstr,c0,g,h,lb,ub);
yvoigt18=laurenvoigt18(c,g);
d=c(1)./(((1+0.05*(g-c(2)).^2)/c(3)^2).*exp((1-0.05)*(log(2)*(g-c(2)).^2)/c(3).^2));
j=c(4)./(((1+0.05*(g-c(5)).^2)/c(6).^2).*exp((1-0.05)*(log(2)*(g-c(5)).^2)/c(6).^2));
m=c(7)./(((1+0.05*(g-c(8)).^2)/c(9).^2).*exp((1-0.05)*(log(2)*(g-c(8)).^2)/c(9).^2));
n=c(10)./(((1+0.05*(g-c(11)).^2)/c(12).^2).*exp((1-0.05)*(log(2)*(g-c(11)).^2)/
c(12).^2));
p=c(13)./(((1+0.05*(g-c(14)).^2)/c(15).^2).*exp((1-0.05)*(log(2)*(g-c(14)).^2)/
c(15).^2));
f=h-yvoigt18;
plot(g,h,‘b’,g,d,‘g’,g,j,‘r’,g,m,‘c’,g,n,‘k’,g,p,‘y’,g,yvoigt18,‘x’,g,f,‘:’);
fprintf(1,‘height1 =%10.5f\n center1 =%10.5f\n beta1 =%10.5f\n height2 =%10.5f\n cen-
ter2 =%10.5f\n beta2 =%10.5f\n height3 =%10.5f\n center3 =%10.5f\n
beta3 =%10.5f\n height4 =%10.5f\n center4 =%10.5f\n beta4 =%10.5f\n
height5 =%10.5f\n center5 =%10.5f\n beta5 =%10.5f\n’,c);
darea=trapz(g,d);
jarea=trapz(g,j);
marea=trapz(g,m);
narea=trapz(g,n);
parea=trapz(g,p);
```

```
fprintf('curve 1 area =%10.5f\n curve 2 area =%10.5f\n curve 3 area =%10.5f\n curve 4
area =%10.5f\n curve 5 area =%10.5f\n',darea,jarea,marea,narea,parea);
chisquared=(sum(0.5*(BS3-yvoigt18).^2))/(ept-9);
fprintf('chi^2 =%10.7f',chisquared);
% end
```

A.5.12 Program File “laurenvoigt19.m”

```
function yvoigt19=laurenvoigt19(c,xdata);
% function.m file for 5 peaks
% f=c(1)/(((1+M*(x-c(2))^2)/c(3)^2)*exp((1-M)*(log(2)*(x-c(2))^2)/c(3)^2))
% c(1)=height (h), c(2)=center (c), c(3)=beta (β),
% c(4)=height2 (h2), c(5)=center2 (c2), c(6)=beta2 (β2),
% c(7)=height3 (h3), c(8)=center3 (c3), c(9)=beta3 (β3),
% c(10)=height4 (h4), c(11)=center4 (c4), c(12)=beta4 (β4),
% c(13)=height5 (h5), c(14)=center5 (c5), c(15)=beta5 (β5),
% c(16)= height6 (h6). c(17)=center6 (c6), c(18)=beta6 (β6)
yvoigt19=c(1)./(((1+0.05*(xdata-c(2)).^2)/c(3).^2).*exp((1-0.05)*(log(2)*
(xdata-c(2)).^2)/c(3).^2))+...
c(4)./(((1+0.05*(xdata-c(5)).^2)/c(6).^2).*exp((1-0.05)*(log(2)*(xdata-c(5)).^2)/
c(6).^2))+...
c(7)./(((1+0.05*(xdata-c(8)).^2)/c(9).^2).*exp((1-0.05)*(log(2)*(xdata-c(8)).^2)/
c(9).^2))+...
c(10)./(((1+0.05*(xdata-c(11)).^2)/c(12).^2).*exp((1-0.05)*(log(2)*(xdata-c(11)).^2)/
c(12).^2))+...
c(13)./(((1+0.05*(xdata-c(14)).^2)/c(15).^2).*exp((1-0.05)*(log(2)*(xdata-c(14)).^2)/
c(15).^2))+...
c(16)./(((1+0.05*(xdata-c(17)).^2)/c(18).^2).*exp((1-0.05)*(log(2)*(xdata-c(17)).^2)/
c(18).^2));
% end
```

A.5.13 Program File “prtc_new_21.m”

```
% start % laurenvoigt19 has 6 Voigt singlets
g=r;
h=s;
funstr='laurenvoigt19';
c0=[14,98.6,0.2,8,99,0.2,8,99.4,0.2,1,100.2,0.2,1,101.3,0.2,1,102.2,0.2];
lb=[0.5,98.4,0.1,0.1,98.8,0.16,0.1,99.3,0.16,0.1,100,0.1,0.1,101,0.16,0.1,101.9,0.1];
ub=[50,98.7,0.22,50,99.1,0.22,25,99.6,0.5,50,100.5,0.6,50,101.7,0.6,50,102.7,0.8];
c=lsqcurvefit(funstr,c0,g,h,lb,ub);
yvoigt19=laurenvoigt19(c,g);
d=c(1)./(((1+0.05*(g-c(2)).^2)/c(3)^2).*exp((1-0.05)*(log(2)*(g-c(2)).^2)/c(3).^2));
j=c(4)./(((1+0.05*(g-c(5)).^2)/c(6).^2).*exp((1-0.05)*(log(2)*(g-c(5)).^2)/c(6).^2));
m=c(7)./(((1+0.05*(g-c(8)).^2)/c(9).^2).*exp((1-0.05)*(log(2)*(g-c(8)).^2)/c(9).^2));
n=c(10)./(((1+0.05*(g-c(11)).^2)/c(12).^2).*exp((1-0.05)*(log(2)*(g-c(11)).^2)/
c(12).^2));
p=c(13)./(((1+0.05*(g-c(14)).^2)/c(15).^2).*exp((1-0.05)*(log(2)*(g-c(14)).^2)/
c(15).^2));
q=c(16)./(((1+0.05*(g-c(17)).^2)/c(18).^2).*exp((1-0.05)*(log(2)*(g-c(17)).^2)/
c(18).^2));
f=h-yvoigt19;
plot(g,h,'b',g,d,'g',g,j,'r',g,m,'c',g,n,'k',g,p,'y',g,q,'m',g,yvoigt19,'x',g,f,':');
fprintf(1,'height1 =%10.5f\n center1 =%10.5f\n beta1 =%10.5f\n height2 =%10.5f\n cen-
ter2 =%10.5f\n beta2 =%10.5f\n height3 =%10.5f\n center3 =%10.5f\n beta3 =%10.5f\n
height4 =%10.5f\n center4 =%10.5f\n beta4 =%10.5f\n height5 =%10.5f\n
center5 =%10.5f\n beta5 =%10.5f\n height6 =%10.5f\n center6 =%10.5f\n
beta6 =%10.5f\n',c);
darea=trapz(g,d);
jarea=trapz(g,j);
marea=trapz(g,m);
```

```
narea=trapz(g,n);
parea=trapz(g,p);
qarea=trapz(g,q);
fprintf('curve 1 area =%10.5f\n curve 2 area =%10.5f\n curve 3 area =%10.5f\n curve 4
area =%10.5f\n curve 5 area =%10.5f\n curve 6 area =%10.5f\n',
darea,jarea,marea,narea,parea,qarea);
chisquared=(sum(0.5*(BS3-yvoigt19).^2))/(ept-9);
fprintf('chi^2 =%10.7f',chisquared);
% end
```

A.6 Data Recording and Archiving

A.6.1 Description

Two Matlab ".m" files were used to record and archive peak fitting results for each fitting program. The x-axis and y-axis data of the original curve, the peak fit, and residuals are printed into one file, "print_dataxx.m," while values for c(1)–c(n), peak areas, and chiˆ2 are printed into a second file, "print_paramxx.m."

A.6.2 Program File "print_data17.m"

```
% start
% fid=fopen('filepath/filename.txt','w'); % write new file for x-axis and y-axis data
fprintf(fid,'%10.5f %10.5f %10.5f % 10.5f %10.5f %10.5f\n',[g h d j yvoigt16 f]');
fclose(fid)
% end
```

A.6.3 Program File "print_param17.m"

```
% start
% fid=fopen('filepath/filename.txt','a'); % write a new file for numerical data
fprintf(fid,'height1 =%10.5f\n center1 =%10.5f\n beta1 =%10.5f\n
height2 =%10.5f\n center2 =%10.5f\n beta2 =%10.5f\n',c);
fprintf(fid,'curve 1 area =%10.5f\n curve 2 area =%10.5f\n',darea,jarea);
fprintf(fid,'chiˆ2 =%10.7f',chisquared);
fclose(fid)
% end
```

A.6.4 Program File “print_data18.m”

```
% start
% fid=fopen(‘filepath/filename.txt’,‘w’);
fprintf(fid,‘%10.5f %10.5f %10.5f %10.5f %10.5f %10.5f %10.5f\n’,[g h d j m yvoigt16
f]’);
fclose(fid)
% end
```

A.6.5 Program File “print_param18.m”

```
% start
% fid=fopen(‘filepath/filename.txt’,‘a’);
fprintf(fid,‘height1 =%10.5f\n center1 =%10.5f\n beta1 =%10.5f\n
height2 =%10.5f\n center2 =%10.5f\n beta2 =%10.5f\n height3 =%10.5f\n
center3 =%10.5f\n beta3 =%10.5f\n’,c);
fprintf(fid,‘curve 1 area =%10.5f\n curve 2 area =%10.5f\n curve 3 area =%10.5f\n’,
darea,jarea,marea);
fprintf(fid,‘chi^2 =%10.7f’,chisquared);
fclose(fid)
% end
```

A.6.6 Program File “print_data19.m”

```
% start
% fid=fopen(‘filepath/filename.txt’,‘w’);
fprintf(fid,‘%10.5f %10.5f %10.5f %10.5f %10.5f %10.5f %10.5f %10.5f\n’,[g h d j m n
yvoigt17 f]’);
fclose(fid)
% end
```

A.6.7 Program File “print_param19.m”

```
% start
% fid=fopen(‘filepath/filename.txt’,‘a’);
fprintf(fid,‘height1 =%10.5f\n center1 =%10.5f\n beta1 =%10.5f\n
height2 =%10.5f\n center2 =%10.5f\n beta2 =%10.5f\n height3 =%10.5f\n
center3 =%10.5f\n beta3 =%10.5f\n height4 =%10.5f\n center4 =%10.5f\n
beta4 =%10.5f\n’,c);
fprintf(fid,‘curve 1 area =%10.5f\n curve 2 area =%10.5f\n curve 3 area =%10.5f\n curve
4 area =%10.5f\n’,darea,jarea,marea,narea);
fprintf(fid,‘chi^2 =%10.7f’,chisquared);
fclose(fid)
% end
```

A.6.8 Program File “print_data20.m”

```
% start
% fid=fopen(‘filepath/filename.txt’,‘w’);
fprintf(fid,‘%10.5f %10.5f %10.5f %10.5f %10.5f %10.5f %10.5f %10.5f
%10.5f\n’,[g h d j m n p yvoigt18 f]’);
fclose(fid)
% end
```

A.6.9 Program File “print_param20.m”

```
% start
% fid=fopen(‘filepath/filename.txt’,‘a’);
fprintf(fid,‘height1 =%10.5f\n center1 =%10.5f\n beta1 =%10.5f\n
height2 =%10.5f\n center2 =%10.5f\n beta2 =%10.5f\n height3 =%10.5f\n
center3 =%10.5f\n beta3 =%10.5f\n height4 =%10.5f\n center4 =%10.5f\n
beta4 =%10.5f\n height5 =%10.5f\n center5 =%10.5f\n beta5 =%10.5f\n’,c);
fprintf(fid,‘curve 1 area =%10.5f\n curve 2 area =%10.5f\n curve 3 area =%10.5f\n curve
4 area =%10.5f\n curve 5 area =%10.5f\n’,darea,jarea,marea,narea,parea);
fprintf(fid,‘chi^2 =%10.7f’,chisquared);
fclose(fid)
% end
```

A.6.10 Program File “print_data21.m”

```
% start
% fid=fopen(‘filepath/filename.txt’,‘w’);
fprintf(fid,‘%10.5f %10.5f %10.5f %10.5f %10.5f %10.5f %10.5f %10.5f %10.5f
%10.5f\n’,[g h d j m n p q yvoigt19 f]’);
fclose(fid)
```

A.6.11 Program File “print_param21.m”

```
% start
% fid=fopen(‘filepath/filename.txt’,‘a’);
fprintf(fid,‘height1 =%10.5f\n center1 =%10.5f\n beta1 =%10.5f\n
height2 =%10.5f\n center2 =%10.5f\n beta2 =%10.5f\n height3 =%10.5f\n
center3 =%10.5f\n beta3 =%10.5f\n height4 =%10.5f\n center4 =%10.5f\n
beta4 =%10.5f\n height5 =%10.5f\n center5 =%10.5f\n beta5 =%10.5f\n
height6 =%10.5f\n center6 =%10.5f\n beta6 =%10.5f\n’,c);
fprintf(fid,‘curve 1 area =%10.5f\n curve 2 area =%10.5f\n curve 3 area =%10.5f\n curve
4 area =%10.5f\n curve 5 area =%10.5f\n curve 6 area =%10.5f\n’,
darea,jarea,marea,narea,parea,qarea);
fprintf(fid,‘chi^2 =%10.7f’,chisquared);
fclose(fid)
% end
```

Bibliography

[1] Himpsel, F. J.; McFeeley, F. R.; Taleb-Ibrahimi, A.; Yarmoff, J. A.; Hollinger, G. *Phys. Rev. B.* **1988,** *38*, 6084–6096.

[2] Himpsel, F. J.; Meyerson, B. S.; McFeeley, F. R.; Morar, J. F.; Taleb-Ibrahimi, A.; Yarmoff, J. A. Core Level Spectroscopy at Silicon Surfaces and Interfaces. In *Proceedings of the 1988 Enrico Fermi School on Photoemission and Absorption Spectroscopy of Solids and Interfaces with Synchrotron Radiation*; Varenna: North Holland, 1988.

[3] Bansal, A.; Li, X.; Yi, S. I.; Weinberg, W. H.; Lewis, N. S. *J. Phys. Chem. B* **2001,** *105*, 10266–10277.

[4] Haber, J. A.; Lewis, N. S. *J. Phys. Chem. B* **2002,** *106*, 3639–3656.

[5] Sherwood, P. M. A. Data Analysis in XPS and AES. In *Practical Surface Analysis*, Vol. 1; Briggs, D.; Seah, M. P., Eds.; John Wiley & Sons Ltd: New York, 1990.

[6] Webb, L. J.; Lewis, N. S. *J. Phys. Chem. B* **2003,** *107*, 5404–5412.

[7] Chan, A. S. Y. **2003,** Personal communication.

[8] Proctor, A.; Sherwood, P. M. A. *Anal. Chem.* **1982,** *54*, 13–19.

[9] Shirley, D. A. *Phys. Rev. B* **1972,** *5*, 4709–4714.

[10] Contini, G.; Turchini, S. *Comput. Phys. Commun.* **1996,** *94*, 49–52.

[11] Seah, M. P. Quantification of AES and XPS. In *Practical Surface Analysis*, Vol. 1, 2nd ed.; Briggs, D.; Seah, M. P., Eds.; John Wiley & Sons: Chichester, 1990.